

Accelerated Aging and Mechanochemical Milling:
Solid State Approaches for Metal Organic Material
Synthesis and Mineral Separation

Feng Qi

A Thesis submitted to McGill University in partial fulfillment of the requirements
of the degree of

Master of Science

Department of Chemistry

McGill University

Montreal Quebec Canada

October 2013

©Feng Qi, 2013. All rights reserved.

*Anyone who thinks science is trying to make
human life easier or more pleasant is utterly
mistaken.*

----- Albert Einstein

Abstract

This thesis illustrates a systematic study of accelerated aging, a mild solid-state synthetic approach inspired by biomineralization (also known as mineral neogenesis or mineral weathering). Similar to mechanochemical milling, accelerated aging is a solvent-free and low energy method for metal organic materials synthesis. It is even more sustainable by avoiding the expensive mechanical mills and the dusty working environment. In this thesis, both main group and transitional metal oxides have been selected as reactants for accelerated aging reactions. Due to their different reactivity towards certain organic acids, solvent-free separation of these minerals has been proposed and demonstrated. By transferring the synthetic strategies developed in solvothermal synthesis, two dimensional and three dimensional metal organic frameworks have been obtained through accelerated aging. The influence of critical aging parameters such as temperature, time and humidity has been systematically demonstrated by a series of kinetic studies. Mechanochemical milling, as the other solid-state synthetic method, has also been introduced in thesis for comparison. The ideas in mechanochemistry such as ion- and liquid- assisted grinding and mechanical activation have thrown light to the improvement of accelerated aging. The scale-up of both mechanosynthesis and accelerated aging are easily achievable, which enables industrial application for more sustainable extractive metallurgical processes and chemical production lines. In this thesis, most of the described aging reactions have been scaled up to 10 grams, and by using their products as precursors, further advanced materials like supramolecular decorated nanoclusters have been successfully obtained.

Keywords: metal organic materials, mechanochemistry, accelerated aging, bio-inspired synthesis, solid-state chemistry, green chemistry, metal oxides, mineral separation, bismuth chemistry, metallodrugs, bismuth salicylate oxo-clusters, supramolecular decoration, nanopharmaceuticals.

Abrégé

Cette thèse montre une étude systématique de vieillissement accéléré, une approche synthétique de l'état solide légère inspirée par biominéralisation (également connu sous le nom néogenèse minérale ou de l'altération des minéraux). Similaire au fraisage mécano, le vieillissement accéléré est une méthode de l'énergie sans solvant et à faible pour le métal la synthèse des matériaux organiques. Il est encore plus durable en évitant les moulins mécaniques coûteux et l'environnement de travail poussiéreux. Dans cette thèse, tant le groupe principal et des oxydes de métaux de transition ont été sélectionnés en tant que réactifs pour les réactions de vieillissement accéléré. En raison de leur réactivité différente à l'égard de certains acides organiques, la séparation sans solvant de ces minéraux a été proposée et démontrée. En transférant les stratégies de synthèse développés dans la synthèse solvothermale, deux cadres organiques métalliques dimensions dimensions et trois ont été obtenus grâce à un vieillissement accéléré. L'influence des paramètres de vieillissement critiques tels que la température, le temps et l'humidité a été systématiquement démontré par une série d'études cinétiques. Broyage mécano, que l'autre méthode de synthèse à l'état solide, a également été introduite dans la thèse de comparaison. Les idées dans mechanochemistry tels que des ions et de broyage liquide assistée par activation mécanique et ont mis en lumière l'amélioration de vieillissement accéléré. La mise à l'échelle à la fois de mécano et un vieillissement accéléré sont facilement réalisables, qui permet l'application industrielle de procédés métallurgiques d'extraction plus durables et des lignes de production de produits chimiques. Dans cette thèse, la plupart des réactions de vieillissement décrites ont été réduits jusqu'à 10 grammes, et en utilisant leurs produits en tant que précurseurs, d'autres matériaux avancés comme les nanoparticules décorées supramoléculaires ont été obtenues avec succès.

Acknowledgements

I want to express my sincere thanks to the many people who accompanied me during my studies at McGill:

My parents, for their never-ending support and encouragement, especially when I was sick or depressed.

My wife, Yingshan Gu, for the love, understanding and happiness she always gave to me. I find my life becomes more enjoyable by holding her hand.

My Supervisor, Prof. Tomislav Friščić, who has an impressive passion for science and a good sense of humor. Talking with him is always fun and ending with interesting ideas. His invaluable input and constant support enabled this work and all other exciting findings.

The wonderful people I met in Friščić Group: Cristina, Neil, Antoine, Davin, Kale, Thanassis, Louis, Vjekoslav, Matthieu, Jose. Working with them is a pleasant experience in my life. Wish all of them live long and prosper.

Prof. David S. Bohle, Dr. Fred Morin, Dr. Mohini Ramkaran, Dr. Petr Fiurasek, Dr. Andrey Moiseev and Dr. Georgios Rizis for their patience and warmness in teaching or helping me with instrumental analysis.

Ms. Chantal Marotte, for her help and detailed responses in dealing with all kinds of documents and forms.

Mr. Ziwen Dai for helping me settle down in Montreal.

My close friends from “The Best THF”: Bo Peng, Lin Liu, and Peiqi Qiao, for the amazing moments we spent together and interesting talks we had through the web.

All my other friends in Montreal and all over the world. Good luck in adventures.

Contributions from Authors

The main body of this thesis consists of two chapters (Chapter 2 and Chapter 3). Chapter 2 has been published while Chapter 3 is being prepared for submission. An introduction to the field is provided in Chapter 1, and conclusions to the work are provided in Chapter 4.

Chapter 2

Title: Mimicking mineral neogenesis for the clean synthesis of metal-organic materials from mineral feedstocks: coordination polymers, MOFs and metal oxide separation

Co-authored by Robin S. Stein and Tomislav Friščić

Green Chem., **2013**, Advanced Article, DOI: 10.1039/C3GC41370E

Chapter 3

Title: Bismuth disalicylate monohydrate: a central compound of bismuth salicylate chemistry

Co-authored by [Kale Laviolette](#) and Tomislav Friščić

Manuscript to be submitted.

In Chapter 2, Dr. Robin S. Stein collected and analyzed solid state NMRs for ammonium templated zinc oxalate frameworks.

In Chapter 3, [Kale Laviolette](#) prepared some single crystals of decorated bismuth salicylate oxo-nanoclusters. Very sadly, Kale passed away in July 2013.

Prof. Tomislav Friščić provided guidance to the work presented in both chapters and contributed to the manuscripts writing. He also solved all crystal structures of decorated bismuth salicylate oxo-nanoclusters in Chapter 3.

Table of Contents

Abstract.....	IV
Abrégé.....	V
Acknowledgements.....	VI
Contributions from Authors.....	VII
Table of Contents.....	VIII
List of Abbreviates.....	X
List of Tables.....	XII
List of Figures.....	XIII
Chapter 1. General Introduction.....	1
1.1 Mechanochemistry: history and applications.....	3
1.2 Transformations of inert inorganic substances: mineral neogenesis and accelerated aging.....	15
1.3 Thesis perspective and outline.....	19
References.....	20
Chapter 2. Mimicking mineral neogenesis for the clean synthesis of metal- organic materials from mineral feedstocks: coordination polymers, MOFs and metal oxide separation.....	26
2.1 Abstract.....	26
2.2 Introduction.....	27
2.3 Experimental Section.....	29
2.4 Results and Discussion.....	31
2.4.1 Structure templating.....	33
2.4.2 Reactivity of other metal oxides, product hydration state.....	36
2.4.3 Formation of open structures based on Co and Ni.....	40
2.4.4 Effect of temperature.....	42
2.4.5 Activation by milling: enabling room temperature reactivity.....	45
2.4.6 Selective transformation of metal oxides in a mixture.....	46

2.5 Conclusions.....	49
2.6 Acknowledgement.....	50
Notes and references.....	50
Connecting text for Chapter 3.....	59
Chapter 3. Bismuth disalicylate monohydrate: a central compound of bismuth salicylate chemistry	60
3.1 Abstract.....	60
3.2 Introduction.....	60
3.3 Experimental Section.....	61
3.4 Results and Discussions.....	63
3.5 Conclusions.....	71
References.....	72
Chapter 4. Conclusions, Contributions to Original Knowledge and Ideas for Future Work	73

List of Abbreviates

MOMs: metal organic materials

MOFs: metal organic frameworks

SSMs: soft supramolecular materials

HTS: high-throughput screening methods

STY: space-time yields

LAG: liquid-assisted grinding

ILAG: ion- and liquid-assisted grinding

APIs: active pharmaceutical ingredients

1D, 2D and 3D: one-, two- and three-dimensional

ZIFs: zeolitic imidazolate frameworks

PXRD: powder X-ray diffraction

RH: relative humidity

TGA: thermogravimetric analysis

FTIR-ATR: Fouriertransform infrared attenuated total reflection

SSNMR: solid-state nuclear magnetic resonance

DSC: differential scanning calorimeter

CSD: Cambridge structure database

BSS: bismuth subsalicylate

NP: Nano particle

x

DLS: dynamic light scattering

AFM: atomic force microscope

List of Tables

Table 1.1. Differentiation of mechanochemical and solution-based methods by η (unit: $\mu\text{L}/\text{mg}$). Reproduced from reference[42].	7
Table 2.1. Time (in days) for the disappearance of X-ray reflections of the metal oxide (with given melting points) in PXRD patterns of mixtures ^a with $\text{H}_2\text{Ox}\cdot 2\text{H}_2\text{O}$ exposed to 98% RH under different conditions.	37

List of Figures

Figure 1.1. Construction of metal-organic-materials from metal nodes and organic linkers. Reproduced from reference [2].....	2
Figure 1.2. Overview of synthetic methods of MOM synthesis. Reproduced from reference [24].....	3
Figure 1.3. Equations of mechanochemical reactions discovered by W. Spring and M. Carey Lea.....	5
Figure 1.4. Magma-plasma model: E – exo-electrons, N – undeformed solid, D – highly deformed surface layer, P – plasma. Reproduced from reference [26].....	6
Figure 1.5. Three-component phase diagrams for cocrystal components that are (a) congruently and (b) incongruently soluble in a solvent. The regions of composition corresponding to typical solution-phase and grinding experiments are marked blue and red, respectively. Reproduced from reference [38].....	8
Figure 1.6. (a) Molecules used in mechanochemical synthesis of pharmaceutical cocrystals by Caira et al.; (b) Mechanochemical reaction of 9-methyladenine and 1-methylthymine to form a cocrystal reported by Etter; (c) Mechanochemical cocrystallization by neat grinding of carbamazepine and saccharin involving an amorphous intermediate. Reproduced from reference [44].....	10
Figure 1.7. Three-component assembly of caffeine, succinic acid and a guest molecule into a ternary inclusion compound based on a two-component hydrogen-bonded host. Reproduced from reference [19].....	11
Figure 1.8. (a) The first reported mechanochemical assembly of a porous MOF by neat grinding; (b) The ligand cyanoguanidine (CNGE) with different metal binding sites indicated by arrows and its reactions with CdCl_2 upon neat grinding under various reaction conditions; (c) Difference in mechanochemical reactivity of bipy towards anhydrous CoCl_2 and $\text{CoCl}_2 \cdot 6\text{H}_2\text{O}$. Reproduced from references [44] and [19].....	12

Figure 1.9. (a) The construction of coordination polymers and frameworks from zinc oxide by LAG; (b) Mechanochemical interconversions of 1-D, 2-D and 3-D MOFs by LAG. Reproduced from references [44] and [19].....	12
Figure 1.10. (a) Topologically specific mechanosynthesis of zeolitic imidazolate frameworks (ZIFs) directly from ZnO and 2-ethylimidazole using ILAG. Pathway A represents ILAG with (NH ₄) ₂ SO ₄ ; B is ILAG with NH ₄ NO ₃ or NH ₄ CH ₃ SO ₃ in the presence of EtOH and C is ILAG with NH ₄ CH ₃ SO ₃ and DMF or DEF as the liquid phase; (b) time-dependent ZIF transformations under ILAG conditions, T/V is the number of tetrahedral sites (T) per nm ³ . Reproduced from reference [44].....	13
Figure 1.11. (a) Sonogashira reaction using a copper vial as the source of the Cu-cocatalyst; (b) Solventless ball milling synthesis of a large organic cage. Reproduced from reference [44].....	14
Figure 1.12. (a) Lead plates before processing by the “Dutch method”. (b) The same plates upon conversion to lead white pigment (basic lead carbonate). Source of photos: http://www.geoffreylaurence.com/leadwhite.html	16
Figure 1.13. Details of solvents used and products obtained in the vapor digestion processes (exposure time = 1 day). Reproduced from reference [87].....	17
Figure 1.14. Accelerated aging reactions toward to ZIF-8 and ZIF-67 in 5g scale. Reproduced from reference [91].....	18
Figure 1.15. a) Reaction scheme of preparation of 1 ; b) Relevant calculated and experimental powder X-ray diffraction (PXRD) patterns for reaction at 0% RH; c) and 98% RH. Characteristic reflections for napht are indicated by “*”. NG is the abbreviation for neat grinding. Reproduced from reference [92].....	18
Figure 2.1. Metal oxalate topologies: a) 1-D; b) 2-D and 3-D.....	29
Figure 2.2. (a) Two coordination polymer chains connected by hydrogen bonds in Zn \mathbf{ox} ·2H ₂ O (CSD QQQBOD04). PXRD patterns for aging reactions of ZnO and H ₂ \mathbf{ox} ·2H ₂ O at 98% RH: (b) H ₂ \mathbf{ox} ·2H ₂ O; (c) simulated for Zn \mathbf{ox} ·2H ₂ O; (d) ZnO; (e) 1 day at room temperature; (f) 5 days at room temperature; (g) 1 day at 45 °C; (h) 5 days at 45 °C; (i) 1 day at room temperature with pre-milling; (j) 5 days at room temperature with pre-milling and (k) 10 days at room temperature with pre-	

milling. (l) Completed 10 gram aging syntheses of $Zn_{ox} \cdot 2H_2O$ and $Ni_{ox} \cdot 2H_2O$32

Figure 2.3. FTIR-ATR spectra of final products of aging reactions for: (a) ZnO, 5 days at 45 °C; (b) CoO, 7 days at 45 °C; (c) NiO, 7 days at 45 °C; (d) CuO, 16 days at 45 °C; (e) MgO, 9 days at 45 °C; (f) MnO, 16 days at room temperature; (g) MnO, 16 days at 45 °C; (h) PbO, 14 days at 45 °C and (i) MnO, aging of a pre-milled sample for 1 day at 45 °C. Spectrum of $H_2Ox \cdot 2H_2O$ is given under (j).....33

Figure 2.4. (a) Planned synthesis of open anionic 2-D and 3-D zinc oxalate frameworks; (b) templates pn^{2+} and pa^+ and (c) a hydrogen-bonded layer in the crystal of $(pa)_2 \cdot (ox)$, with propyl chains omitted for clarity.....34

Figure 2.5. PXRD patterns for templated aging syntheses of zinc oxalate MOFs: (a) $Zn_{ox} \cdot 2H_2O$; (b) ZnO, $H_2Ox \cdot 2H_2O$ and $[pn][ox]$ in ratio 2:2:1 after 5 days; (c) $Zn_{ox} \cdot 2H_2O$ and $[pn][ox]$ in ratio 2:1 after 5 days; (d) simulated for 2-D MOF $[pn][Zn_2(ox)_3] \cdot 3H_2O$ (SEYQAO); (e) ZnO, $H_2Ox \cdot 2H_2O$ and $[pa]_2[ox]$ in ratio 2:2:1 after 5 days and (f) simulated for 3-D MOF $[pa]_2[Zn_2(ox)_3] \cdot 3H_2O$ (SEYQIW). Reactions were done at room temperature, 98% RH. Characteristic reflection of $Zn_{ox} \cdot 2H_2O$ is marked with '*'......36

Figure 2.6. Aging reactivity of ZnO, CoO and NiO towards $H_2Ox \cdot 2H_2O$ with and without organoammonium templates.....37

Figure 2.7. PXRD patterns for selected reactions at 98% RH: (a) MgO; (b) $Mg_{ox} \cdot 2H_2O$ (5 days, 45°C); (c) MnO; (d) $Mn_{ox} \cdot 2H_2O$ (pre-milled MnO, 45 1 day, room temperature); (e) $Mn_{ox} \cdot 2H_2O$ (9 days, 45°C); (f) simulated α - $Mn_{ox} \cdot 2H_2O$ (FOZHUX11); (g) simulated γ - $Mn_{ox} \cdot 2H_2O$ (FOZHUX10); (h) NiO; (i) $Ni_{ox} \cdot 2H_2O$ (3 days, 45°C); (j) $Co_{ox} \cdot 2H_2O$ (6days, room temperature, data collected using $CuK\alpha$ radiation and energydiscriminating LynxEye detector); (k) CuO; (l) $Cu_{ox} \cdot 0.5H_2O$ (16 days, 45°C; (m) $Cu_{ox} \cdot 0.5H_2O$ (pre-milled CuO, 10 days, room temperature); (n) PbO; (o) Pb_{ox} (pre-milled PbO, 9 days, 45°C); (p) simulated Pb_{ox} (JAHVUJ). (q) Visual comparison of samples of oxide reactants with corresponding oxalate products obtained by aging (98%RH, 45°C).....39

Figure 2.8. Selected PXRD patterns for templated aging synthesis of Ni(II) (green) and Co(II) (red) oxalate MOFs: (a) $Ni_{ox} \cdot 2H_2O$; (b) $Co_{ox} \cdot 2H_2O$; (c) NiO,

H₂ox·2H₂O and [pn][ox] in ratio 2:2:1 after 5 days; (d) Ni₂ox·2H₂O and [pn][ox] in ratio 2:1 after 5 days; (e) CoO, H₂ox·2H₂O and [pn][ox] in ratio 2:2:1 after 5 days; (f) simulated 2-D MOF [pn][Zn₂(ox)₃]·3H₂O (SEYQAO); (g) NiO, H₂ox·2H₂O and [pa]₂[ox] in ratio 2:2:1 after 5 days; (h) Ni₂ox·2H₂O and [pa]₂[ox] in ratio 2:1 after 5 days; (i) CoO, H₂ox·2H₂O and [pa]₂[ox] in ratio 2:2:1 after 5 days; (j) simulated 3-D MOF [pa]₂[Zn₂(ox)₃]·3H₂O (SEYQIW). Reactions were done at room temperature, 98% RH. Patterns of cobalt samples were recorded using CuK α radiation and an energy-discriminating detector. Characteristic reflections of Ni₂ox·2H₂O, Co₂ox·2H₂O are marked with '*'. 41

Figure 2.9. Solid-state reflectance UV-Vis spectra of cobalt(II) (top) and nickel(II) (bottom) oxalate dihydrates obtained by aging reactions. 42

Figure 2.10. (a) Crystal structures of α - (top) and γ -Mn₂ox·2H₂O (bottom). PXRD patterns collected using CoK α radiation: (b) MnO; (c) MnO after 5min milling; (d) reaction of MnO and H₂ox·2H₂O, room temperature, 98% RH; (e) reaction of MnO and H₂ox·2H₂O, 45°C, 98% RH; (f) reaction of pre-milled MnO and H₂ox·2H₂O, room temperature, 98% RH; (g) reaction of pre-milled MnO and H₂ox·2H₂O, 45°C, 98% RH. Full set of PXRD patterns is given in the Supplementary Material. 44

Figure 2.11. Selected FTIR-ATR spectra for the reaction of MnO and H₂ox·2H₂O. Characteristic bands are labeled for α - (red line) and γ -forms (blue line) of Mn₂ox·2H₂O. 46

Figure 2.12. PXRD patterns for the aging of a 1:1:1 mixture of ZnO, CuO and H₂ox·2H₂O: (a) after 5 days at 45°C, 98% RH; (b) bottom layer from gravity separation using CH₂I₂; (c) top layer obtained by gravity separation using CH₂I₂; (d) Zn₂ox·2H₂O; (e) Cu₂ox; (f) ZnO and (g) CuO. (h) Reflectance UV-Vis spectra (top to bottom): average of Cu₂ox and Zn₂ox·2H₂O; reaction mixture after 5 days at 45°C, 98% RH; pure Zn₂ox·2H₂O and pure Cu₂ox. PXRD and UV-Vis spectra indicate selective transformation of ZnO into Zn₂ox·2H₂O, leaving behind CuO. To highlight the selective conversion, selected X-ray reflections of CuO and Zn₂ox·2H₂O are designated with * and •, respectively. 48

Figure 3.1. (a) The interconversion of **Bi-1** and **Bi-2**; (b) PXRD patterns for interconversion of **Bi-1**, **Bi-2** and **Bi-3**. From top to bottom: commercial **H₂Sal**; commercial **Bi-1**; synthesized **Bi-2** (washed by room temperature water and dried in the open air); synthesized **Bi-3** (kept in dry desiccator); **Bi-2** after reflux in boiling water for 3 hours; 1:1 mixture of **Bi-1** and **H₂Sal** after LAG with water ($\eta=0.25\mu\text{L}/\text{mg}$); **Bi-3** after 1 day in air; **Bi-3** washed with room temperature water.....64

Figure 3.2. (a) Images of 10 gram scale accelerated aging reaction to form **Bi-2**; (b) PXRD patterns for accelerated aging reactions forming **Bi-2** and **Bi-1**. From top to bottom: bismuth oxide (**Bi₂O₃**); salicylic acid (**H₂Sal**); **Bi-1**; **Bi-2**; 1:4 mixture of **Bi₂O₃** and **H₂Sal** after 4 days aging at 80°C 100% RH; 10 g scale 1:4 mixture of **Bi₂O₃** and **H₂Sal** after 3 days aging at 95°C 100% RH; 1:2 mixture of **Bi₂O₃** and **H₂Sal** after 1 day aging at 95°C 100% RH; 1:2 mixture of **Bi₂O₃** and **H₂Sal** after 3 days aging at 95°C 100% RH; 1:2 mixture of **Bi₂O₃** and **H₂Sal** after 5 days aging at 95°C 100% RH; 1:2 mixture of **Bi₂O₃** and **H₂Sal** after 7 days aging at 95°C 100% RH.....66

Figure 3.3. PXRD patterns for equilibrium study of **Bi-2** and **Bi-1+H₂Sal** at 95°C 100% RH aging condition. From top to bottom: 1:1 mixture of **Bi-1** and **H₂Sal** after 4 days aging at 80°C 100% RH (no reaction); 1:1 mixture of **Bi-1** and **H₂Sal** after 3 days aging at 95°C 100% RH; 1:1 mixture of **Bi-1** and **H₂Sal** after 7 days aging at 95°C 100% RH; 1:1 mixture of **Bi-1** and **H₂Sal** after 11 days aging at 95°C 100% RH; **Bi-2** after 8 months aging at room temperature 100%RH (no reaction); **Bi-2** after 3 days aging at 95°C 100%RH; **Bi-2** after 7 days aging at 95°C 100%RH; **Bi-2** after 11 days aging at 95°C 100%RH; 10% **Bi-1**+90% **Bi-2** manually mixture; 20% **Bi-1**+80% **Bi-2** manually mixture.....67

Figure 3.4. (a) Proposed mechanism of the **Bi-2** and **Bi₂O₃** aging reactions; (b) PXRD patterns for **Bi-2** and **Bi₂O₃** aging reactions, from top to bottom: bismuth oxide (**Bi₂O₃**); salicylic acid (**H₂Sal**); **Bi-1**; **Bi-2**; 2:1 stoichiometric mixture of **Bi-2** and **Bi₂O₃** after 10 days aging at room temperature and 100% RH (no reaction); 2:1 mixture of **Bi-2** and **Bi₂O₃** after 1 day aging at 95°C and 100% RH; 2:1

mixture of **Bi-2** and Bi_2O_3 after 3 days aging at 95°C and 100% RH; 2:1 mixture of **Bi-2** and Bi_2O_3 after 7 days aging at 95°C 100% RH; 2:1 mixture of **Bi-2** and Bi_2O_3 after 9 days aging at 95°C 100% RH.....68

Figure 3.5. (a) A series single crystals of surface-decorated bismuth salicylate oxo-nanoclusters; (b) DLS measurements of the size of nanoclusters in their respective solvents of decoration; (c) FTIR-ATR spectra of different decorated nanoclusters. The characteristic absorption bands are located in the $1500\text{-}1700\text{ cm}^{-1}$ region.....70

Figure 3.6. AFM image and analysis of aqueous suspension of proposed water-decorated bismuth salicylate oxo-nanoclusters.....71

Chapter 1: General Introduction

Our knowledge of inorganic chemistry has been extremely extended since Alfred Werner proposed his structural model of octahedral transition metal complexes in 1893.¹ Although Werner could not explain the detailed mechanism of how coordination bonds were generated, the modern coordination chemistry which he pioneered enables the modern chemists to rationally design structures by deliberately combining specific ligands and metal ions. Modern coordination and organometallic chemistry have evolved to the point that desired molecular architectures are readily constructed, offering the study of structure-property relationships as the next challenge of materials science. Synthesis of materials with designed properties provides solutions to our technological challenges like global warming, energy depletion and industrial pollution. Metal organic materials (MOMs), a broad family of materials constructed by metal nodes and organic ligands (Figure 1.1),² includes simple metal-organic complexes, coordination polymers, organometallic catalysts, metal organic frameworks (MOFs), and supramolecular coordination complexes. Although the term MOMs is the preferred one for the purpose of this thesis, it should be noted that alternative and complementary names also exist, such as hybrid inorganic-organic materials introduced by Rao and Cheetham,³ coordination polymers as discussed by Kitagawa's group,⁴ or even soft supramolecular materials (SSMs) initially developed by Soldatov and Ripmeester.⁵ Despite minor differences, all these terms refer to an up-and-coming family of materials whose unique properties (electrical, magnetic, optical, catalytic, self-assembly and porosity) are obtained by combining properties of metal ions and organic molecules in a modular way.²⁻⁹

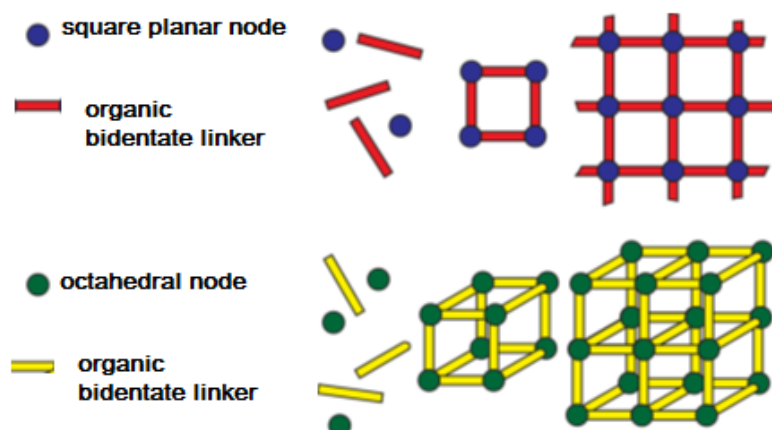


Figure 1.1. Construction of metal-organic-materials from metal nodes and organic linkers. Reproduced from reference [2].

After establishing the principles of designing MOMs using metals and ligands of specific geometry, the next and fundamentally important step is the choice of synthetic method. In general, the chosen synthetic method should help the desired phase to grow in a crystallization process as well as limit the formation of byproducts and prevent the decomposition of the organic linkers which could be sensitive to acidic ions, temperature or light. From the same reactants mixture, different synthetic methods may selectively provide specific structures, or lead to different reaction times, particle sizes, crystal morphology, yield, and potential for scaling up. The history of development of MOMs synthesis is an excellent example of interdisciplinary inspiration and scientific collaboration. Chemists with different synthetic backgrounds introduced a variety of synthetic methods over the past 20 years. As shown in Figure 1.2, high-throughput screening methods (HTS) initially developed in the area of pharmaceutical research have been applied to accelerate conventional MOMs synthetic methods like slow evaporation, diffusion, elevated temperature synthesis, and synthesis under solvothermal conditions.¹⁰⁻¹¹ New means of introducing energy into a chemical reaction such as electricity,¹² microwave,¹³⁻¹⁵ ultrasound¹⁶⁻¹⁷ and mechanical grinding¹⁸⁻¹⁹ have been established as alternatives of simple heating. Bottom-up techniques including thin films and membrane synthesis²⁰⁻²¹ have also been used to control the morphology of particles and investigate nanoscale MOM crystals.

Besides providing potential benefits for the control of the structure and particular morphology of the final product, non-conventional synthetic methods are also expected to decrease reaction temperature, lower solvent usage, provide high space-time yields (STY), *i.e.* “the mass of a product formed per volume of the reactor and time”,²² and reduce risks associated with nitrate, perchlorate and chloride anions which often raise challenges to reactor layout or process control. Indeed, the underlying ideas of green chemistry and sustainable manufacturing processes expect that the conventional high energy and solvent consuming synthetic processes will be eventually phased out by solventless technologies with mild reactants and low energy input.²³

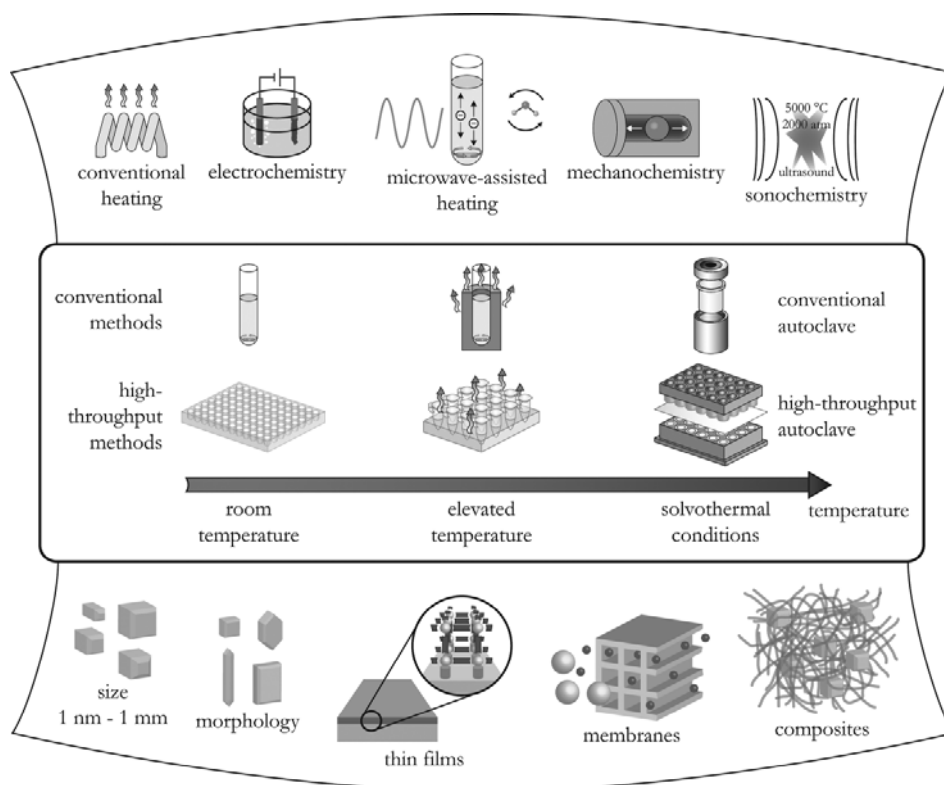


Figure 1.2. Overview of synthetic methods of MOM synthesis. Reproduced from reference [24]

1.1. Mechanochemistry: history and applications

In the classification of a textbook written by Wilhelm Ostwald, a highly influential German chemist who received the Nobel Prize in 1909, the term “mechanochemistry” initially appeared as a branch of physical chemistry like thermochemistry, photochemistry and electrochemistry. Ostwald defined this type of chemistry based on the source of energy: “*Mechanochemistry is a branch of chemistry which is concerned with chemical and physico-chemical changes of substances of all states of aggregation due to the influence of mechanical energy.*”²⁵ However, the chemical application of mechanical activation can be traced back to prehistoric times. Specifically, mechanochemistry conducted by friction and grinding has been used since the Stone Age for ignition and food preparation.²⁶⁻²⁷ In 4th century BC, elemental mercury has been made by grinding cinnabar (HgS) with acetic acid in a copper vessel. It is the first documented mechanochemical reaction and may be the first time in human history to extract a metal in the elemental form from a compound.²⁸ Unfortunately, despite these early findings, the development of mechanochemistry has followed a much slower path than the connected disciplines like mineralogy, inorganic synthesis, organic synthesis and tribology. Thus, the high-speed development of mechanochemistry did not really begin until 1960s.

In the history of mechanochemistry, the case of mechanical alloying suitably illustrates the interdisciplinary nature of mechanochemistry research and problems in communication of scientists from various backgrounds. The mechanical alloying technique has been developed in 1966 by metallurgists from Western Europe.²⁹ Meanwhile, in Soviet Union and Eastern Europe, several mechanochemistry groups have been established in the area of triboemission research and mineral processing applications.³⁰⁻³¹ For almost 20 years, the researchers from East and West conducted parallel work using very similar ball milling equipment without mutual communication. In early 1990s, the development of internet finally connected two groups of scientists. However, due to the tradition and history, mechanical alloying is still a unique branch within

mechanochemistry even though the ideas from both sides are being continuously exchanged.³²

Although many early scholars like Theophrastus and Faraday discovered mechanochemical reactions and recorded them in their work,²⁶ the first extensive investigations of mechanochemistry were separately carried out by W. Spring in 1880s in Belgium and by the American scientist M. Carey Lea in 1890s. Spring's metathesis reaction (Figure 1.3) induced by repeated compression and pulverization was the first large scale mechanochemical synthesis.³³ Lea's systematical investigation revealed that mechanochemical grinding can bring different outcome than heating of the same system. His significant experiment addressed the behavior of mercuric chloride which sublimes under heating, but decomposes during grinding.³⁴⁻³⁵ (Figure 1.3)

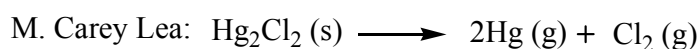
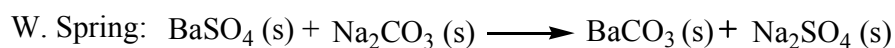


Figure 1.3. Equations of mechanochemical reactions discovered by W. Spring and M. Carey Lea.

Obviously, during impact and friction much mechanical work must be converted to thermal effect. It has been reported that when using a Retsch MM200 mill, a stainless steel jar and two 7mm diameter stainless steel balls, a typical 30min grinding experiment at a frequency of 30 Hz will increase the temperature of the milling vessel (jar) by ca. 4°C.³⁶ However, as proved by Lea's experiments, it would be one-sided to attribute all chemical changes during milling or grinding to local heating. The first model of mechanochemical reactivity, the "Magma-Plasma Model", was introduced by Thiessen in 1967.³⁷ According to this model, the mechanical impact upon grinding releases a large quantity of energy which helps the formation of a special plasmatic state during grinding. (Figure 1.4) Other models like "spherical model", "dislocation and phonon theory", "short-live-active center theory" "kinetic and impulse model" were proposed in the

following 30 years,²⁶ but due to the complex and multivariable processes of mechanochemistry, the fundamental nature of mechanochemical reactions is still a challenging issue to both experimental and theoretical chemists.

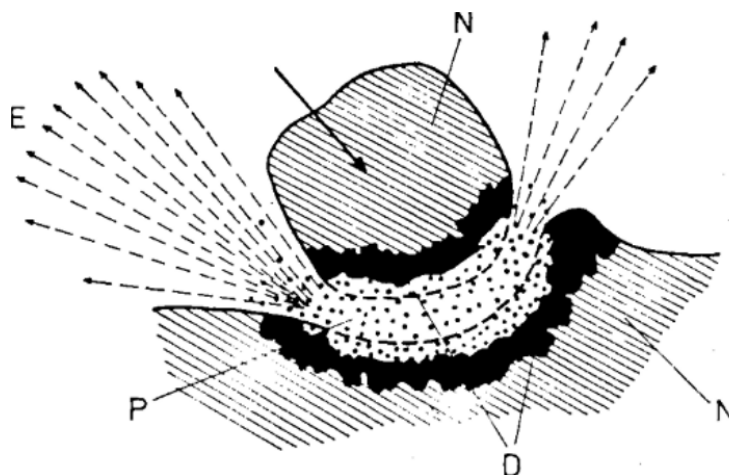


Figure 1.4. Magma-plasma model: E – exo-electrons, N – undeformed solid, D – highly deformed surface layer, P – plasma. Reproduced from reference [26].

During the investigation in numerous research fields, further advances like “liquid-assisted grinding” (LAG) (also known as solvent drop grinding or kneading), and “ion- and liquid-assisted grinding” (ILAG) have been developed. It was recently discovered that mechanochemical reactions can be dramatically accelerated and efficiently controlled by digressing from the general view of mechanochemistry as a purely solid-state method and introducing a small, sub-stoichiometric amount of a liquid into the reaction mixture.³⁸⁻⁴⁰ Compared to neat grinding, such LAG could increase molecular mobility and give more crystalline product. In a way, the liquid in LAG resembles the function of solvent in solution-based chemistry. But in contrast to using bulk solvents, the amount of liquid in LAG is too small to impose any solubility-related limitations on chemical reactions.^{41,42} The parameter η (unit: $\mu\text{L}/\text{mg}$), corresponding to the ratio of the liquid phase to the amount of solid reactants, was introduced to distinguish different synthetic methods.⁴² (Table 1.1) In the case of cocrystal synthesis, analysis of the three-component phase diagrams has shown that it is difficult to obtain a cocrystal from solution-based methods, especially when two components

are incongruently soluble. In Figure 1.5, the red area in the bottom, corresponding to the conditions of LAG, indicates that the function of liquid in LAG is apparently different from that of bulk solvents.³⁸ ILAG has been initially introduced in the field of porous MOFs synthesis,⁴³ and then extended to other metal organic materials like bismuth salicylate complexes.³⁶ In ILAG, the use of catalytic amounts of simple ions such as NO_3^- , SO_4^{2-} and NH_4^+ from inorganic salts demonstrated previously unknown templating effects in mechanochemistry and accelerated the formation of topologically specific structures.

As a non-conventional solventless time-efficient synthetic approach, mechanochemistry is turning into a mainstream technique aimed at resolving challenges of sustainable chemical manufacturing and the depletion of fossil energy resources. The number of patents related to mechanochemistry has dramatically increased since late 1990s.⁴⁴ Recently, the solvent usage in several pharmaceutical processes, for example the manufacture of Viagra (sildenafil), has been successfully reduced by introducing mechanochemical techniques.⁴⁵⁻⁴⁶ Mechanochemical research in various fields such as inorganic materials, pharmaceutical cocrystals, organic synthesis, porous MOFs, discrete metal complexes, and supramolecular synthesis has strongly supported the growing applications of mechanochemistry and at the same time contributed new solventless perspectives to the improvements of these research fields.

Table 1.1. Differentiation of mechanochemical and solution-based methods by η (unit: $\mu\text{L}/\text{mg}$). Reproduced from reference [42].

Synthetic methods	Neat grinding	LAG	Slurring	Solution synthesis
H	0	0-2	2-12	>12

As mentioned previously, synthesis of inorganic materials is the first established area in mechanochemistry. Mechanical alloying, the process of combining alloys and elements to produce a homogenous alloy, is dominant in this field.⁴⁷⁻⁴⁸ With reactants like oxides, sulfides and other minerals, high-energy milling can also be

treated as a top-down route to nano-materials. Nanoparticles and amorphous phases can be produced by the significant reduction of particle size and crystallite during milling.⁴⁹ Mechanical activation of inorganic materials can also be applied in mineral processing, extractive metallurgy, material engineering, or even solid waste treatment.²⁶

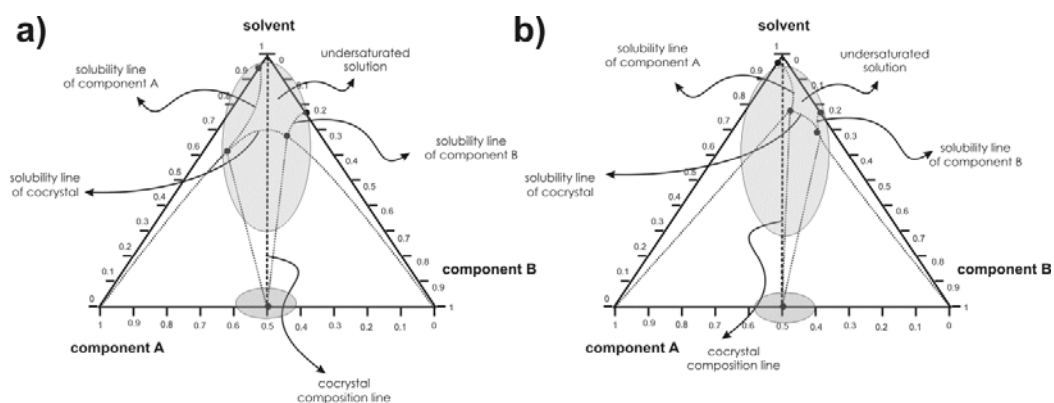


Figure 1.5. Three-component phase diagrams for cocrystal components that are (a) congruently and (b) incongruently soluble in a solvent. The regions of composition corresponding to typical solution-phase and grinding experiments are marked blue and red, respectively. Reproduced from reference [38].

Cocrystals, defined as “multi-component molecular crystals”, are another influential area of mechanochemistry application.⁵⁰ Held by intermolecular interactions like hydrogen bonds, ionic forces, halogen bonds, π - π stacking, Van der Waals force and charge transfer interactions, different molecules can assemble into well-defined crystal structures with new physicochemical properties. In solution-based chemistry, the synthesis of cocrystals is usually hindered by preferential crystallization of the least soluble cocrystal component. (Figure 1.5) By avoiding this limitation, mechanochemistry becomes a better choice for cocrystal synthesis and screening, especially for ternary (*i.e.* three-component) cocrystals. The modular design of pharmaceutical cocrystals, which rests on combining active pharmaceutical ingredients (APIs) with suitable ancillary molecules known as cocrystal formers (or “coformers”), has provided a huge opportunity for the development and application of mechanochemical methods.⁵¹

Derivatization of the crystal lattice of API by cocrystallization can improve pharmaceutical properties like solubility, thermal stability, dissolution rate and compressibility.⁵² The first pharmaceutically relevant cocrystals made by neat grinding were reported independently by Caira and by Etter in 1993.⁵³⁻⁵⁴ As shown in Figure 1.6, hydrogen bonds between donors and acceptors have been stoichiometrically established during grinding. The later work of Rodríguez-Hornedo on cocrystals of the API carbamazepine, conducted by low-temperature grinding (cryogrinding) reveals an intermediate amorphous phase below glass transition temperature (T_g), followed by polymorphic transformations after heating.⁵⁵⁻⁵⁶ Compared to neat grinding, LAG is a more preferred synthetic and screening method for its universality, high efficiency and ability to provide highly crystalline products.⁵⁷ In terms of the assembly of pharmaceutical ternary inclusion compounds shown in Figure 1.7, LAG is more efficient in the incorporation of guest molecules (liquid, solid or gas) at mild conditions than alternative methods.⁵⁸

Besides hydrogen bonding and other weak interactions, mechanochemistry is also potent in constructing metal-ligand coordination bonds,⁵⁹ which makes it an efficient tool for MOMs synthesis. Many discrete metal complexes can be readily formed by grinding simple metal precursors (chlorides, oxides, etc.) with organic ligands.⁶⁰⁻⁶¹ Ligand addition reactions in mechanochemistry can be used to convert inert polymeric species to more tractable molecules. For example, anionic bidentate ligands LL (dithiocarbamates, xanthates and oxalates) have been used to convert inert $[\text{Nb}_2(\text{E}_2)_2\text{Cl}_4]_\infty$ ($\text{E}=\text{S}, \text{Se}$) to $[\text{Nb}_2(\text{E}_2)_2(\text{LL})_4]$ with the elimination of chloride.⁶² Air-sensitive or moisture-sensitive metal complexes and organometallics are perfect targets for inert atmosphere milling techniques. Complexes of main group metals such as magnesium and bismuth with pharmaceutical ligands have also been achieved by LAG and ILAG,^{36,63} illustrating a new perspective to metallodrug research.

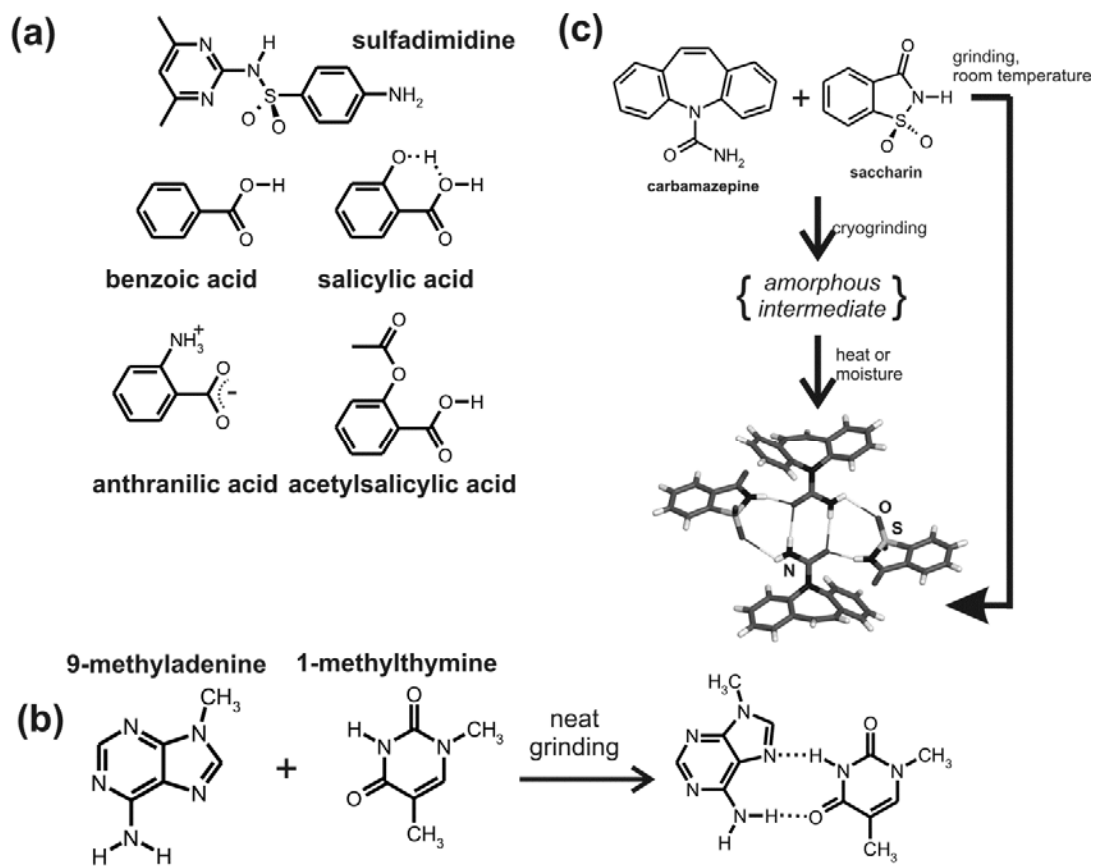


Figure 1.6. (a) Molecules used in mechanochemical synthesis of pharmaceutical cocrystals by Caira et al.; (b) Mechanochemical reaction of 9-methyladenine and 1-methylthymine to form a cocrystal reported by Etter; (c) Mechanochemical cocrystallization by neat grinding of carbamazepine and saccharin involving an amorphous intermediate. Reproduced from reference [44].

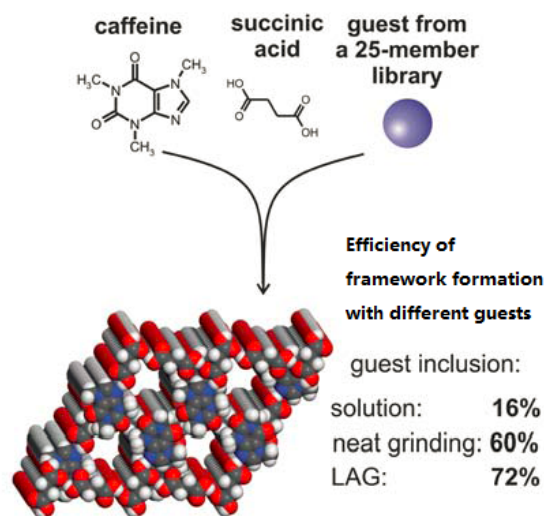


Figure 1.7. Three-component assembly of caffeine, succinic acid and a guest molecule into a ternary inclusion compound based on a two-component hydrogen-bonded host. Reproduced from reference [19].

One of the most intensely researched areas in mechanochemistry over the past decade is the construction of coordination polymers and porous MOFs. In 2001, Bourne *et al.* generated the first mechanochemically synthesized coordination polymer $\text{ZnBr}_2(\text{pyrazine})_2$ by grinding 1D zig-zag polymer $\text{ZnBr}_2(\text{pyrazine})$ with a further equivalent of neutral pyrazine.⁶⁴ Five years later, with the same strategy of adding extra organic ligand to known metal-containing building blocks, Pichon *et al.* ground copper(II) acetate paddlewheel complex with isonicotinic acid and constructed the first mechanochemically synthesized MOF.⁶⁵ (Figure 1.8a) In neat grinding experiments, different grinding conditions lead to different coordination modes⁶⁶ (Figure 1.8b) and the important role of water in mechanochemical reactions has been noticed⁶⁷ (Figure 1.8c). In LAG experiments, different liquid additives result in different structures⁶⁸ (Figure 1.9a) and mechanochemical interconversions of one-, two- and three-dimensional (1D, 2D and 3D, respectively) MOFs have been observed.⁶⁹ (Figure 1.9b) In ILAG experiments, different inorganic salts can specifically lead the same mixture of reactants to different topological products and time-dependent structure transformations has also been reported.⁷⁰ (Figure 1.10) In terms of green

chemistry and up-scale production, mechanochemistry nowadays can stoichiometrically convert inexpensive and inert metal oxides to functional porous MOFs without using bulk solvents and high temperatures.^{68,70} Such synthetic possibilities simplify the screening of functional MOFs and greatly reduce the manufacture cost of MOMs.

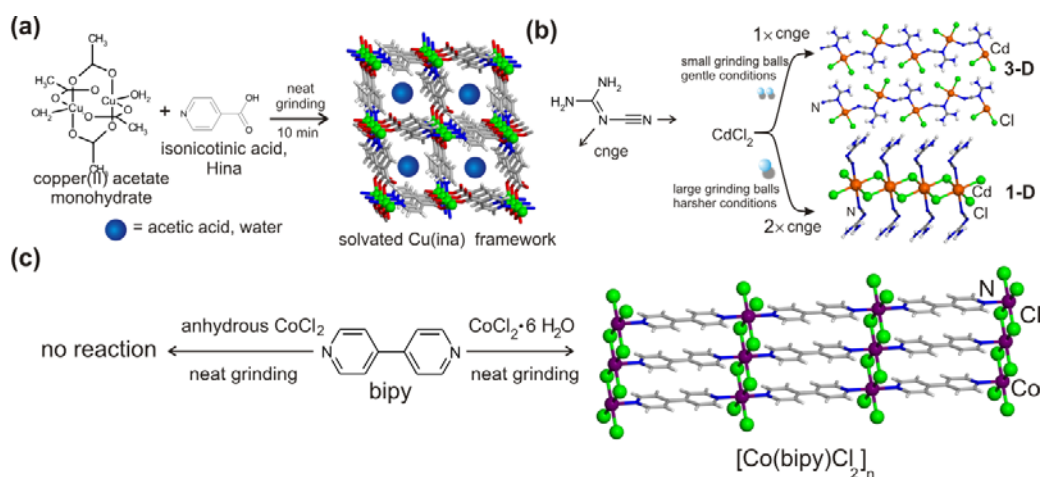


Figure 1.8. (a) The first reported mechanochemical assembly of a porous MOF by neat grinding; (b) The ligand cyanoguanidine (CNGE) with different metal binding sites indicated by arrows and its reactions with CdCl_2 upon neat grinding under various reaction conditions; (c) Difference in mechanochemical reactivity of bipy towards anhydrous CoCl_2 and $\text{CoCl}_2 \cdot 6\text{H}_2\text{O}$. Reproduced from references [44] and [19].

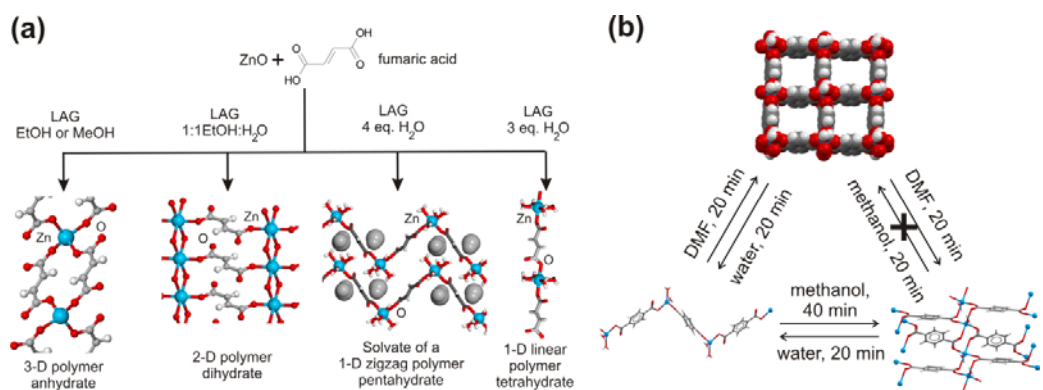


Figure 1.9. (a) The construction of coordination polymers and frameworks from zinc oxide by LAG; (b) Mechanochemical interconversions of 1-D, 2-D and 3-D MOFs by LAG. Reproduced from references [44] and [19].

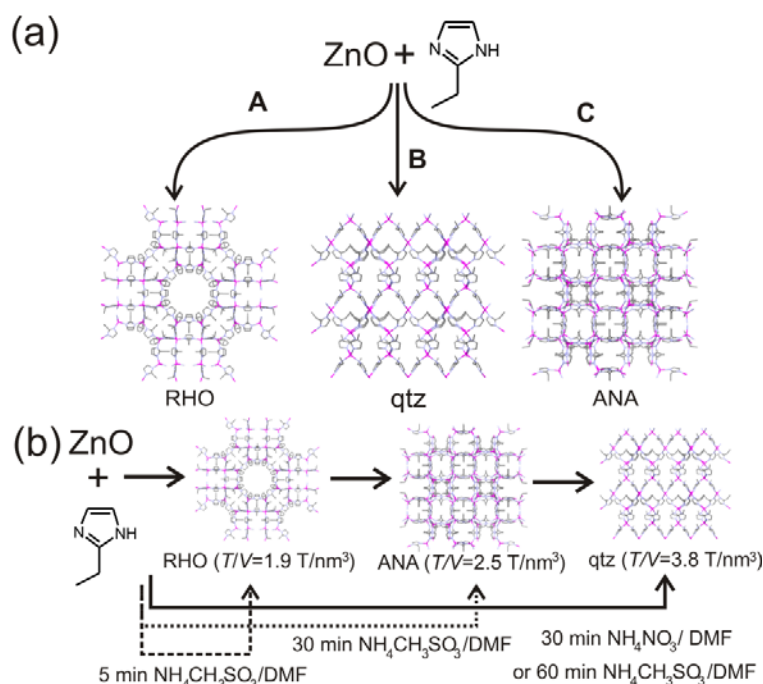


Figure 1.10. (a) Topologically specific mechanochemical synthesis of zeolitic imidazolate frameworks (ZIFs) directly from ZnO and 2-ethylimidazole using ILAG. Pathway A represents ILAG with $(\text{NH}_4)_2\text{SO}_4$; B is ILAG with NH_4NO_3 or $\text{NH}_4\text{CH}_3\text{SO}_3$ in the presence of EtOH and C is ILAG with $\text{NH}_4\text{CH}_3\text{SO}_3$ and DMF or DEF as the liquid phase; (b) time-dependent ZIF transformations under ILAG conditions, T/V is the number of tetrahedral sites (T) per nm^3 . Reproduced from reference [44].

Last but not least, organic synthesis, which is heavily dominated by solution-based methods, has recently become enriched by a number of solvent-free mechanochemical procedures. A major benefit brought about by mechanochemical synthesis is the stoichiometric conversion of organic reactants. In examples such as the Knoevenagel condensation and Wittig reactions,⁷¹⁻⁷² only stoichiometric amounts of reactants were used to achieve 99% (quantitative) yields. In traditional organic synthesis with slightly soluble biological molecules, such as nucleosides and nucleobases, toxic polar aprotic solvents like dimethylformamide or pyridine must be used. However, in mechanochemical synthesis, these solvents can be entirely avoided and a high yield (95%) of the final product obtained.⁷³ In terms of metal-catalyzed organic reactions, the solvent-free ball milling technique with inert atmosphere inside the vial can easily protect air- and

moisture-sensitive catalysts and simplify all procedures of the experiment. Interestingly, the metallic vial can sometimes catalyze the reaction in the absence of catalyst.⁷⁴ (Figure 1.11a) Even the organocatalytic asymmetric reactions and large organic cage syntheses can be conducted mechanochemically.⁷⁵⁻⁷⁶ (Figure 1.11b) Compared to traditional solution synthesis, organic mechanochemistry minimizes the use of hazardous and unpleasant solvents. The energy requirements of mechanosynthesis are even lower than for other non-conventional methods like microwave heating.⁷¹ Solid-state synthetic conditions with new mechanisms also encourage organic chemists to explore reactions thought to be not possible under conventional conditions.⁷⁷

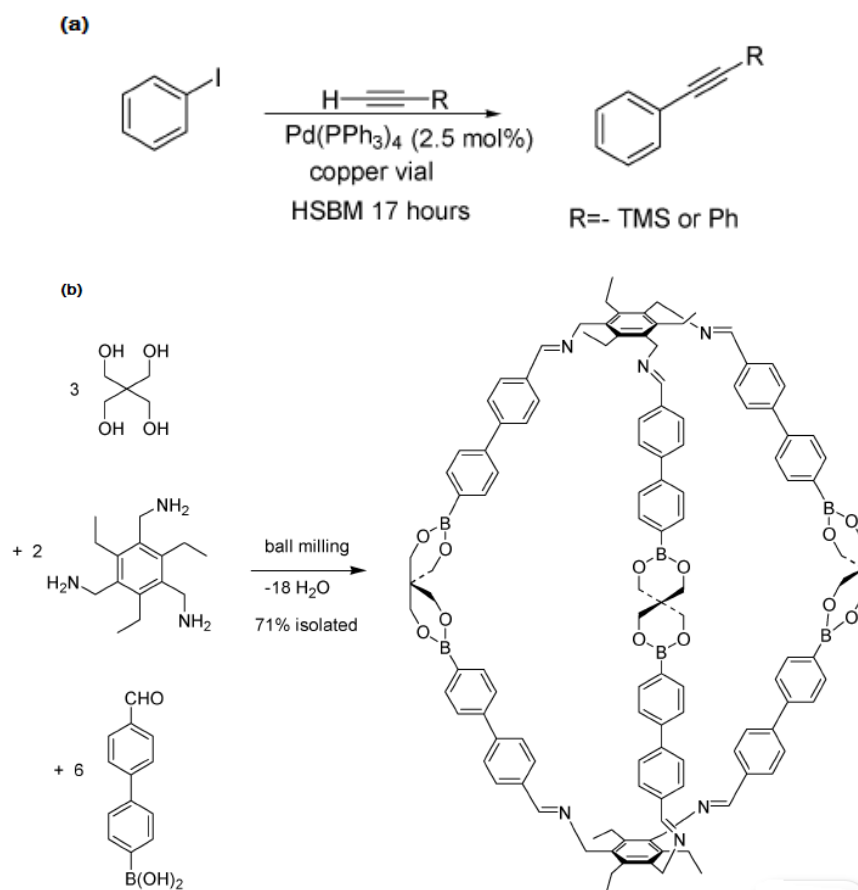


Figure 1.11. (a) Sonogashira reaction using a copper vial as the source of the Cu-cocatalyst; (b) Solventless ball milling synthesis of a large organic cage. Reproduced from reference [44]

1.2. Transformations of inert inorganic substances: mineral neogenesis and accelerated aging

Although the speedy development of mechanochemistry in the past 20 years enables stoichiometric synthesis of MOMs without bulk solvents and high temperature conditions, mechanochemistry still has three “unsustainable” aspects: the cost of high-frequency mills, electricity consumption as well as dusty and noisy working environment. Apparently, compared to traditional synthetic methods these “unsustainable” aspects are not unacceptable, and seem inevitable to a material synthetic approach. However, as Ralph Waldo Emerson said: “Science does not know its debt to imagination”⁷⁸. In the case of searching for a more sustainable synthetic approach than mechanochemistry, our imagination stems from the interface of biology and geology.

In “geological biomineralization” processes, known as mineral neogenesis or mineral weathering, small molecules such as oxalic acid generated by lichens or found as ammonium oxalate in guano, slowly transform inert metal-containing minerals like oxides and sulfides into MOMs.⁷⁹⁻⁸¹ The process may take several years and the resulting MOMs (known as secondary organic minerals) such as Moolooite, Humboldtine and Lindbergite are more tractable for industry use and processing than original oxides or sulfides.⁸²⁻⁸³ Notably, this inconspicuous natural process takes place everyday in a mild and low energy environment. Indeed, the reactants in this process are inexpensive and rarely used in synthetic chemistry due to their low solubilities and high stabilization. For example, the lattice energy of ZnO is 4142 kJ/mol while the lattice energy of Zn(NO₃)₂ (one of the most commonly used sources of zinc in inorganic synthesis) is 2376 kJ/mol.⁸⁴

If this “mineral weathering” process could be accelerated and applied to syntheses of other MOMs, it will have high transformative potential to the current solvent- and energy-intensive metallurgical industry and chemical production. In fact, the principles of “mineral weathering” have been applied in traditional techniques such as the “Dutch process” for production of the pigment (basic lead carbonate)

established since ancient times.⁸⁵ (Figure 1.12) The importance of high humidity and large surface area have been demonstrated, but the process is time-consuming and requires 12 weeks.

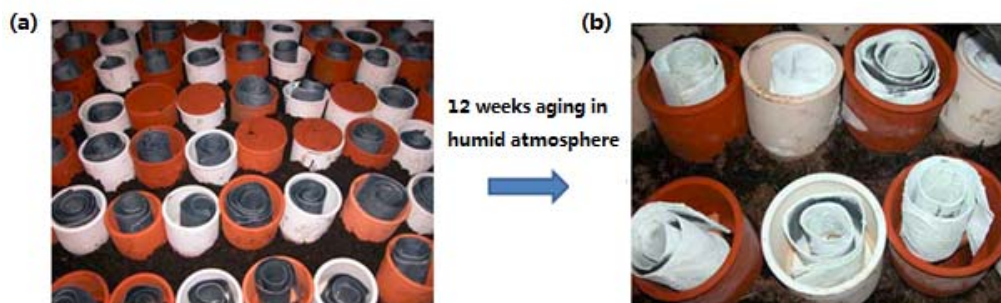


Figure 1.12. (a) Lead plates before processing by the “Dutch method”. (b) The same plates upon conversion to lead white pigment (basic lead carbonate). Source of photos: <http://www.geoffreylaurence.com/leadwhite.html>

In the context of laboratory synthesis, Nakamatsu *et al.* in 2005 reported that certain organic reactions can be efficiently and selectively performed in the solid state in the presence of a small amount of methanol or acetonitrile vapour.⁸⁶ Two years later, a similar phenomenon in cocrystal formation has been described by Braga *et al.* Specifically, exposing a manual mixture of $\text{Fe}(\eta^5\text{-C}_5\text{H}_4\text{-C}_5\text{H}_4\text{N})_2$ and $\text{HOOC}(\text{CH}_2)_5\text{COOH}$ to vapors of different organic liquids led to the formation of different molecular solids. Strongly hydrogen bonding liquids such as methanol, ethanol and water led to the formation of $\text{Fe}(\eta^5\text{-C}_5\text{H}_4\text{-C}_5\text{H}_4\text{N})_2$: $\text{HOOC}(\text{CH}_2)_5\text{COOH} = 1:2$ cocrystal (supramolecular macrocycle). In contrast, less polar liquids yielded the $\text{Fe}(\eta^5\text{-C}_5\text{H}_4\text{-C}_5\text{H}_4\text{N})_2$: $\text{HOOC}(\text{CH}_2)_5\text{COOH} = 1:1$ cocrystal (zig-zag chain). (Figure 1.13) This process was named “vapor digestion” by the authors, who recognized it as an interesting “solvent effect” in a solvent-free reaction.⁸⁷

Solvent vapour	Product obtained	Solvent vapour	Product obtained
CH ₂ Cl ₂	1	CH ₃ OH	2
CHCl ₃	1	EtOH	2
Et ₂ O	1	H ₂ O	2
CH ₃ NO ₂	1	Isopropyl alcohol	2
Ethyl lactate	1		

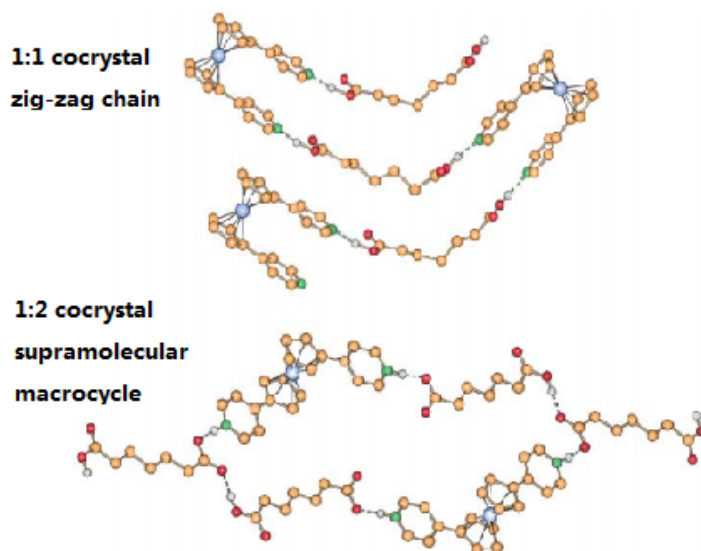


Figure 1.13. Details of solvents used and products obtained in the vapor digestion processes (exposure time = 1 day). Reproduced from reference [87]

In the pharmaceutical field, Byrn *et al.* have conducted systematic research on moisture-induced solid-state conversion of MgO and carboxylic acid-containing pharmaceuticals to magnesium complexes.⁸⁸⁻⁸⁹ In 2012, this moisture-induced solid-state reaction has been named “accelerated aging” and used to synthesize 3D zeolitic imidazolate frameworks (ZIFs) from ZnO and various imidazoles.⁹⁰ Inspired by ILAG, substoichiometric amount of ammonium salt has been added into the static solid mixture as catalyst. However, such process led only to the formation of non-porous ZIFs. In the following work published in 2013, the porous sodalite-topology ZIF-8, its cobalt analogue ZIF-67, and a related zeolite RHO framework have been obtained in up to 5g scale by replacing ammonium catalysts with organic salts.⁹¹ (Figure 1.14) Besides MOMs, similar investigations have also been reported on the amine–aldehyde condensation reactions which

yield imines as products.⁹² As shown in Figure 1.15, the high humidity environment (98% relative humidity) significantly accelerates the reaction and enables a complete conversion has been obtained after 2 days of standing.

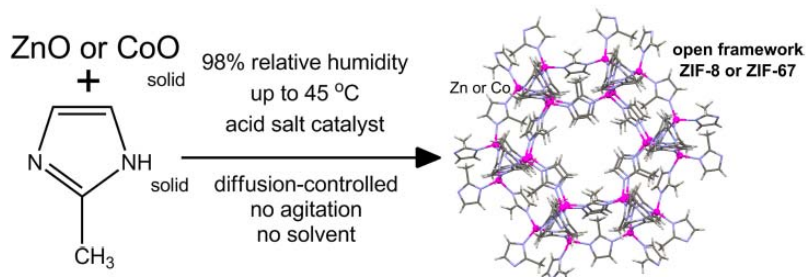


Figure 1.14. Accelerated aging reactions toward to ZIF-8 and ZIF-67 in 5g scale. Reproduced from reference [91].

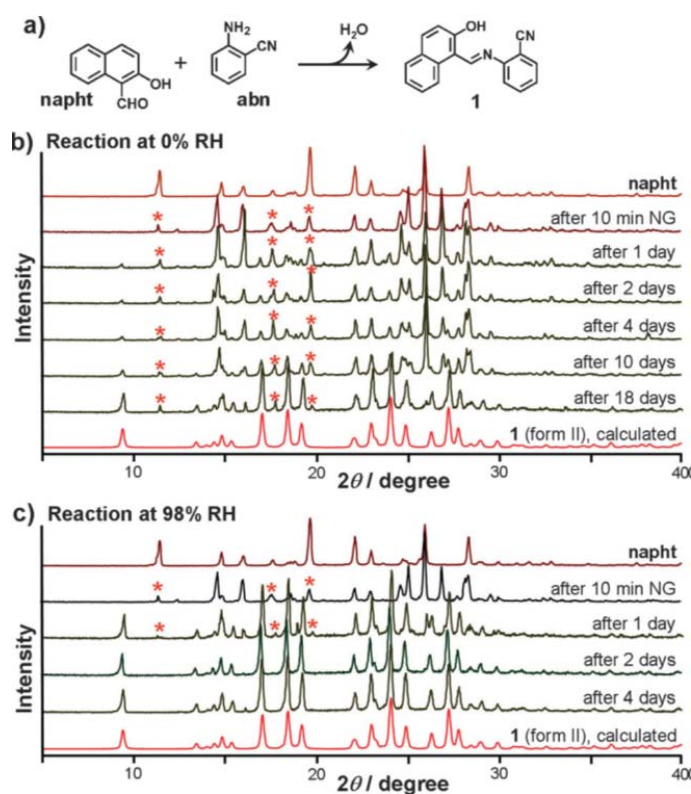


Figure 1.15. a) Reaction scheme of preparation of **1**; b) Relevant calculated and experimental powder X-ray diffraction (PXRD) patterns for reaction at 0% relative humidity (RH); c) and 98% RH. Characteristic reflections for **napht** are indicated by '*'. NG is the abbreviation for neat grinding. Reproduced from reference [92].

By mimicking and accelerating the neogenesis of minerals, accelerated aging can enable stoichiometric solid-state synthesis of MOMs and organic molecules at very mild conditions like room temperature or 45°C (a reasonably achievable temperature in summer). The energy input is even lower than steam cooking which is conducted under 100% relative humidity and boiling point of water. By simply extending the exposing surface, accelerated aging reactions can be easily scaled up for industry use. Besides the energy- and solvent- saving benefits, accelerated aging as a solid state approach can save more operation space than solution based methods and minimize both the risk and the cost of chemical productions.

1.3. Thesis perspective and outline

Although the reactivity and benefits are obvious, accelerated aging as a new synthetic technique has only been demonstrated in isolated cases and a systematic study including kinetic and mechanistic investigations is still rare in the field. This thesis reports the first systematic research of accelerated aging reactions towards MOMs. The reactants were selected across the periodic table including main group metals (Bi, Pb, Mg) and transitional metals (Zn, Cu, Ni, Co, Mn.). In Chapter 2, accelerated aging reactions of different metal oxides with stoichiometric oxalic acid dihydrate have been monitored by solid state techniques at both room temperature and 45°C. The kinetic study shows that besides increasing humidity and temperature, the reactions can also be accelerated by applying a 5min pre-milling of the metal oxides. In some cases, different aging temperatures and mechanical activation can also lead to different polymorphs of the product. Further kinetic research of these aging parameters such as humidity, temperature, time and mechanical activation will be beneficial for extending the aging reactions to more inert mineral feedstocks. In terms of MOF synthesis, synthetic strategies like ionic templating agents in solvothermal synthesis are proved to be transferrable to solid-state aging reactions. In Chapter 2, similar

metal oxides like ZnO and CuO have shown big difference in reactivity towards oxalic acid in the same aging conditions, which enables the solvent-free separation of these minerals and opens an influential possibility for using accelerated aging to simplify our metallurgical process.

In Chapter 3, both mechanochemistry and accelerated aging have been used as solid-state synthetic tools to study water-insoluble bismuth salicylate complexes. The up to 10 grams solid-state synthesis and interconversions of three kinds of bismuth salicylate complexes including bismuth subsalicylate (the API of Pepto-Bismol) have been demonstrated. It is the first time that accelerated aging reactions have been conducted at 95°C and a solid-state equilibrium under aging conditions has been described. Indeed, a series of decorated bismuth oxo-nanoclusters have been obtained by dissolving solid-state synthesized bismuth disalicylate in a variety of organic solvents. These nanosized oxo-clusters may help the investigation of the structure of bismuth subsalicylate and could be considered as potential nano-pharmaceuticals in gastrointestinal and related fields.

Reference

- (1) K. Bowman-James, *Acc. Chem. Res.* **2005**, *38*, 671.
- (2) T. R. Cook, Y-R. Zheng, P. J. Stang, *Chem. Rev.* **2013**, *113*, 734.
- (3) A. K. Cheetham, C. N. R. Rao, R. K. Feller, *Chem. Commun.* **2006**, 4780.
- (4) S. Kitagawa, R. Kitaura, S. Noro, *Angew. Chem. Int. Ed.* **2004**, *43*, 2334.
- (5) D. V. Soldatov, *J. Inclusion Phenom. Macrocyclic Chem.* **2004**, *48*, 3.
- (6) U. Mueller, M. Schubert, F. Teich, H. Puetter, K. Schierle-Arndt and J. Pastré, *J. Mater. Chem.* **2006**, *16*, 626.
- (7) J-R. Li, J. Sculley and H-C, Zhou, *Chem. Rev.* **2013**, *113*, 734.
- (8) J-Y. Lee, O. K. Farha, J. Roberts, K. A. Scheidt, S. T. Nguyen and J. T. Hupp, *Chem. Soc. Rev.* **2009**, *38*, 1450.
- (9) R Chakrabarty, P. S. Mukherjee and P. J. Stang, *Chem. Rev.* **2011**, *111*, 6810.

- (10) R. Banerjee, A. Phan, B. Wang, C. Knobler, H. Furukawa, M. O’Keeffe, O. M. Yaghi, *Science* **2008**, *319*, 939.
- (11) N. Stock, *Microporous Mesoporous Mater.* **2010**, *129*, 287.
- (12) U. Mueller, H. Puetter, M. Hesse, H. Wessel, WO 2005/ 049892.
- (13) S. H. Jung, J.-H. Lee, J.-S. Chang, K. Bull, *Chem. Soc.* **2005**, *26*, 880.
- (14) S. H. Jung, J.-H. Lee, J. W. Yoon, C. Serre, G. Ferey, J.-S. Chang, *Adv. Mater.* **2007**, *19*, 121.
- (15) K. M. L. Taylor-Pashow, J. D. Rocca, Z. Xie, S. Tran, W. Lin, *J. Am. Chem. Soc.* **2009**, *131*, 14261.
- (16) L.-G. Qiu, Z.-Q. Li, Y. Wu, W. Wang, T. Xu, S. Jiang, *Chem. Commun.* **2008**, 3642.
- (17) J. Kim, S.-T. Yang, S. B. Choi, J. Sim, J. Kim, W.-S. Ahn, *J. Mater. Chem.* **2011**, *21*, 3070.
- (18) A. Pichon, A. Lazuen-Garay, S. L. James, *CrystEngComm.* **2006**, *8*, 211.
- (19) T. Friščić, *J. Mater. Chem.* **2010**, *20*, 7599.
- (20) C. Munuera, O. Shekhah, H. Wang, C. Woll, C. Ocal, *Phys. Chem. Chem. Phys.* **2008**, *10*, 7257.
- (21) A. Demessence, P. Horcajada, C. Serre, C. Boissiere, D. Grosso, C. Sanchez, G. Ferey, *Chem. Commun.* **2009**, 7149.
- (22) G. Gritzner, G. Kreysa, *Pure Appl. Chem.* **1993**, *65*, 1009.
- (23) P. T. Anastas, J. C. Warner, *Green Chemistry: Theory and Practice*, Oxford University Press, New York, **1998**, 30.
- (24) N. Stock, S. Biswas, *Chem. Rev.* **2012**, *112*, 933.
- (25) W. Ostwald, *Die chemische Literatur und die Organisation der Wissenschaft, in Handbuch der allgemeinen Chemie*, ed. W. Ostwald and C. Drucker, Akademische Verlagsgesellschaft. m. b. H. Leipzig, **1919**, pp. 70 and 77.
- (26) P. Baláž, *Mechanochemistry in Nanoscience and Minerals Engineering*, Springer-Verlag Berlin Heidelberg. (**2008**)
- (27) A. J. Lynch and C. A. Rowland, *The History of Grinding*, Society of Mining, Metallurgy and Exploration, Inc. Littleton, CO. (**2005**)

- (28) L. Takacs, *J. Mineral Met. Mater. Soc.* **2000**, 52, 12.
- (29) J. S. Benjamin, in *New Materials by Mechanical Alloying Techniques*, ed. E. Artz and L. Schultz, DGM Informationsgesellschaft, Oberursel, **1989**, 3.
- (30) K. Beneke, *Die Kolloidwissenschaftler Peter Adolf Thiessen, Gerhart Jander, Robert Havemann, Hanz Witzmann und ihre Zeit*, Verlag Reinhard Knof, Nehnten, (**2000**)
- (31) V. V. Boldyrev, *Russ. Chem. Rev.*, **2006**, 75, 17.
- (32) L. Takacs, *Chem. Soc. Rev.* **2013**, DOI: 10.1039/C2CS35442J.
- (33) W. Spring, *Bull. Soc. Chim. Fr.* **1885**, 44, 166.
- (34) M. C. Lea, *Am. J. Sci.* **1893**, 46, 413.
- (35) L. Takacs, *Journal of Materials Science*, **2004**, 4987.
- (36) V. André, *et al. Angew. Chem. Int. Ed.* **2011**, 50, 1.
- (37) P. A. Thiessen, K. Meyer and G. Heinicke, *Grundlagen der Tribochemie*, Akademie Verlag, Berlin, (**1967**)
- (38) T. Friščić and W. Jones, *Cryst. Growth Des.* **2009**, 9, 1621.
- (39) D. Braga, S. L. Giaffreda, F. Grepioni, A. Pettersen, L. Maini, M. Curzi and M. Polito, *Dalton Trans.* **2006**, 1249.
- (40) A. V. Trask, W. D. S. Motherwell and W. Jones, *Chem. Commun.* **2004**, 890.
- (41) S. Karki, L. Fábíán, T. Friščić and W. Jones, *Org. Lett.* **2007**, 9, 3133.
- (42) T. Friščić, S. L. Childs, S. A. A. Rizvi and W. Jones, *CrystEngComm*, **2009**, 11, 418.
- (43) T. Friščić, D. G. Reid, I. Halasz, R. S. Stein, R. E. Dinnebier, M. J. Duer *Angew. Chem. Int. Ed.* **2010**, 49, 712.
- (44) S. L. James, *et al. Chem. Soc. Rev.*, **2012**, 41, 413.
- (45) C. P. F. Marcos, A. P. Martins, D. N. Moreira, L. Buriol, P. Machado, *Chem. Rev.* **2009**, 109, 4140.
- (46) P. J. G. Dunn, S. Galvin and K. Hettenbach, *Green Chem.* **2004**, 6, 43.
- (47) M. Karolus, E. Jartych and D. Oleszak, *Acta Phys. Pol. A*, **2002**, 102, 253.
- (48) L. M. Kubalova, V. I. Fadeeva, I. A. Sviridov and S. A. Fedotov, *J. Alloys Compd.* **2009**, 483, 86.

- (49) P. Solsona, S. Doppiu, T. Spassov, S. Surinach and M. D. Baro, *J. Alloys Compd.* **2004**, *381*, 66.
- (50) D. Braga, L. Maini and F. Grepioni, *Chem. Soc. Rev.* **2013**, DOI: 10.1039/C3CS60014A.
- (51) N. Shan and M. J. Zaworotko, *Drug Discov. Today*, **2008**, *13*, 440.
- (52) D. P. McNamara, S. L. Childs, J. Giordano, A. Iarriccio, J. Cassidy, M. S. Shet, R. Mannion, E. O'Donnell and A. Park, *Pharm. Res.* **2006**, *23*, 1888.
- (53) M. R. Caira, L. R. Nassimbeni and A. F. Wildervanck, *J. Chem. Soc. Perkin. Trans. 2*, **1995**, 2213.
- (54) M. C. Etter, S. M. Reutzel and C. G. Choo, *J. Am. Chem. Soc.* **1993**, *115*, 4411.
- (55) A. Jayasankar, D. J. Good and N. Rodriguez-Hornedo, *Mol. Pharmaceutics*, **2007**, *4*, 360.
- (56) C. Maheshwari, A. Jayasankar, N. A. Khan, G. E. Amidon and N. Rodriguez-Hornedo, *CrystEngComm*, **2009**, *11*, 493.
- (57) K. L. Nguyen, T. Friščić, G. M. Day, L. F. Gladden and W. Jones, *Nat. Mater.* **2007**, *6*, 206.
- (58) T. Friščić, A. V. Trask, W. Jones and W. D. S. Motherwell, *Angew. Chem. Int. Ed.* **2006**, *45*, 7546.
- (59) A. Lazuen-Garay, A. Pichon and S. L. James, *Chem. Soc. Rev.* **2007**, *36*, 846.
- (60) P. J. Nichols, C. L. Raston and J. W. Steed, *Chem. Commun.* **2001**, 1062.
- (61) T. Ohshita, D. Nakajima, A. Tsukamoto, N. Tsuchiya, T. Isobe, M. Senna, N. Yoshioka and H. Inoue, *Ann. Chim. Sci. Mater.* **2002**, *27*, 91.
- (62) M. N. Sokolov, A. L. Gushchin, S. V. Tkachev, D. Y. Naumov, P. Nunez, P. Gili, J. G. Platas and V. P. Fedin, *Inorg. Chim. Acta*, **2005**, *358*, 2371.
- (63) E. H. H. Chow, F. C. Strobridge, and T. Friščić, *Chem. Commun.* **2010**, *46*, 6368.
- (64) S. A. Bourne, M. Kilkenny and L. R. Nassimbeni, *J. Chem. Soc. Dalton Trans.* **2001**, 1176.

- (65) A. Pichon, A. Lazuen-Garay and S. L. James, *CrystEngComm*, **2006**, *8*, 211.
- (66) V. Štrukil, L. Fábíán, D. G. Reid, M. J. Duer, G. J. Jackson, M. Eckert-Maksić and T. Frišćić, *Chem. Commun.* **2010**, *46*, 9191.
- (67) C. J. Adams, H. M. Colquhoun, P. C. Crawford, M. Lusi and A. G. Orpen, *Angew. Chem., Int. Ed.* **2007**, *46*, 1124.
- (68) T. Frišćić and L. Fábíán, *CrystEngComm*, **2009**, *11*, 743.
- (69) W. Yuan, T. Frišćić, D. Apperley and S. L. James, *Angew. Chem. Int. Ed.* **2010**, *49*, 3916.
- (70) P. J. Beldon, L. Fábíán, R. S. Stein, A. Thirumurugan, A. K. Cheetham, and T. Frišćić, *Angew. Chem. Int. Ed.* **2010**, *49*, 9640.
- (71) G. Kaupp, M. R. Naimi-Jamal and J. Schmeyers, *Tetrahedron*, **2003**, *59*, 3753.
- (72) V. P. Balema, J. W. Wiench, M. Pruski and V. K. Pecharsky, *J. Am. Chem. Soc.* **2002**, *124*, 6244.
- (73) N. Giri, C. Bowen, J. S. Vyle and S. L. James, *Green Chem.* **2008**, *10*, 627.
- (74) D. A. Fulmer, W. C. Shearouse, S. T. Medonza and J. Mack, *Green Chem.* **2009**, *11*, 1821.
- (75) T. Rantanen, I. Schiffers and C. Bolm, *Org. Process Res. Dev.* **2007**, *11*, 592.
- (76) B. Içli, N. Christinat, J. Tonnemann, C. Schuttler, R. Scopelliti and K. Severin, *J. Am. Chem. Soc.* **2009**, *131*, 3154.
- (77) J. J. Gilman, *Science*, **1996**, *274*, 65.
- (78) R. W. Emerson, *Poetry and Imagination*, (1872)
- (79) O. W. Purvis, C. Halls, *Lichenologist* **1996**, *28*, 571.
- (80) G. M. Gadd, Y. J. Rhee, K. Stephenson, Z. Wei, *Env. Microb. Rep.* **2012**, *4*, 270.
- (81) P. Adamo, P. Violante, *Appl. Clay Sci.* **2000**, *16*, 229.
- (82) T. Echigo, M. Kimata, *Canadian Mineralogist* **2010**, *48*, 1329.
- (83) R. M. Clarke, I. R. Williams, *Miner. Mag.* **1986**, *50*, 295.

- (84) D. R. Lide, *et al. Handbook of Chemistry and Physics - 88th Edition*, (2008)
- (85) R. J. Gettens, H. Kühn, W. T. Chase, *Studies in Conservation*, **1967**, **12**, 125.
- (86) S. Nakamatsu, S. Toyota, W. Jones, F. Toda, *Chem. Commun.* **2005**, 3808.
- (87) D. Braga, *et al. CrystEngComm*, **2007**, **9**, 879.
- (88) X. Chen, J. G. Stowell, K. R. Morris and S. R. Byrn, *J. Pharm. Biomed. Anal.* **2010**, **51**, 866.
- (89) S. R. Byrn, W. Xu and A. W. Newman, *Adv. Drug Delivery Rev.* **2001**, **48**, 115.
- (90) M. J. Cliffe, *et al. Chem. Sci.* **2012**, **3**, 2495.
- (91) C. Mottillo, *et al. Green Chem.*, **2013**, **15**, 2121.
- (92) D. Cinčič, I. Brekalo and B. Kaitner, *Chem. Commun.* **2012**, **48**, 11683.

Chapter 2: Mimicking mineral neogenesis for the clean synthesis of metal-organic materials from mineral feedstocks: coordination polymers, MOFs and metal oxide separation*

** This paper (Green Chem, 2013, Advanced Article, DOI: 10.1039/C3GC41370E, <http://pubs.rsc.org/en/content/articlepdf/2013/gc/c3gc41370e>) was reproduced by permission of The Royal Society of Chemistry. It is coauthored by Robin S. Stein and Tomislav Friščić. The acknowledgement forms from co-authors are separately provided. The text below is the verbatim copy of the published paper.*

2.1 Abstract

We present a systematic study of a mild approach for the activation of metal oxides, involving reactivity and self-assembly in the solid state, which enables their solvent-free chemical separation and direct solvent-free and low-energy conversion into coordination polymers and open metal-organic frameworks (MOFs). The approach is inspired by geological biomineralization processes known as mineral weathering, in which long-term exposure of oxide or sulfide minerals to molecules of biological origin leads to their conversion into simple coordination polymers. This proof-of-principle study shows how mineral neogenesis can be mimicked in the laboratory to provide coordination polymers directly from metal oxides without a significant input of either thermal or mechanical energy, or solvents. We show that such "aging" is accelerated by increased humidity, mild temperature increase and/or brief mechanical activation, enabling the transformation of a variety of high-melting (800°C-2800°C) transition (Mn^{II} , Co^{II} , Ni^{II} , Cu^{II} , Zn) and main group (Mg , Pb^{II}) oxides at or near room temperature. Accelerated aging reactions are readily scaled to at least 10 grams and can be templated for the synthesis of two-dimensional and three-dimensional anionic frameworks of Zn, Ni(II) and Co(II). Finally, we demonstrate how this biomineralization-inspired approach allows an unprecedented

opportunity for solvent-free chemical segregation of base metals, such as Cu, Zn and Pb, in their oxide form under mild conditions.

2.2 Introduction

The development of environmentally-friendly and sustainable synthesis is one of the central tasks of modern science and technology.¹ As the number of potential applications for coordination polymers and metal-organic frameworks (MOFs) grows to include hydrogen or methane storage, carbon sequestration, catalysis and even light-harvesting,² it becomes of critical importance to address how such materials can be manufactured in a clean, sustainable and scalable manner from slightly soluble natural feedstocks (*e.g.* mineral concentrates consisting of metal oxides or sulfides), rather than from conventionally used derivatives that are also toxic or corrosive³ (metal nitrates, chlorides, acetates).³ While the clean synthesis of coordination polymers and MOFs⁴ from soluble salts has been explored using sonochemistry,⁵ microwave synthesis,⁶ electrochemistry,⁷ mechanochemical synthesis⁸ and near-critical water conditions,⁹ we are interested in developing mild processes for directly transforming metal minerals or mineral concentrates into metal-organic materials. Metal oxides are recognized by researchers¹⁰ and industry³ as the ideal feedstock for inexpensive and clean synthesis. Also, the development of mild methods for metal oxide and sulfide transformation and separation offers benefits in mineral processing and refining industries by improving energy- and solvent-intensive pyro- and hydrometallurgical protocols.¹¹

However, metal oxides are rarely used as starting materials due to their low solubility, high melting points and a generally inert nature resulting from high lattice energies (typically 4-6 MJ mol⁻¹). Transformations of metal oxides into metal-organic materials are energy-intensive, *e.g.* conversion of ZnO or CoO into porous frameworks *via* melt reactions can last several days at 120°C-160°C.¹² Consequently, activation of metal oxides near room temperature and without bulk solvents is a challenge that must be met by non-conventional approaches.

Although mechanochemistry⁸ has recently enabled the conversion of main group or d^{10} -oxides (ZnO, MgO, CdO, Bi₂O₃)¹³⁻¹⁸ into MOFs and pharmaceuticals, it has been less efficient with transition metal oxides. Instead, mechanosyntheses of coordination compounds of Co, Ni or Cu use acetates, carbonates or halides.^{19,20} We are exploring a novel and potentially general methodology for converting transition metal oxides into metal-organic derivatives, which minimizes energy use and completely avoids organic solvents. Microorganisms, such as lichens, can transform inert minerals into metal-organic derivatives by excreting small molecules known as lichen acids.²¹ Such geological biomineralization, known as mineral weathering (neogenesis), is essential to the formation of secondary metal-organic minerals (also called "organic" minerals).²² For example, oxalic acid (H₂ox) generated by lichens or found as ammonium oxalate in guano can slowly convert copper ores into the copper(II) oxalate mineral Moolooite.^{23,24} Other examples of mineral weathering by microorganisms include readily extractable deposits of metal oxalate biominerals Humboldtine, Lindbergite⁵ and Glushinskite, based on iron(II), manganese(II) and magnesium respectively.²⁵ *In vitro* experiments have also demonstrated the biomineralization of lead oxalate by *Aspergillus niger* or the lichen *Diploschistes muscorum*. Most oxalate biominerals are one-dimensional (1-D) coordination polymers (Figure 2.1a). We are exploring whether such weathering of metal oxides can be reproduced in the synthetic chemical laboratory and adapted into an environmentally-friendly path to metal-organic materials. In this study we establish: (1) conditions that enable the conversion of laboratory-scale samples of metal oxides into metal-organic materials; (2) the applicability of this methodology to a variety of metals and scale-up to multi-gram amounts; and (3) the use of templating to drive such biomineralization-inspired reactivity for the synthesis of open MOFs.

Our work is influenced by that of Byrn and co-workers, who noted the complexation of MgO upon aging with pharmaceuticals.²⁶ Our first report of "accelerated aging" demonstrated conversion of ZnO into zeolitic MOFs by aging with imidazole ligands at high humidity with an acid catalyst.²⁷ For this

systematic study we selected metal oxalates as models for three principal reasons. Firstly, oxalates are of obvious geological and biomimetic significance as the dominant type of "organic" secondary minerals and are of continuous interest as functional (magnetic, proton conducting) materials.²⁸ Secondly, oxalic acid is more acidic than previously explored imidazoles and, consequently, might not require acid catalysts. Finally, there is a large variety of framework topologies accessible through oxalate ligands, providing an opportunity to explore how reactions of geological weathering can be adapted for the synthesis of open MOFs.²⁹ Most significant metal oxalate topologies are the neutral 1-D polymer $M\text{ox}\cdot 2\text{H}_2\text{O}$ in monoclinic α -dihydrates of divalent metal oxalates (Figure 2.1a),³⁰ and the open two-dimensional (2-D) honeycomb and three-dimensional (3-D) topologies³¹ of the anion $M_2(\text{ox})_3^{2-}$ (M=divalent metal ion) (Figure 2.1b). Formation of 2-D or 3-D $M_2(\text{ox})_3^{2-}$ MOFs is controlled by templates and depends on the configuration of the octahedral $M(\text{ox})_3$ subunits.³² Formation of oxalate MOFs in solution was extensively studied^{28,29} and particularly important for this study is the work by Cheetham³³ and Rao³⁴ on template solvothermal synthesis using organoammonium cations.

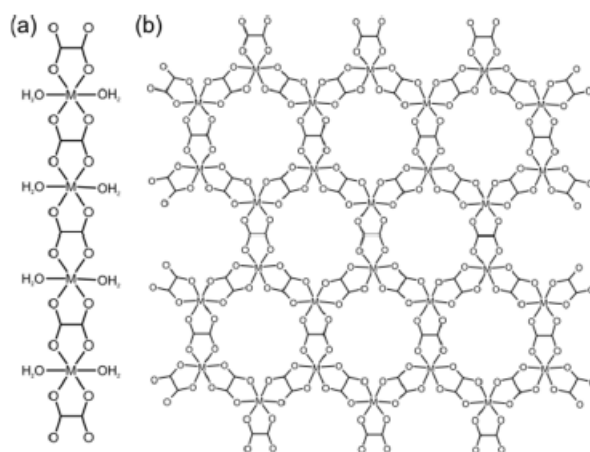


Figure 2.1. Metal oxalate topologies: a) 1-D; b) 2-D and 3-D

2.3 Experimental Section

All chemicals were reagent grade and obtained from commercial sources. MgO, MnO, CoO, NiO, ZnO and PbO were of 99%+ purity, obtained from Sigma-

Aldrich, CuO was 96% purity from Riedel-de Haën and H₂ox·2H₂O was 99%+ purity from American Chemicals Ltd. ZnO and MgO have been calcined (400°C) to remove potential hydroxide and carbonate impurities, and were kept in a dry desiccator over P₄O₁₀. Aging reactions were conducted either in a walk-in incubator held at 45°C, or at room temperature without particular means of temperature control. The samples aged at high humidity were kept at 98% RH atmosphere established in a Secador® cabinet equilibrated with saturated aqueous K₂SO₄. In a typical experiment, 1 mmol of a metal oxide was mixed with 1 mmol of H₂ox·2H₂O and gently ground in an agate mortar and pestle for 30 seconds. The solid mixture was placed in a 20 mL open vial and stored under controlled conditions. All reactions were investigated by powder X-ray diffraction (PXRD), thermogravimetric analysis (TGA), Fouriertransform infrared attenuated total reflection (FTIR-ATR) spectroscopy and, in some cases, UV-Vis reflectance, solid-state NMR (SSNMR) and differential scanning calorimetry (DSC). Thermogravimetric analysis was conducted on TA Instruments Q500 Thermogravimetric System with a Pt pan under dynamic atmosphere of N₂ or air with 40ml/min balance flow and 60ml/min purge flow. The upper temperature limit ranged from 500°C to 800°C with a heating rate of 10°C/min. DSC was performed on a TA Instruments Q2000 Differential Scanning Calorimeter using a standard aluminum pan of 40 µL. Nitrogen flow was set at 50 mL/min and the upper temperature limit ranged from 105°C to 150°C with a constant heating rate of 10°C/min. UV-Vis reflectance was measured on Ocean Optics Jaz-Combo spectrometer using LS-1 Tungsten Halogen Light Source 80 (360-2000 nm), 0.4 mm fiber optic reflection R400-Angle-UV probe with RPH-1 reflection probe holder and WS-1 PTFE diffuse reflection standard, from 400 nm to 800 nm. SSNMR spectra of [pa]₂[Zn₂(ox)₃]·3H₂O were recorded on a standard-bore Bruker Avance III spectrometer operating at 500.13 MHz using a Bruker 4 mm double-resonance probe spinning at 5 kHz. Spectra were referenced using the chemical shift of the carbonyl carbon of glycine at 174.1 ppm with respect to TMS. SSNMR spectra of [pn][Zn₂(ox)₃]·3H₂O were recorded on a 400 MHz Varian VNMRS spectrometer operating at 100.52MHz using a T3HX probe,

7.5mm zirconia rotor spinning at 4.5 kHz. Spectrum was acquired in 1000 scans using crosspolarization for 1 ms and 2 s recycle delay. PXRD patterns were collected in 2 θ -range 3 $^{\circ}$ -60 $^{\circ}$ on Bruker D2 Phaser diffractometer using a CuK α ($\lambda=1.54$ Å) source. Data were analyzed using Panalytical X'pert HighScore Plus.

2.4 Results and Discussion

As an initial foray into investigating the aging reactivity of oxalic acid and metal oxides, we prepared a stoichiometric 1:1 mixture of oxalic acid dihydrate (H₂ox·2H₂O) with ZnO. The mixture was prepared by gently grinding the reactants in a mortar and pestle for 30 seconds. Care was taken to avoid harsh grinding that could cause uncontrolled mechanical activation and, therefore, difficulties in reproducibility. Powder X-ray diffraction (PXRD) after 24 hours aging at room temperature (18 $^{\circ}$ C-22 $^{\circ}$ C) and high (98%) relative humidity (RH) revealed the formation of a new product (Figure 2.2).

Comparison with PXRD patterns simulated for known zinc oxalate structures revealed the product was the 1-D coordination polymer zinc oxalate dihydrate (Znox·2H₂O, CSD QQQBOD04) in the α -type structure.³⁵ In one week, the conversion to the 1-D coordination polymer was complete. The composition Znox·2H₂O was confirmed by thermogravimetric analysis (TGA) in air, which provided the assessment of weight fractions for included water (measured: 18.5%, calculated: 19.0%) and ZnO residue (measured: 42.9%, calculated: 43.0%). Aging reactivity was further improved by storing the sample in 98% RH conditions at the mild temperature of 45 $^{\circ}$ C. Under such conditions, complete formation of α -Znox·2H₂O, as established by PXRD (Supplementary Fig. S1), was achieved in 5 days. When scaled to 10 grams, the reaction completed in seven days (Figure 2.12). Transformation was also detected by Fouriertransform infrared attenuated total reflection (FTIR-ATR) spectroscopy (Figure 2.3), specifically by the disappearance of O-H stretching bands of H₂ox·2H₂O at 3380 cm⁻¹ and 3470 cm⁻¹ and the appearance of the O-H stretching bands of Znox·2H₂O at 3350 cm⁻¹, as

well as the appearance of characteristic $\text{ZnOx}\cdot 2\text{H}_2\text{O}$ bands at 1604 cm^{-1} , 1356 cm^{-1} and 1311 cm^{-1} .

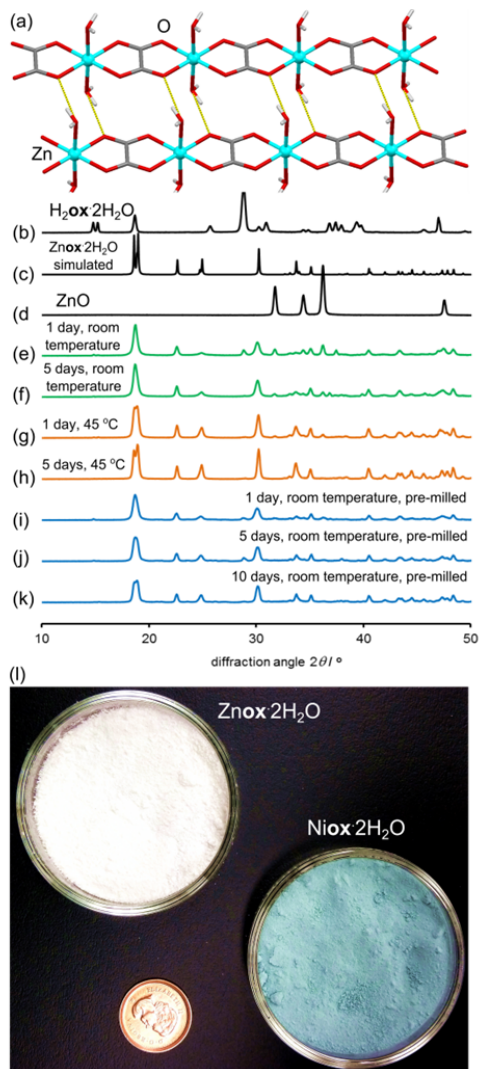


Figure 2.2. (a) Two coordination polymer chains connected by hydrogen bonds in $\text{ZnOx}\cdot 2\text{H}_2\text{O}$ (CSD QQQBOD04). PXRD patterns for aging reactions of ZnO and $\text{H}_2\text{Ox}\cdot 2\text{H}_2\text{O}$ at 98% RH: (b) $\text{H}_2\text{Ox}\cdot 2\text{H}_2\text{O}$; (c) simulated for $\text{ZnOx}\cdot 2\text{H}_2\text{O}$; (d) ZnO ; (e) 1 day at room temperature; (f) 5 days at room temperature; (g) 1 day at $45\text{ }^\circ\text{C}$; (h) 5 days at $45\text{ }^\circ\text{C}$; (i) 1 day at room temperature with pre-milling; (j) 5 days at room temperature with pre-milling and (k) 10 days at room temperature with pre-milling. (l) Completed 10 gram aging syntheses of $\text{ZnOx}\cdot 2\text{H}_2\text{O}$ and $\text{NiOx}\cdot 2\text{H}_2\text{O}$.

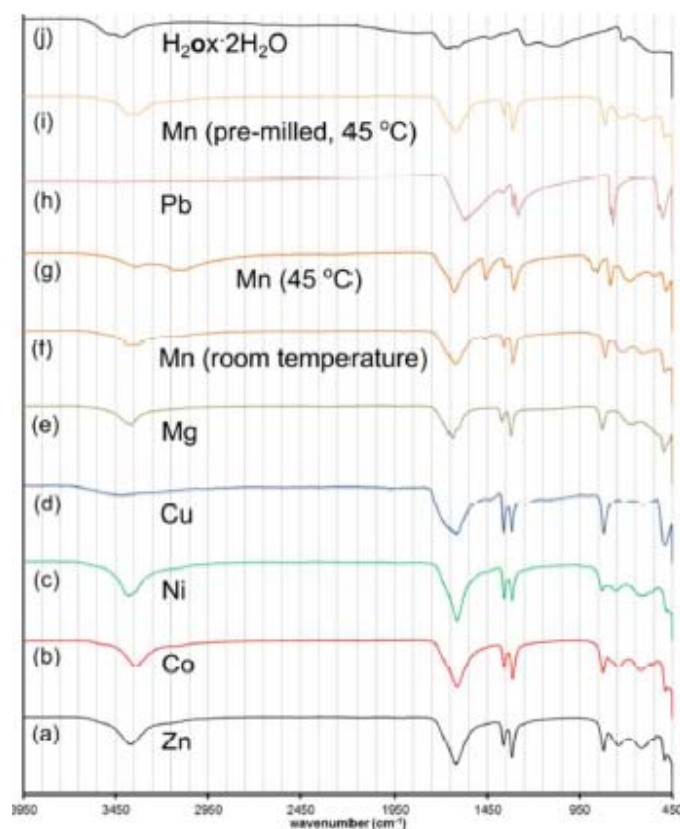


Figure 2.3. FTIR-ATR spectra of final products of aging reactions for: (a) ZnO, 5 days at 45 °C; (b) CoO, 7 days at 45 °C; (c) NiO, 7 days at 45 °C; (d) CuO, 16 days at 45 °C; (e) MgO, 9 days at 45 °C; (f) MnO, 16 days at room temperature; (g) MnO, 16 days at 45 °C; (h) PbO, 14 days at 45 °C and (i) MnO, aging of a pre-milled sample for 1 day at 45 °C. Spectrum of $\text{H}_2\text{ox}\cdot 2\text{H}_2\text{O}$ is given under (j).

2.4.1 Structure templating

After establishing that oxalic acid reacts with ZnO to form the close packed $\text{ZnOx}\cdot 2\text{H}_2\text{O}$, a templated synthesis of open structures was attempted. Rao and Cheetham have established that solvothermal syntheses of metal oxalates can be directed towards the formation of open MOFs by organoammonium templates.³⁶⁻³⁸ The design to introduce structure templating into aging reactivity involved mixtures of ZnO, $\text{H}_2\text{ox}\cdot 2\text{H}_2\text{O}$ and either 1,3-propanediammonium oxalate [**pn**][**ox**] or propylammonium oxalate [**pa**]₂[**ox**] in the respective stoichiometric ratio 2:2:1.

Such templated aging reactions were expected to yield known materials $[\mathbf{pn}][\text{Zn}_2(\mathbf{ox})_3] \cdot 3\text{H}_2\text{O}$ ³⁷ and $[\mathbf{pa}]_2[\text{Zn}_2(\mathbf{ox})_3] \cdot 3\text{H}_2\text{O}$,³⁶ based on the 2-D and 3-D forms of the $[\text{Zn}_2(\mathbf{ox})_3]^{2-}$ anionic framework, respectively (Figure 2.4a).

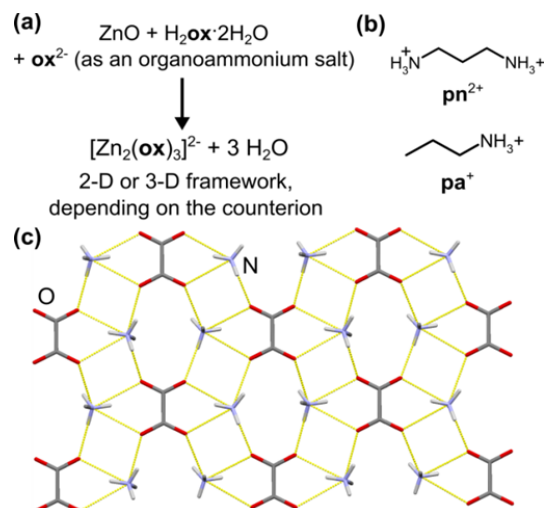


Figure 2.4. (a) Planned synthesis of open anionic 2-D and 3-D zinc oxalate frameworks; (b) templates \mathbf{pn}^{2+} and \mathbf{pa}^+ and (c) a hydrogen-bonded layer in the crystal of $(\mathbf{pa})_2 \cdot (\mathbf{ox})$, with propyl chains omitted for clarity.

The synthesis of $[\mathbf{pn}][\mathbf{ox}]$ and $[\mathbf{pa}]_2[\mathbf{ox}]$ provided a minor challenge. Presence of water readily induced the formation of hydrogen oxalate hydrate salts $[\mathbf{pa}][\mathbf{Hox}] \cdot \text{H}_2\text{O}$ (CSD QIGCOY, QIGCOY01)³⁶ and $[\mathbf{pn}][\mathbf{Hox}]_2 \cdot 2\text{H}_2\text{O}$ (CSD PEPQEG, PEPQEG01).³⁸ Hydrogenoxalates are not suitable for planned templating experiments, due to the inadequate ratio of cationic organoammonium templates and oxalate building blocks. The synthesis of $[\mathbf{pn}][\mathbf{ox}]$ and $[\mathbf{pa}]_2[\mathbf{ox}]$ was devised by reacting anhydrous oxalic acid (obtained by drying $\text{H}_2\mathbf{ox} \cdot 2\text{H}_2\text{O}$ overnight at 125 °C) with the amine in methanol. In ethanol, the product contained a significant fraction of the hydrated hydrogenoxalate. The anhydrous nature of the material from methanol was confirmed by TGA. The structure and composition of $[\mathbf{pn}]_2[\mathbf{ox}]$ were also confirmed by single crystal X-ray diffraction (crystallographic data given in Supplementary Material, Section 1). The structure consists of sheets of \mathbf{pa}^+ and \mathbf{ox}^{2-} held by $\text{N}^+ \cdots \text{O}^-$ hydrogen bonds (Figure 2.4c).

After 5 days at room temperature and 98% RH, PXRD analysis (Figure 2.5a,b) of the mixture of ZnO, $\text{H}_2\text{ox}\cdot 2\text{H}_2\text{O}$ and $[\text{pn}][\text{ox}]$ in 2:2:1 ratio revealed the presence of $\text{Znox}\cdot 2\text{H}_2\text{O}$, but also X-ray reflections consistent with the expected honeycomb topology $[\text{pn}][\text{Zn}_2(\text{ox})_3]\cdot 3\text{H}_2\text{O}$ (Figure 2.6a). Aging for a total of 16 days led to the complete disappearance of reflections of ZnO reactant and the $\text{Znox}\cdot 2\text{H}_2\text{O}$ intermediate, and the diffraction pattern displayed an excellent fit to that expected for the pn^{2+} salt of the $\text{Zn}_2(\text{ox})_3^{2-}$ framework. Since $\text{Znox}\cdot 2\text{H}_2\text{O}$ was an intermediate in the assembly of $[\text{pn}][\text{Zn}_2(\text{ox})_3]\cdot 3\text{H}_2\text{O}$, a room-temperature aging reaction of $[\text{pn}][\text{ox}]$ with $\text{Znox}\cdot 2\text{H}_2\text{O}$ was attempted. After five days, the reaction mixture fully converted into $[\text{pn}][\text{Zn}_2(\text{ox})_3]\cdot 3\text{H}_2\text{O}$. Quantitative conversion was evident from PXRD (Figure 2.5c,d) and TGA.

Aging of a mixture of $(\text{pa})_2(\text{ox})$, H_2ox and ZnO at room temperature and 98% RH was explored next. After five days PXRD (Figure 2.5e,f) and TGA indicated complete conversion to the expected 3-D framework $[\text{pa}]_2[\text{Zn}_2(\text{ox})_3]\cdot 3\text{H}_2\text{O}$ (CSD SEYQIW, Figure 2.6a).³⁶

Cross-polarization magic angle spinning ^{13}C solid-state NMR (SSNMR, see Supplementary Material, Section 5) was consistent with the product being $[\text{pa}]_2[\text{Zn}_2(\text{ox})_3]\cdot 3\text{H}_2\text{O}$, displaying the signals of ox^{2-} and pa^+ . The ^1H - ^{13}C HETCOR and ^1H - ^1H INADEQUATE experiments enabled tentative assignment of the ^1H SSNMR spectra of $[\text{pa}]_2[\text{Zn}_2(\text{ox})_3]\cdot 3\text{H}_2\text{O}$, but with multiple signals expected from partially disordered water molecules unresolved. The HETCOR spectrum was consistent with the reported structure in which the framework interacts mostly with the methyl and ammonium moieties of the pa^+ . The ^{13}C SSNMR spectrum of $[\text{pn}][\text{Zn}_2(\text{ox})_3]\cdot 3\text{H}_2\text{O}$ was also consistent with the published structure. Difference between $\text{Znox}\cdot 2\text{H}_2\text{O}$, $[\text{pn}][\text{Zn}_2(\text{ox})_3]\cdot 3\text{H}_2\text{O}$ and $[\text{pa}]_2[\text{Zn}_2(\text{ox})_3]\cdot 3\text{H}_2\text{O}$ was also evident using FTIR-ATR (Supplementary Fig. S13).

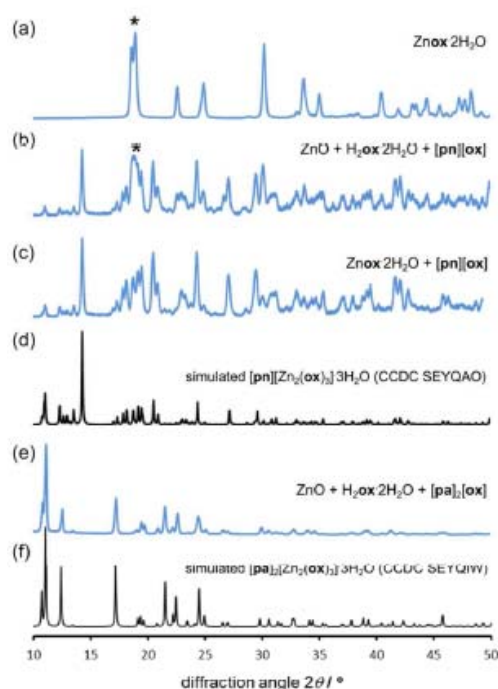


Figure 2.5. PXRD patterns for templated aging syntheses of zinc oxalate MOFs: (a) $\text{Zn ox} \cdot 2\text{H}_2\text{O}$; (b) ZnO , $\text{H}_2\text{ ox} \cdot 2\text{H}_2\text{O}$ and $[\text{pn}][\text{ox}]$ in ratio 2:2:1 after 5 days; (c) $\text{Zn ox} \cdot 2\text{H}_2\text{O}$ and $[\text{pn}][\text{ox}]$ in ratio 2:1 after 5 days; (d) simulated for 2-D MOF $[\text{pn}][\text{Zn}_2(\text{ox})_3] \cdot 3\text{H}_2\text{O}$ (SEYQAO); (e) ZnO , $\text{H}_2\text{ ox} \cdot 2\text{H}_2\text{O}$ and $[\text{pa}]_2[\text{ox}]$ in ratio 2:2:1 after 5 days and (f) simulated for 3-D MOF $[\text{pa}]_2[\text{Zn}_2(\text{ox})_3] \cdot 3\text{H}_2\text{O}$ (SEYQIW). Reactions were done at room temperature, 98% RH. Characteristic reflection of $\text{Zn ox} \cdot 2\text{H}_2\text{O}$ is marked with '*'.

2.4.2 Reactivity of other metal oxides, product hydration state

The reactivity of other metal oxides with oxalic acid was also explored in 98% RH, at room temperature and at 45°C. PXRD analysis revealed the complete conversion of the metal oxide into a metal oxalate structure for all investigated oxides, specifically MgO (Figure 2.7a,b), MnO (Figure 2.7c-g), NiO and CoO (Figure 2.7h-j), CuO (Figure 2.7k,l) and PbO (Figure 2.7n-p). Table 2.1 lists the times required for the reflections of the metal oxide to disappear from the PXRD pattern of the reaction mixture (Figure 2.7, Supplementary Figs. S2-S7), demonstrating that aging reactions are applicable to a variety of metal oxides.

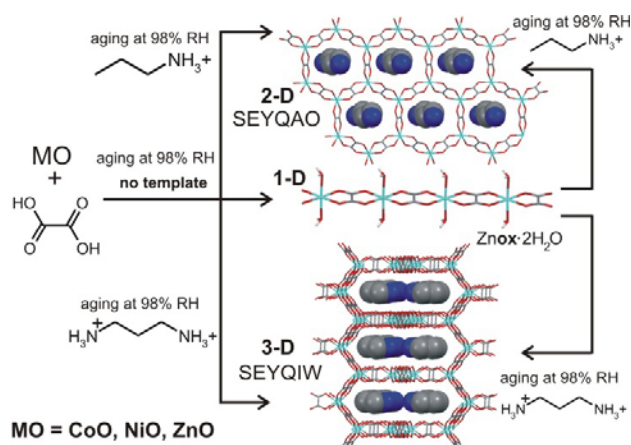


Figure 2.6. Aging reactivity of ZnO, CoO and NiO towards $\text{H}_2\text{Ox} \cdot 2\text{H}_2\text{O}$ with and without organoammonium templates.

The reactions could also be observed by FTIR-5 ATR spectroscopy (Supplementary Figs. S8-S12). The results in Table 2.1 demonstrate the ability to transform metal oxides at mild conditions of temperature, despite their very high melting points. This is relevant in comparison to mechanochemistry, as analogous milling transformations of CoO, NiO, MnO or PbO into metal-organic derivatives have not yet been reported.⁸ The composition of the products was elucidated by the similarity of the PXRD patterns to those simulated for published structures (Figure 2.7, Supplementary Figs. S2-S7).

Table 2.1. Time (in days) for the disappearance of X-ray reflections of the metal oxide (with given melting points) in PXRD patterns of mixtures^a with $\text{H}_2\text{Ox} \cdot 2\text{H}_2\text{O}$ exposed to 98% RH under different conditions.

Oxide (melting point/ $^{\circ}\text{C}$)	RT ^b	Reaction time (days)	
		45 $^{\circ}\text{C}$	RT ^b with pre-milling ^c
MgO (2852)	>9	9 ^d	5 ^d
MnO (1945)	>16	9 ^d	1 ^d
NiO (1955)	>25	3 ^d	>10
CuO (1201)	>25	16	10 ^{e,f}
ZnO (1975)	>5	3 ^d	5 ^d
PbO (888)	>30	9 ^d	>10

a) Reactions were conducted using 2 mmol of the oxide and 2 mmol of $\text{H}_2\text{Ox}\cdot 2\text{H}_2\text{O}$; b) room temperature; c) milling was conducted for 5 minutes in a 10 mL stainless steel jar; d) PXRD pattern displayed no reflections of $\text{H}_2\text{Ox}\cdot 2\text{H}_2\text{O}$ or the metal oxide; e) very weak reflections of $\text{H}_2\text{Ox}\cdot 2\text{H}_2\text{O}$ were observable in the PXRD pattern; f) identical result was obtained at 45°C and 98% RH after 1 day.

Product composition, indicating complete conversion, was corroborated by TGA (Supplementary Figs. S15-S28). Notably, NiO demonstrated similar level of reactivity as ZnO, with complete transformation to $\text{NiOx}\cdot 2\text{H}_2\text{O}$ ³⁹ (isostructural to monoclinic $\text{ZnOx}\cdot 2\text{H}_2\text{O}$) taking place within three days at 98% RH and 45°C. The structural resemblance of $\text{NiOx}\cdot 2\text{H}_2\text{O}$ to the zinc-based polymer was also evident from the similarity of the FTIR-ATR spectra (Figure 2.3). Similar to ZnO, the synthesis of $\text{NiOx}\cdot 2\text{H}_2\text{O}$ was also readily scaled to 10 grams (Figure 2.12). The slowest reaction was with CuO, for which the oxide was no longer observable by PXRD after 16 days aging at 98% RH and 45°C. The product was partially hydrated copper(II) oxalate²³ with traces of $\text{H}_2\text{Ox}\cdot 2\text{H}_2\text{O}$ evident in the PXRD pattern, explained by the technical (96%) purity of CuO. Product was analyzed as $\text{CuOx}\cdot 0.5\text{H}_2\text{O}$, consistent with previous investigations.⁴⁰ Like the oxides listed in Table 2.1, CoO also readily (in six days) converted to a pink material isostructural to $\text{NiOx}\cdot 2\text{H}_2\text{O}$ and $\text{ZnOx}\cdot 2\text{H}_2\text{O}$.

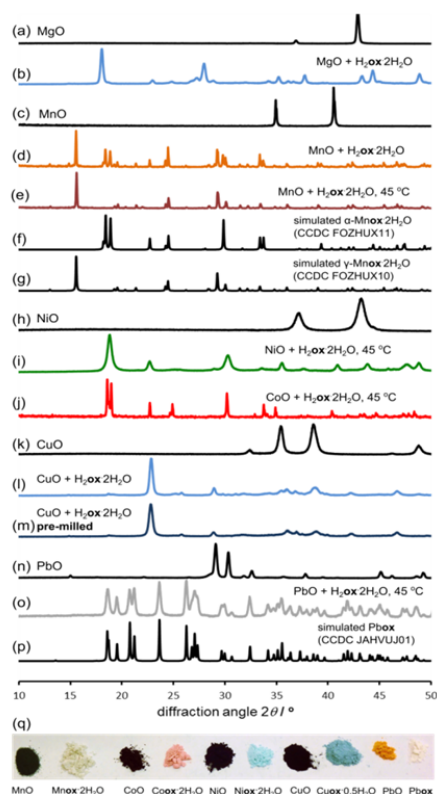


Figure 2.7. PXRD patterns for selected reactions at 98% RH: (a) MgO; (b) $\text{MgOx}\cdot 2\text{H}_2\text{O}$ (5 days, 45°C); (c) MnO; (d) $\text{MnOx}\cdot 2\text{H}_2\text{O}$ (pre-milled MnO, 45 1 day, room temperature); (e) $\text{MnOx}\cdot 2\text{H}_2\text{O}$ (9 days, 45°C); (f) simulated $\alpha\text{-MnOx}\cdot 2\text{H}_2\text{O}$ (FOZHUX11); (g) simulated $\gamma\text{-MnOx}\cdot 2\text{H}_2\text{O}$ (FOZHUX10); (h) NiO; (i) $\text{NiOx}\cdot 2\text{H}_2\text{O}$ (3 days, 45°C); (j) $\text{CoOx}\cdot 2\text{H}_2\text{O}$ (6 days, room temperature, data collected using $\text{CuK}\alpha$ radiation and energydiscriminating LynxEye detector); (k) CuO; (l) $\text{CuOx}\cdot 0.5\text{H}_2\text{O}$ (16 days, 45°C); (m) $\text{CuOx}\cdot 0.5\text{H}_2\text{O}$ (pre-milled CuO, 10 days, room temperature); (n) PbO; (o) PbOx (pre-milled PbO, 9 days, 45°C); (p) simulated PbOx (JAHVUJ). (q) Visual comparison of samples of oxide reactants with corresponding oxalate products obtained by aging (98%RH, 45°C).

Diffraction pattern of the product exhibited X-ray fluorescence which impaired the detection of trace CoO or $\text{H}_2\text{Ox}\cdot 2\text{H}_2\text{O}$ using $\text{CuK}\alpha$ radiation. TGA was consistent with the formula $\text{CoOx}\cdot 2\text{H}_2\text{O}$,⁴¹ and the FTIR-ATR spectrum was almost identical to those of isostructural Ni(II) and Zn oxalates (Figure 2.3). Subsequent PXRD studies using $\text{CoK}\alpha$ and $\text{CuK}\alpha$ radiation after energy

discrimination by the LynxEye detector (Figure 2.7j) confirmed the absence of reactants and formation of $\text{Coox} \cdot 2\text{H}_2\text{O}$. Although all transformations in Table 2.1 are conducted under 98% relative humidity, the obtained products are not the highest known hydrates of corresponding metal oxalates. MnO yielded $\text{Mnox} \cdot 2\text{H}_2\text{O}$ although a higher hydrate⁴² is also known. Similarly, PbO yields the anhydrous Pbox (CSD JAHVUJ, JAHVUJ01, Figure 2.7n-p)⁴³ although a dihydrate is also known.⁴⁴ Copper produced the well-known partially hydrated structure, despite the existence of a trihydrate.⁴⁵ For Pb(II) and Cu(II) the low content of water in products was also evidenced by FTIR-ATR spectra lacking the broad water absorption band at 3400 cm^{-1} (Figure 2.3, also Supplementary Figs. S10,S12). These observations differentiate the herein reported reactions from previously studied cases of solid-gas reactivity⁴⁶ where the reacting vapor becomes a structural component of the metal-organic product.

2.4.3 Formation of open structures based on Co and Ni

Structure templating by organoammonium cations to form MOFs was also applicable to aging reactions of CoO and NiO. Aging of either NiO or CoO (Figure 2.8a-j) with oxalic acid dihydrate and $[\text{pn}][\text{ox}]$ and $[\text{pa}]_2[\text{ox}]$ yielded materials that were, as established by PXRD, iso-structural to the hydrated 2-D and 3-D MOFs $[\text{pn}][\text{Zn}_2(\text{ox})_3]$ and $[\text{pa}]_2[\text{Zn}_2(\text{ox})_3]$, respectively. Framework formation was also corroborated by FTIR-ATR spectroscopy which demonstrated a high degree of mutual similarity in the set of three (Zn-, Co- and Ni-based) materials obtained in the presence of $[\text{pn}][\text{ox}]$ (Supplementary Fig. S13), and also in the set of analogous three materials obtained with $[\text{pa}]_2[\text{ox}]$ template. TGA was consistent with compositions $[\text{pn}][\text{Co}_2(\text{ox})_3] \cdot 3\text{H}_2\text{O}$, $[\text{pn}][\text{Ni}_2(\text{ox})_3] \cdot 3\text{H}_2\text{O}$ and $[\text{pn}][\text{Zn}_2(\text{ox})_3] \cdot 3\text{H}_2\text{O}$. For pa^+ -templated systems, the analyses indicated formulas $[\text{pa}]_2[\text{Co}_2(\text{ox})_3] \cdot 4\text{H}_2\text{O}$, $[\text{pa}]_2[\text{Ni}_2(\text{ox})_3] \cdot 4\text{H}_2\text{O}$ and $[\text{pa}]_2[\text{Zn}_2(\text{ox})_3] \cdot 3\text{H}_2\text{O}$. It is not clear if additional water in these systems is a result of impurity, or a real difference in stoichiometric composition with respect to zinc MOFs. Formation of MOFs was also investigated by solid-state UV/Vis reflectance spectroscopy (Figure 2.9). Reflectance measurements showed a notable difference between the

absorption spectra of either $\text{Coox} \cdot 2\text{H}_2\text{O}$ or $\text{Niox} \cdot 2\text{H}_2\text{O}$ and products of templated reactions. In contrast, the reflectance spectra of pa^+ - and pn^{2+} -templated materials were similar to each other. Such observations are consistent with the difference in the coordination environment of the metal in the 1-D hydrated metal oxalate polymer, where the cation is octahedrally coordinated by two oxalate and two water ligands, and MOFs in which the metal is octahedrally surrounded by three oxalates.

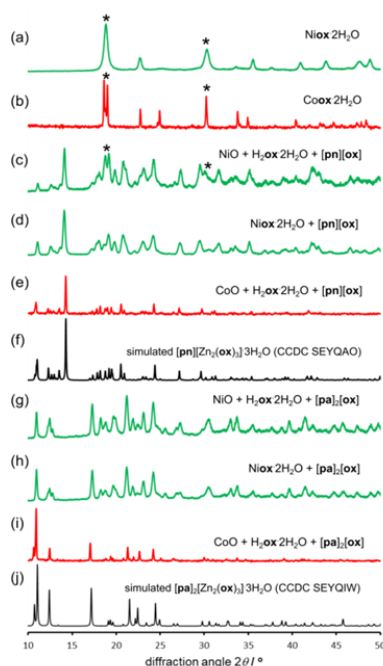


Figure 2.8. Selected PXRD patterns for templated aging synthesis of Ni(II) (green) and Co(II) (red) oxalate MOFs: (a) $\text{Niox} \cdot 2\text{H}_2\text{O}$; (b) $\text{Coox} \cdot 2\text{H}_2\text{O}$; (c) NiO, $\text{H}_2\text{ox} \cdot 2\text{H}_2\text{O}$ and $[\text{pn}][\text{ox}]$ in ratio 2:2:1 after 5 days; (d) $\text{Niox} \cdot 2\text{H}_2\text{O}$ and $[\text{pn}][\text{ox}]$ in ratio 2:1 after 5 days; (e) CoO, $\text{H}_2\text{ox} \cdot 2\text{H}_2\text{O}$ and $[\text{pn}][\text{ox}]$ in ratio 2:2:1 after 5 days; (f) simulated 2-D MOF $[\text{pn}][\text{Zn}_2(\text{ox})_3] \cdot 3\text{H}_2\text{O}$ (SEYQAO); (g) NiO, $\text{H}_2\text{ox} \cdot 2\text{H}_2\text{O}$ and $[\text{pa}]_2[\text{ox}]$ in ratio 2:2:1 after 5 days; (h) $\text{Niox} \cdot 2\text{H}_2\text{O}$ and $[\text{pa}]_2[\text{ox}]$ in ratio 2:1 after 5 days; (i) CoO, $\text{H}_2\text{ox} \cdot 2\text{H}_2\text{O}$ and $[\text{pa}]_2[\text{ox}]$ in ratio 2:2:1 after 5 days; (j) simulated 3-D MOF $[\text{pa}]_2[\text{Zn}_2(\text{ox})_3] \cdot 3\text{H}_2\text{O}$ (SEYQIW). Reactions were done at room temperature, 98% RH. Patterns of cobalt samples were recorded using $\text{CuK}\alpha$ radiation and an energy-discriminating detector. Characteristic reflections of $\text{Niox} \cdot 2\text{H}_2\text{O}$, $\text{Coox} \cdot 2\text{H}_2\text{O}$ are marked with '*'

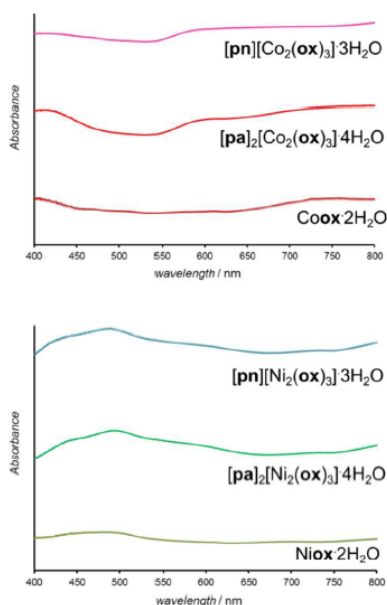


Figure 2.9. Solid-state reflectance UV-Vis spectra of cobalt(II) (top) and nickel(II) (bottom) oxalate dihydrates obtained by aging reactions.

2.4.4 Effect of temperature

For all oxides, except MnO, switching from room temperature to 45°C only increased the reaction rate without changing the product. However, PXRD measurements using CuK α radiation (Supplementary Fig. S6) showed that MnO produced the α -polymorph of Mn $\text{ox}\cdot 2\text{H}_2\text{O}$ by aging at room temperature and only the reportedly more stable γ -form at 45°C. The α -form is structurally similar the other metal oxalate dihydrates (CSD FOZHUX11). In the γ -form inorganic connectivity between octahedrally coordinated Mn $^{2+}$ ions is established by μ^3 -bridging oxalate oxygen atoms (Figure 2.10a). The difference in polymorphic composition was also observable using FTIR-ATR (Figure 2.10). For example, the O-H stretching bands in the α -form are located in a narrow region between 3300 cm^{-1} and 3360 cm^{-1} , while the γ -form exhibits two broad maxima at 3090 cm^{-1} and 3320 cm^{-1} . The earlier solution-based study⁴⁷ indicated the α -polymorph is metastable with respect to the γ -form. Therefore, the temperature-dependent change in polymorphic composition of the aging product suggests the formation of a kinetic product at lower temperatures. The formation of the thermodynamically stable form at 45°C can be explained by higher mobility of

molecules at a higher temperature. Subsequent PXRD study of the aged samples using a CoK α X-ray source (Figure 2.10b-g), to avoid the X-ray fluorescence of manganese-based samples, indicated the presence of the γ -form also in the room temperature product. As the CuK α -based PXRD and FTIR-ATR measurements were all performed without delay and are mutually consistent, we explain the γ -form detected in the PXRD patterns obtained using CoK α radiation as a result of a spontaneous room-temperature transformation during sample transport and storage.

Indeed, the transformation of the α -polymorph to the γ -form in moist air was noted by Huizing *et al.*⁴⁷ and traces of the γ -polymorph are visible in the samples of the α -form after 16 days at room temperature and 98% RH. The $\alpha \rightarrow \gamma$ transformation is not thermally reversible, since heating of the α -form did not result in a structural transformation, shown by DSC.

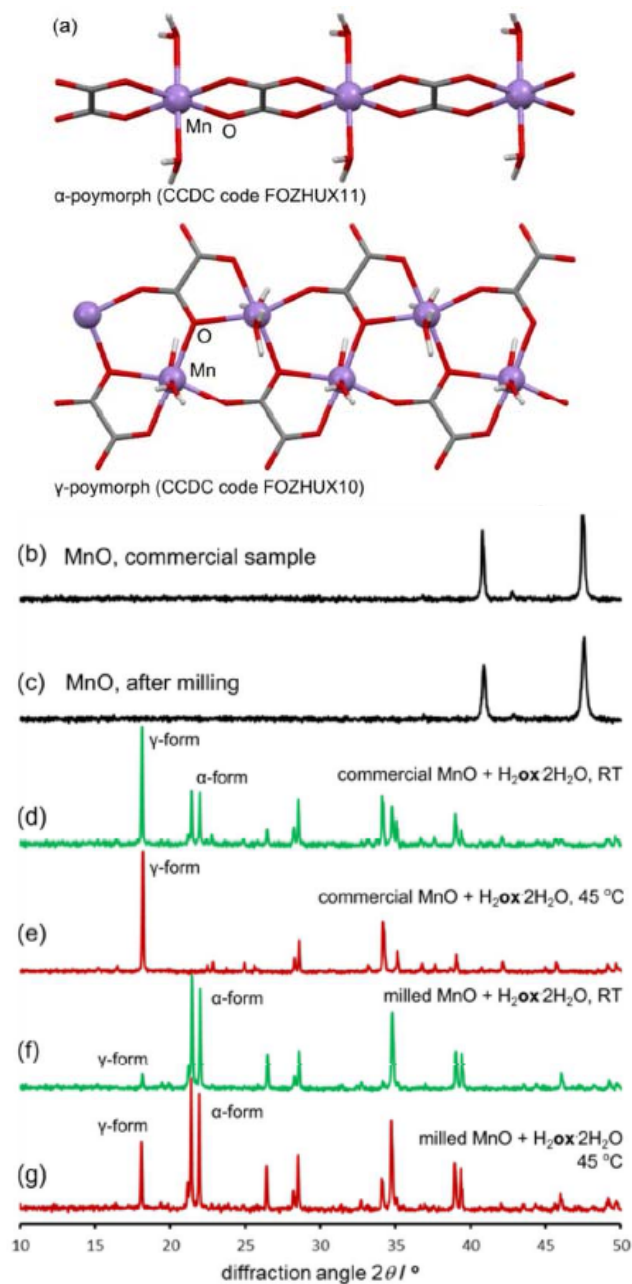


Figure 2.10. (a) Crystal structures of α - (top) and γ -MnO_x·2H₂O (bottom). PXRD patterns collected using CoK α radiation: (b) MnO; (c) MnO after 5min milling; (d) reaction of MnO and H₂ox·2H₂O, room temperature, 98% RH; (e) reaction of MnO and H₂ox·2H₂O, 45°C, 98% RH; (f) reaction of pre-milled MnO and H₂ox·2H₂O, room temperature, 98% RH; (g) reaction of pre-milled MnO and H₂ox·2H₂O, 45°C, 98% RH. Full set of PXRD patterns is given in the Supplementary Material.

2.4.5 Activation by milling: enabling room temperature reactivity

Although the ability to conduct aging reactions in the absence of solvent and at mildly elevated temperature represents a considerable improvement over solution-based processes, the energy benefit can be reduced for long reaction times. Consequently, we explored means to further accelerate the reactions by mechanically activating the reaction mixture by brief ball milling. Initial milling (Retsch MM400 mill operating at 30Hz) of the reaction mixture for 5 minutes enabled most aging reactions to be completed at room temperature, eliminating the need for thermal treatment.⁴⁸ The exception was the reaction of CuO that displayed traces of $\text{H}_2\text{Ox}\cdot 2\text{H}_2\text{O}$ even after 10 days. Most notable was the effect of milling on reactions of MnO, which completely converted to $\text{MnOx}\cdot 2\text{H}_2\text{O}$ in one day (Figure 2.10f,g; Figure 2.11). The product was the metastable $\alpha\text{-MnOx}\cdot 2\text{H}_2\text{O}$ with minor amount of the γ -form. Reaction acceleration was also achieved by pre-milling only MnO, and we speculate the success of pre-milling is due to introducing defects in the oxide structure.⁴⁹ If the milled mixture of MnO and $\text{H}_2\text{Ox}\cdot 2\text{H}_2\text{O}$ was left to age at 45°C and 98% RH the product was a mixture of the α - and γ -forms, indicating that pre-milling of reactants facilitates the kinetic formation of the metastable form, whereas increased temperature favors the thermodynamically stable one.

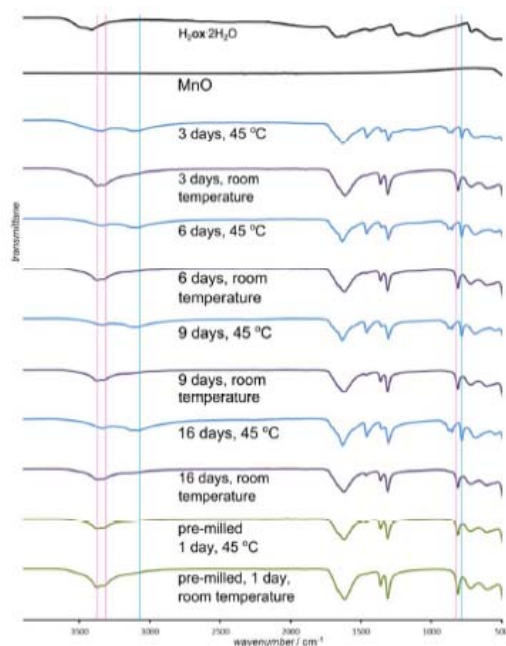


Figure 2.11. Selected FTIR-ATR spectra for the reaction of MnO and $\text{H}_2\text{Ox}\cdot 2\text{H}_2\text{O}$. Characteristic bands are labeled for α - (red line) and γ -forms (blue line) of $\text{MnOx}\cdot 2\text{H}_2\text{O}$.

2.4.6 Selective transformation of metal oxides in a mixture

That different metal oxides underwent aging reactions with oxalic acid at different rates implies the possibility of solvent-free segregation of metal oxide mixtures. A potential benefit of such selectivity in aging reactions would be the transformation of one of the metal oxides into a low density metal oxalate, allowing for its separation from the mixture using gravity, rather than aggressive dissolution reagents. A competitive aging experiment was conducted with a 1:1 stoichiometric mixture of CuO, the slowest reacting metal oxide in our study, with ZnO, one of the most reactive oxides in the study. The mixture contained only one equivalent of $\text{H}_2\text{Ox}\cdot 2\text{H}_2\text{O}$. After five days aging at 45°C and 98% RH the initially black reaction mixture (5 grams) turned to gray. PXRD analysis indicated that the mixture underwent spontaneous and solvent-free chemical separation of zinc from copper by selective conversion of ZnO into $\text{ZnOx}\cdot 2\text{H}_2\text{O}$ (Equation 1):



PXRD revealed the formation of a crystalline material isostructural to $\text{ZnOx}\cdot 2\text{H}_2\text{O}$ and the complete disappearance of X-ray reflections of ZnO (Figure 2.12a-g). In contrast, the X-ray reflections of CuO were clearly observable and reflections of Cu(II) oxalate did not appear in the pattern, consistent with oxalic acid selectively reacting with ZnO. TGA (Supplementary Fig. S29) indicated the complete conversion of ZnO, while the less reliable analysis of water loss upon heating indicated the selective conversion of ZnO over CuO in the stoichiometric ratio 9:1. The FTIR-ATR spectrum of the reaction mixture was consistent with the formation of $\text{ZnOx}\cdot 2\text{H}_2\text{O}$, but could not confirm the absence of copper(II) oxalate (Supplementary Fig. S14). The near absence of copper(II) oxalate in the reaction mixture was confirmed by UV/Vis reflectance spectroscopy (Figure 2.12h). The spectrum of the aged mixture was almost identical to that of pure $\text{ZnOx}\cdot 2\text{H}_2\text{O}$ and different from the spectrum expected for a 1:1 mixture of Cu(II) and Zn oxalates. Thus, UV/Vis spectra are consistent with the absence of any significant amounts of copper(II) oxalate in the aged mixture. Presumably, the large difference in densities of $\text{ZnOx}\cdot 2\text{H}_2\text{O}$ (density=2.2 g/cm³) and CuO (density=6.3 g/cm³) could allow for mechanical separation of copper from zinc by gravity,⁵⁰ which is not possible for a mixture of raw oxides. Indeed, gravity separation with a "heavy liquid" CH_2I_2 (density=3.3 g/cm³)^{50,51} separated the reaction mixture into top and bottom layers that were identified by PXRD as $\text{ZnOx}\cdot 2\text{H}_2\text{O}$ and CuO, respectively (Figure 2.12c,d). Thus, combining the solvent-free chemical separation of zinc and copper oxides with gravity separation allows the separation of copper and zinc oxides without the need for dissolution⁵⁰ in aggressive solvents, such as sulfuric acid, or high temperatures. Preliminary results on accelerated aging mixtures of PbO and ZnO indicate similar selectivity (Supplementary Fig. S30).

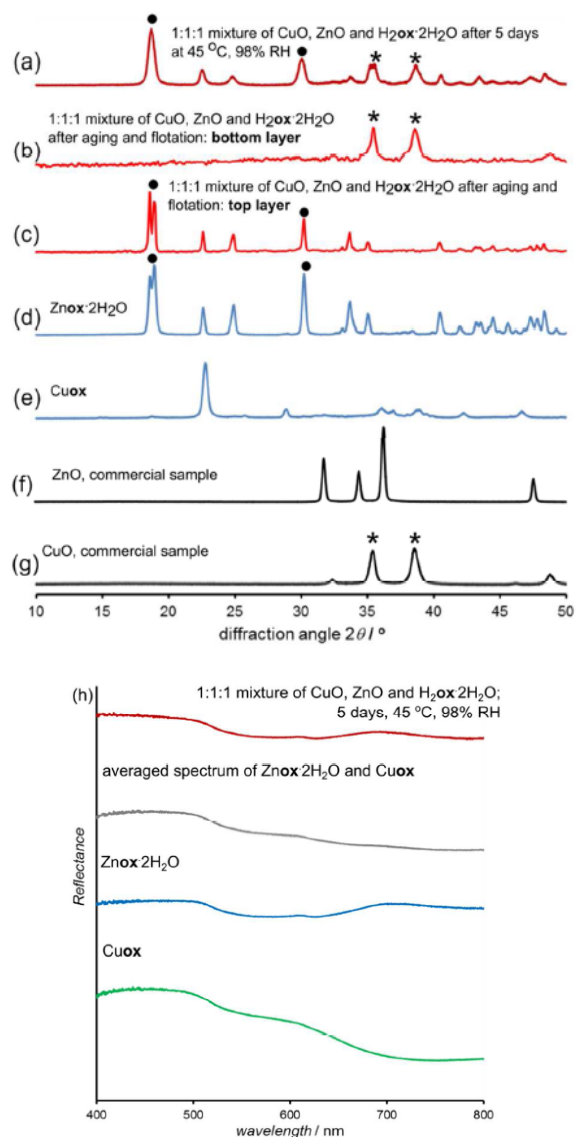


Figure 2.12. PXRD patterns for the aging of a 1:1:1 mixture of ZnO, CuO and $\text{H}_2\text{Ox}\cdot 2\text{H}_2\text{O}$: (a) after 5 days at 45 °C, 98% RH; (b) bottom layer from gravity separation using CH_2I_2 ; (c) top layer obtained by gravity separation using CH_2I_2 ; (d) $\text{ZnOx}\cdot 2\text{H}_2\text{O}$; (e) CuOx ; (f) ZnO and (g) CuO. (h) Reflectance UV-Vis spectra (top to bottom): average of CuOx and $\text{ZnOx}\cdot 2\text{H}_2\text{O}$; reaction mixture after 5 days at 45 °C, 98% RH; pure $\text{ZnOx}\cdot 2\text{H}_2\text{O}$ and pure CuOx . PXRD and UV-Vis spectra indicate selective transformation of ZnO into $\text{ZnOx}\cdot 2\text{H}_2\text{O}$, leaving behind CuO. To highlight the selective conversion, selected X-ray reflections of CuO and $\text{ZnOx}\cdot 2\text{H}_2\text{O}$ are designated with * and •, respectively.

2.5 Conclusions

This proof-of-principle study demonstrated how mimicking the conditions responsible for mineral weathering can lead to solvent-free, low-energy approaches to making coordination polymers and open frameworks from mineral-like feedstocks, as well as to novel mild methodologies applicable in mineral industry. The transformation of a variety of metal (Mg, Mn, Co, Ni, Cu, Zn, Pb) oxides was accessible at room temperature in mixtures prepared by gentle mixing of powders, despite high lattice stabilization energies⁵² and melting points of the oxides (800°C-2500°C). Mechanical activation or mild temperature increase accelerated the reactions, enabled the complete transformation of all explored metal oxides, and provided control over the polymorphic composition of the product (exemplified by reactions of MnO). The difference in aging reactivity of metal oxides enabled the solvent-free separation of metals in their oxide form without strong acids or high temperatures. As transition metal oxides are often slightly soluble and highly inert, the ability to conduct their chemical segregation in a solvent-free manner and under mild conditions is particularly surprising.⁵³ After chemical separation, the metals were also mechanically separated by gravity. We believe solvent-free separation by aging has considerable potential for reducing energy and solvent use in mineral industry.⁵⁰

It was demonstrated how the reactions can be directed for the formation of 2D or 3D open MOFs. In our hands, this yielded two known open frameworks based on zinc, and four previously not described frameworks based on Co(II) or Ni(II). Whereas a potential criticism can be directed towards reactivity requiring several days, we note that accelerated aging reactions can take place over times that are comparable to those for conventional solvothermal syntheses, whilst being conducted quantitatively from a metal oxide⁵⁴ and near room temperature. As demonstrated here for nickel and zinc oxalates, and recently reported synthesis of porous zeolitic imidazolate frameworks, accelerated aging can be conducted at a multi-gram scale.

It is worth noting that aging transformations are not unknown in large-scale applications, as illustrated by the Dutch process for manufacturing lead white paint. Mechanistic details of herein presented aging reactivity are not known. We believe that the mobility of the organic phase plays a significant role, consistent with reports⁵⁵ of vapor or gas-induced transformations of organic and organometallic solids, such as those by Atwood⁵⁶ and Braga groups.⁵⁷ We are currently pursuing the reactivity of three- and four-valent metals, such as Sc, Ti, Cr.

2.6 Acknowledgement

We acknowledge McGill University, the FRQNT Nouveaux Chercheurs fund, the Canada Foundation for Innovation Leaders Opportunity Fund, the NSERC Discovery Grant and the FRQNT Centre for Self-Assembled Chemical Structures. Prof. D. S. Bohle is acknowledged for aid in obtaining single crystal X-ray diffraction data. Bruker UK are acknowledged for SSNMR measurements. Drs N. Henderson and S. Pharesi, Bruker AXS, are acknowledged for help with X-ray fluorescence. Preliminary results that inspired the research were obtained during the principal investigator's appointment as a Herchel Smith Research Fellow at the University of Cambridge. The support of the Royal Society (Research Grant) and the Herchel Smith fund during that period is acknowledged. Advice from Prof. A. K. Cheetham, University of Cambridge, is appreciated.

Notes and references

Electronic Supplementary Information (ESI) available: Crystallographic information for **(pa)₂(ox)** in CIF format. This data has also been deposited with the CCDC, deposition number 933546. Additional PXRD, FTIR-ATR, SSNMR and thermogravimetric data. See

<http://www.rsc.org/suppdata/gc/c3/c3gc41370e/c3gc41370e.pdf>

TGA of **[pn][Zn₂(ox)₃]·3H₂O** prepared by templated aging gave an excellent fit for the expected loss of three equivalents of water before 200°C (measured weight

loss=10.1%, expected weight loss=10.3%), followed by the decomposition of the metal-organic residue into ZnO (measured residue weight=31.3%, calculated ZnO residue for $[\text{pn}][\text{Zn}_2(\text{ox})_3]\cdot 3\text{H}_2\text{O}$ =31.0 %). Such thermal behavior is consistent with that previously reported for solvothermally grown $[\text{pn}][\text{Zn}_2(\text{ox})_3]\cdot 3\text{H}_2\text{O}$.³⁶ An excellent fit was also observed for TGA of $[\text{pa}]_2[\text{Zn}_2(\text{ox})_3] \cdot 3\text{H}_2\text{O}$ (measured water content=9.1%, calculated=9.5%; measured ZnO residue=29.4%, calculated=28.6%). Also see Supplementary Material.

Potential metallurgical and mineral processing applications of concepts and results of the work described in this manuscript are covered by the provisional patent application US 61/826,172.

- (1) (a) J. C. Crittenden and H. S. White, *J. Am. Chem. Soc.* **2010**, *132*, 4503; (b) D. J. C. Constable, P. J. Dunn, J. D. Hayler, G. R. Humphret, J. L. Leazer Jr., R. J. Linderman, K. Lorenz, J. Manley, B. A. Pearlman, A. Wells, A. Zaks and T. Y. Zhang, *Green Chem.* **2007**, *9*, 411; (c) W. J. W. Watson, *Green Chem.* **2012**, *14*, 251; (d) P. Anastas and N. Eghbali, *Chem. Soc. Rev.* **2010**, *39*, 301.
- (2) (a) S. R. Batten, N. R. Champness, X.-M. Chen, J. Garcia-Martinez, S. Kitagawa, L. Ohrstrom, M. O'Keeffe, M. P. Suh and J. Reedijk, *CrystEngComm* **2012**, *14*, 3001; (b) O. M. Yaghi, M. O'Keeffe, N. W. Ockwig, H. K. Chae, M. Eddaoudi and J. Kim, *Nature*, **2003**, *423*, 705; (c) S. A. K. Robinson, M.-V. L. Mempin, A. J. Cairns, K. T. Holman, *J. Am. Chem. Soc.* **2011**, *133*, 1634; (b) L. E. Kreno, K. Leong, O. K. Farha, M. Allendorf, R. P. Van Duyne and J. T. Hupp, *Chem. Rev.* **2012**, *112*, 1105. (c) J. J. Gassensmith, H. Furukawa, R. A. Smaldone, R. S. Forgan, Y. Y. Botros, O. M. Yaghi and J. F. Stoddart, *J. Am. Chem. Soc.* **2011**, *133*, 15312; (d) R. Vaidhyanathan, S. S. Iremonger, G. K. H. Shimizu, P. G. Boyd, S. Alavi and T. K. Woo, *Science* **2010**, *330*, 650; (e) C. Y. Lee, O. K. Farha, B. J. Hong, A. A. Sarjeant, S. T. Nguyen and J. T. Hupp, *J. Am.*

- Chem. Soc.*, **2011**, *133*, 15858; (f) C. Wang, T. Zhang and W. Lin, *Chem. Rev.* **2012**, *112*, 1084.
- (3) (a) A. Czaja, E. Leung, N. Trukhan and U. Müller, *Industrial MOF Synthesis* in: *Metal-Organic Frameworks: Applications from Catalysis to Gas Storage*, 1st Ed. Editor D. Farrusseng, Wiley-VCH (2011); (b) B. Yilmaz, N. Trukhan and U. Müller *Chin. J. Catal.* **2012**, *33*, 3.
- (4) (a) S. Horike, S. Shimomura and S. Kitagawa, *Nature. Chem.* **2009**, *1*, 695; (b) S. Kitagawa, R. Kitaura and S.-i. Noro, *Angew. Chem. Int. Ed.* **2004**, *43*, 2334; (c) S. T. Meek, J. A. Greathouse and M. D. Allendorf, *Adv. Mater.* **2011**, *23*, 249; (d) U. Mueller, M. Schubert, F. Teich, H. Puetter, K. Schierle-Arndt and J. Pastré, *J. Mater. Chem.* **2006**, *16*, 626; (e) G. Férey, *Chem. Soc. Rev.* **2008**, *37*, 191.
- (5) W.-J. Son, J. Kim, J. Kim and W.-S. Ahn, *Chem. Commun.* **2008**, *15*, 6336.
- (6) (a) S. H. Jung, J.-H. Lee, P. M. Forster, G. Férey, A. K. Cheetham and J.-S. Chang, *Chem. Eur. J.* **2006**, *12*, 7899; (b) J.-S. Choi, W.-J. Son, J. Kim and W.-S. Ahn, *Micropor. Mesopor. Mater.* **2008**, *116*, 727; (c) C.-M. Lu, J. Liu, K. Xiao and A. T. Harris, *Chem. Eng. J.* **2010**, *156*, 465.
- (7) A. M. Joaristi, J. Juan-Alcañiz, P. Serra-Crespo, F. Kapteijn and J. Gascon, *Cryst. Growth Des.* **2012**, *12*, 3489.
- (8) (a) A. Pichon, A. Lazuen-Garay and S. L. James, *CrystEngComm.* **2006**, *8*, 211; (b) F. Kotaro, A. Lazuen-Garay, J. Hill, E. Sbircea, Z. Pan, M. Xu, D. C. Apperley, S. L. James and K. D. M. Harris, *Chem. Commun.*, **2010**, *46*, 7572; (c) S. L. James, P. Collier, I. Parkin, G. Hyatt, D. Braga, L. Maini, W. Jones, C. Bolm, A. Krebs, J. Mack, D. Waddell, W. Shearouse, A. G. Orpen, C. J. Adams, T. Friščić, J. W. Steed and K. D. M. Harris, *Chem. Soc. Rev.* **2012**, *41*, 413; (d) T. Friščić, *J. Mat. Chem.* **2010**, *20*, 7599; (e) D. Braga, S. L. Giuffreda, F. Grepioni, A. Pettersen, L. Maini, M. Curzi, and M. Polito, *Dalton Trans.* **2006**, 1249; (f) H. Sakamoto, R. Matsuda and S. Kitagawa, *Dalton Trans.* **2012**, *41*, 3956
- (9) I. A. Ibarra, P. A. Bayliss, E. Pérez, S. Yang, A. J. Blake, H. Nowell, D. R. Allan, M. Poliakoff and M. Schroder *Green Chem.* **2012**, *14*, 117.

- (10) (a) T. Friščić and L. Fábíán, *CrystEngComm*. **2009**, *11*, 743; (b) A.-X. Zhu, R.-B. Lin, X.-L. Qi, Y. Liu, Y.-Y. Lin, J.-P. Zhang and X.-M. Chen *Micropor. Mesopor. Mater.* **2012**, *157*, 42.
- (11) W. Zhang, Z. Zhu and C. Y. Cheng, *Hydrometallurgy*, **2011**, *108*, 177.
- (12) (a) J.-B. Lin, R.-B. Lin, X.-N. Cheng, J.-P. Zhang and X.-M. Cheng, *Chem. Commun.* **2011**, *47*, 9185; (b) M. Lanchas, D. Vallejo-Sánchez, G. Beobide, O. Castillo, A. T. Aguayo, A. Luque and P. Román, *Chem. Commun.* **2012**, *48*, 9930.
- (13) T. Friščić and W. Jones, *Cryst. Growth Des.* **2009**, *9*, 1621.
- (14) T. Friščić, *Chem. Soc. Rev.* **2012**, *41*, 3493.
- (15) W. Yuan, T. Friščić, D. Apperley and S. L. James *Angew. Chem. Int. Ed.* **2010**, *49*, 3916.
- (16) (a) E. H. H. Chow, F. C. Strobridge and T. Friščić *Chem. Commun.* **2010**, *46*, 6368; (b) T. Friščić, I. Halasz, F. C. Strobridge, R. E. Dinnebier, R. S. Stein, L. Fábíán and C. Curfs *CrystEngComm*. **2011**, *13*, 3125.
- (17) P. Wang, G. Li, Y. Chen, S. Chen, S. L. James and W. Yuan *CrystEngComm*. **2012**, *14*, 1994.
- (18) V. M. André, A. Hardeman, I. Halasz, R. S. Stein, G. J. Jackson, D. G. Reid, M. J. Duer, C. Curfs, M. T. Duarte and T. Friščić *Angew. Chem. Int. Ed.* **2011**, *50*, 7858.
- (19) C. J. Adams, M. A. Kurawa, M. Lusi and A. G. Orpen, *CrystEngComm*, **2008**, *10*, 1790.
- (20) Mechanochemical transformation of CuO into copper(II) acetate can be achieved only by extended milling with traces of water: F. C. Strobridge, N. Judaš, and T. Friščić, *CrystEngComm*. **2010**, *12*, 2409.
- (21) (a) G. M. Gadd, Y. J. Rhee, K. Stephenson, and Z. Wei, *Env. Microb. Rep.* **2012**, *4*, 270; (b) P. Adamo and P. Violante, *Appl. Clay Sci.* **2000**, *16*, 229; (c) G. M. Gadd, *Microbiology* **2010**, *156*, 609; (d) J. A. Sayer, M. Kierans and G. M. Gadd, *FEMS Microbiol. Lett.* **1997**, *154*, 29; (e) M. Fomina, S. Hillier, J. M. Charnock, K. Melville, I. J. Alexander and G. M. Gadd, *Appl. Envir. Microb.* **2005**, *71*, 371; (f) W. W. Barker and J. F. Banfield, *Chem.*

- Geology*, **1996**, *132*, 55; (g) Z. Wei, S. Hillier and G. M. Gadd, *Environ. Microb.* **2012**, *14*, 1744; (h) J. A. Sayer and G. M. Gadd, *Mycol. Res.* **1997**, *101*, 653; (i) Z. Wei, M. Kierans and G. M. Gadd, *Geomicrobiol. J.* **2012**, *29*, 323.
- (22) (a) O. W. Purvis, *Lichenologist*, **1984**, *16*, 197; (b) J. Chen, H.-P. Blume and L. Beyer, *Catena*, **2000**, *39*, 121; (c) G. Sarret, A. Maceau, D. Cuny, C. van Haluwyn, S. Déruelle, J.-L. Hazemann, Y. Soldo, L. Eybert-Bérard and J.-J. Methonnex, *Environ. Sci. Technol.* **1998**, *32*, 3325.
- (23) O. W. Purvis and C. Halls, *Lichenologist* **1996**, *28*, 571.
- (24) R. M. Clarke and I. R. Williams, *Miner. Mag.* **1986**, *50*, 295.
- (25) (a) T. Echigo and M. Kimata, *Canadian Mineralogist* **2010**, *48*, 1329; (b) U. M. Cowgill, *Min. Mag.* **1989**, *53*, 505; (c) M. M. Smits, A. M. Herrmann, M. Duane, O. W. Duckworth, S. Bonneville, L. G. Benning and U. Lundstrom, *Fung. Biol. Rev.* **2009**, *23*, 122; (d) G. M. Gadd and J. A. Raven, *Geomicrobiol. J.* **2010**, *27*, 491; (e) E. J. Baran and P. V. Monje, *Met. Ions. Life Sci.* **2008**, *4*, 219.
- (26) (a) S. R. Byrn, W. Xu and A. W. Newman, *Adv. Drug. Deliv. Rev.* **2001**, *48*, 115; (b) X. Chen, J. G. Stowell, K. R. Morris and S. R. Byrn, *J. Pharm. Biomed. Anal.* **2010**, *51*, 866.
- (27) (a) M. J. C. Cliffe, C. Mottillo, R. S. Stein, D.-K. Bučar and T. Friščić, *Chem. Sci.* **2012**, *3*, 2495; (b) C. Mottillo, Y. Lu, M.-H. Pham, T.-O. Do and T. Friščić, *Green Chem.* **2013**, DOI: 10.1039/C3GC40520F
- (28) (a) M. Sadakiyo, H. Ōkawa, A. Shigematsu, M. Ohba, T. Yamada and H. Kitagawa, *J. Am. Chem. Soc.* **2012**, *134*, 5472; (b) J.-C. Tan., J. D. Furman and A. K. Cheetham, *J. Am. Chem. Soc.* **2009**, *131*, 14252; (c) E. Coronado, C. Martí-Gastaldo, J. R. Galán-Mascarós and M. Cavallini, *J. Am. Chem. Soc.* **2010**, *132*, 5456; (d) M. Clemente-León, E. Coronado, C. Martí-Gastaldo and F. M. Romero, *Chem. Soc. Rev.* **2011**, *40*, 473; (e) J. Ling, C. M. Wallace, J. E. S. Szymanowski and P. C. Burns, *Angew. Chem. Int. Ed.* **2010**, *49*, 7271; (f) J. Ling, J. Qiu and P. C. Burns, *Inorg. Chem.* **2012**, *51*, 2403; (g) E. Cariati, R. Macchi, D. Roberto, R. Ugo, S. Galli, N.

- Casati, P. Macchi, A. Sironi, L. Bogani, A. Caneschi and D. Gatteschi, *J. Am. Chem. Soc.* **2007**, *129*, 9410; (h) P. A. Prasad, S. Neeraj, S. Natarajan and C. N. R. Rao, *Chem. Commun.* **2000**, 1251; (i) E. Gavilan, N. Audebrand and E. Jeanneau, *Solid State Sci.* **2007**, *9*, 985; (j) E. Jeanneau, N. Audebrand and D. Louer, *Chem. Mater.* **2002**, *14*, 1187.
- (29) (a) C. N. R. Rao, S. Natarajan and R. Vaidhyanathan, *Angew. Chem. Int. Ed.* **2004**, *43*, 1466; (b) A. K. Cheetham and C. N. R. Rao, *Mat. Res. Bull.* **2005**, *30*, 93; (c) Q. Pan, Q. Chen, W.-C. Song, T.-L. Hu and X.-H. Bu, *CrystEngComm*, **2010**, *12*, 4198; (d) G. De Munno, M. Julve, F. Nicolo, F. Lloret, J. Faus, R. Ruiz and E. Sinn, *Angew. Chem. Int. Ed.* **1993**, *32*, 613; (e) G. De Munno, R. Ruiz, F. Lloret, J. Faus, R. Sessoli and M. Julve, *Inorg. Chem.* **1995**, *34*, 408; (f) U. Baisch and D. Braga, *CrystEngComm* **2009**, *11*, 40; (g) T. Bataille, J. P. Auffredic and D. Louer, *Chem. Mater.* **1999**, *11*, 1559.
- (30) (a) D. Yu. Naumov, N. V. Podberezskaya, E. V. Boldyreva and A. V. Virovets, *J. Struct. Chem.* **1996**, *37*, 480; (b) R. Deyrieux and A. Peneloux, *Bull. Chim. Soc. Fr.* **1969**, 2675.
- (31) S. Descurtin, R. Pellaux, G. Antorrena and F. Palacio, *Coord. Chem. Rev.* **1999**, *190-192*, 841.
- (32) (a) S. Decurtins, H. W. Schmalle, P. Schneuwly, J. Enslin and P. Gütllich, *J. Am. Chem. Soc.* **1994**, *116*, 9521; (b) S. Decurtins, H. W. Schmalle, P. Schneuwly and H. R. Oswald, *Inorg. Chem.* **1993**, *32*, 1888; (c) F. Luo, Y.-X. Che and J.-M. Zheng, *J. Mol. Struct.* **2007**, *827*, 206; (d) O. R. Evans and W. Lin, *Cryst. Growth Des.* **2001**, *1*, 9.
- (33) (a) S. Ayyapan, A. K. Cheetham, S. Natarajan and C. N. R. Rao, *Chem. Mater.* **1998**, *10*, 3746; (b) S. Natarajan, R. Vaidhyanathan, C. N. R. Rao, S. Ayyapan and A. K. Cheetham, *Chem. Mater.* **1999**, *11*, 1633.
- (34) (a) M. Dan and C. N. R. Rao, *Angew. Chem. Int. Ed.* **2006**, *45*, 281; (b) A. K. Cheetham, C. N. R. Rao and R. K. Feller, *Chem. Commun.* **2006**, 135, 4780.
- (35) G. Giester, *Z. Kristallogr.* **1997**, *212*, 720.

- (36) R. Vaidhyanathan, S. Natarajan and C. N. R. Rao *J. Chem. Soc. Dalton Trans.* **2001**, 699.
- (37) R. Vaidhyanathan, S. Natarajan, A. K. Cheetham, C. N. R. Rao *Chem. Mater.* **1999**, *11*, 3636.
- (38) (a) R. Vaidhyanathan, S. Natarajam and C. N. R. Rao, *J. Mol. Struc.* **2002**, *608*, 123; b) J. C. Barnes, R. W. Longhurst and T. J. R. Weakley, *Acta Cryst. C.*, **1998**, *54*, 1347.
- (39) R. Deyrieux, C. Berro and A. Peneloux, *Bull. Soc. Chim. Fr.* **1973**, 25.
- (40) (a) A. Michalowicz, J. J. Girered and J. Goulon, *Inorg. Chem.* **1979**, *18*, 3004; (b) H. Fichtner-Schmittler, *Cryst. Res. Tech.* **1984**, *19*, 1225.
- (41) (a) J. Bacsa, D. Eve and K. R. Dunbar, *Acta Crystallogr. C*, **2005**, *61*, m58; (b) E. Wisgerhof and J. W. Geus, *Mat. Res. Bull.* **1983**, *18*, 993.
- (42) (a) W.-Y. Wu, Y. Song, Y-Z. Li and X.-Z. You *Inorg. Chem. Commun.* **2005**, *8*, 732; (b) X. Fu, C. Wang and M. Li, *Acta Cryst. E*, **2005**, *61*, m1348.
- (43) A. N. Christensen, D. E. Cox and M. S. Lehmann *Acta Chem. Scand.* **1989**, *43*, 19.
- (44) A; V. Virovets, D. Yu. Naumov, E. V. Boldyreva and N. V. Podberezskaya, *Acta Crystallogr. C* **1993**, *49*, 1882.
- (45) W.-Y. Wu and L.-X. Zhai, *Acta Cryst. E* **2007**, *63*, m429.
- (46) (a) S. Libri, M. Mahler, G. M. Espallargas, D. C. N. G. Singh, J. Soleimannejad, H. Adams, M. D. Burgard, N. P. Rath, M. Brunelli and L. Brammer *Angew. Chem. Int. Ed.* **2008**, *47*, 1693; (b) G. M. Espallargas, M. Hippler, A. J. Florence, P. Fernandes, J. van de Streek, M. Brunelli, W. I. F. David, K. Shankland and L. Brammer *J. Am. Chem. Soc.* **2007**, *129*, 15606.
- (47) A. Huizing, H. A. M. van Hal, W. Kwestroo, C. Langereis and P. C. van Loosdregt, *Mat. Res. Bull.* **1977**, *12*, 605.
- (48) Consequently, the energy cost for such mechanically activated reaction is reduced to the short period of operating the mill. At the laboratory scale this amounts to a small total input of 15 kJ per reaction, as measured in

our laboratory for a Retsch MM400 mill which operates at 100W (comparable to a light bulb) for two milling stations.

- (49) (a) V. Šepelak, S. Bégin-Colin and G. Le Caer *Dalton Trans.* **2012**, *41*, 11927; (b) V. Šepelak, S. M. Becker, I. Bergmann, S. Indris, M. Scheuermann, A. Feldhoff, C. Kübel, M. Bruns, N. Stürzl, A. S. Ulrich, M. Ghafari, H. Hahn, C. P. Grey, K. D. Becker and P. Heitjans *J. Mat. Chem.* **2012**, *22*, 3117.
- (50) The heavy liquid in gravity separation experiments does not act as a solvent, but serves for physical separation of substances without dissolving them. Whereas the use of CH₂I₂ heavy liquid is still a standard practice in a number of geology, chemistry and mineralogy laboratories, we note there is a greener, but more costly, alternative based on aqueous sodium or lithium polytungstate solutions.⁵¹ In large-scale applications, heavy liquid separation is replaced by froth flotation in aqueous systems. For an overview of industrial froth flotation methods, see: (a) S. Bulatovic, *Handbook of Flotation Reagents, Chemistry, Theory and Practice. Vol. 1 Flotation of Sulfide Ores and Vol. 2 Flotation of gold, PGM and oxide minerals*, Elsevier (2007)
- (51) (a) M. R. Gregory and K. A. Johnston *New Zeal. J. Geol. Geop.* **1987**, *30*, 317; (b) G. A. Andreev and M. Hartmanová *Phys. Stat. Sol.* **1989**, *116*, 4571; (c) T. L. Threlfall, *Analyst* **1995**, *120*, 2435.
- (52) Lattice energies of herein explored oxides range from 3.5 MJ/mol to 4.2 MJ/mol, see *CRC Handbook of Chemistry and Physics*, 61st Edn, ed. R. C. Weast, M. J. Astle, CRC Press Inc. Boca Raton, FL, (1981).
- (53) Herein presented solvent-free metal oxide separation is based on solid-state reactivity which has a potential to be generalized, and should not be confused with magnetic procedures unique to certain iron oxides (maghemite, magnetite).
- (54) Reported rapid (minutes to hours) syntheses of MOFs in solution exhibit either poor yields (below 60%) or require additional stoichiometric base, see: (a) A. F. Gross, E. Sherman and J. J. Vajo *Dalton Trans.* **2012**, *41*,

- 5458; (b) D. J. Tranchemontagne, J. R. Hunt and O. M. Yaghi, *Tetrahedron*, **2008**, *64*, 8553.
- (55) (a) D. Cinčić, I. Brekalo and B. Kaitner, *Chem. Commun.* **2012**, *48*, 11683; (b) D. Cinčić, I. Brekalo and B. Kaitner, *Cryst. Growth Des.* **2012**, *12*, 44; (c) M. A. Ziganshin, I. G. Efimova, V. V. Gorbachuk, S. A. Ziganshina, A. P. Chuklanov, A. A. Bukharaev, D. V. Soldatov, *J. Peptide Sci.* **2012**, *18*, 209; (d) R. Annedo, D. V. Soldatov, I. L. Moudrakovski, M. Casu and J. A. Ripmeester, *Chem. Mater.* **2008**, *20*, 2908; (e) G. M. Espallargas, M. Hippler, A. J. Florence, P. Fernandes, J. van de Streek, M. Brunelli, W. I. F. David, K. Shankland and L. Brammer, *J. Am. Chem. Soc.* **2007**, *129*, 15606; (f) B. D. Chandler, G. D. Enright, K. A. Udachin, S. Pawsey, J. A. Ripmeester, D. T. Cramb and G. K. H. Shimizu, *Nature Mater.* **2008**, 229.
- (56) (a) J. Tian, S. J. Dalgarno and J. L. Atwood, *J. Am. Chem. Soc.* **2011**, *133*, 1399; (b) J. Tian, P. Thallapally, J. Liu, G. J. Exarhos and J. L. Atwood, *Chem. Commun.* **2011**, *47*, 701; (c) P. K. Thallapally, B. P. McGrail, S. J. Dalgarno, H. T. Schaefer, J. Tian and J. L. Atwood, *Nature Mater.* **2008**, *7*, 146.
- (57) (a) D. Braga, S. L. Giaffreda, F. Grepioni, M. R. Chierotti, R. Gobetto, G. Palladino and M. Polito, *CrystEngComm* **2007**, *9*, 879; (b) L. Maini, D. Braga, P. P. Mazzeo and B. Ventura, *Dalton Trans.* **2012**, *41*, 531.

Connecting text for Chapter 3

Chapter 2 introduced the inspiration, development and applications of accelerated aging which has been proven as an effective, solvent-free and green synthetic approach for MOMs synthesis and mineral separation. In Chapter 3, the synthesis of bismuth salicylate complexes, including bismuth subsalicylate (API of the drug “Pepto-Bismol®”) and bismuth salicylate oxo-nanoclusters have been targeted. Solid-state synthetic tools including both mechanochemical milling and accelerated aging have been used in the investigation. Accelerated aging at 95°C and solid-state equilibrium are described in this Chapter. By using bismuth disalicylate monohydrate as a central precursor, a series of decorated bismuth salicylate oxo-nanoclusters have been synthesized and structurally characterized. Some of them may find use as nano-pharmaceuticals and alternatives to bismuth subsalicylate.

Chapter 3. Bismuth disalicylate monohydrate: a central compound of bismuth salicylate chemistry

* *This paper is being prepared for publication. It is coauthored by [Kale Laviolette](#) and Tomislav Friščić.*

3.1 Abstract

We propose bismuth disalicylate monohydrate as a versatile, well-defined, readily prepared precursor for a variety of bismuth salicylate materials, ranging from the metallodrug bismuth subsalicylate to surface-decorated bismuth salicylate oxo-nanoclusters; the attractive aspect of bismuth disalicylate monohydrate is its facile preparation through low-energy and low-solvent methods of mechanochemical and accelerated aging synthesis.

3.2 Introduction

Inspired by the anti-inflammatory and bactericidal action of bismuth subsalicylate (BSS, commercially known as Pepto-Bismol®), the investigation of bismuth complexes with salicylic acid and its anions remains a highly active area of metallodrug research.¹ Due to the low solubility of bismuth salicylate complexes, structures of these pharmaceutically important compounds have remained largely unknown and most structural information has been gathered on systems involving auxiliary organic ligands.² In 2006 the Andrews group recognised the formation of bismuth salicylate oxo-clusters based on $\text{Bi}_{38}\text{O}_{44}$ and Bi_9O_7 units externally coordinated with salicylate anions and acetone solvent, representing exciting new models for BSS structure and reactivity.³ Our group has recently reported⁴ the facile, clean and selective synthesis of BSS (**Bi-1**) and two previously poorly characterised bismuth salicylate materials, bismuth disalicylate monohydrate (**Bi-2**) and bismuth trisalicylate (**Bi-3**), using mechanochemical ion- and liquid-assisted grinding (ILAG).⁵ Importantly, the use of mechanochemistry has enabled the quantitative formation of bismuth salicylates directly from the simplest metal

oxide precursor, with water as the only byproduct, and without the need for corrosive metal nitrate reagents and acid byproducts. The purity of **Bi-2** obtained in that way enabled its structural characterization from powder X-ray diffraction (PXRD) data, which was a long-standing challenge of the Structure Determination by Powder Diffraction Round Robin competition.⁶ Currently, **Bi-2** is the only bismuth salicylate material without auxiliary organic ligands whose crystal structure has been determined.⁴

Compared to mechanochemical milling, accelerated aging inspired by mineral neogenesis is an even milder synthetic approach for metal organic materials (MOMs) synthesis. It has been successfully applied for the synthesis of zeolitic imidazolate frameworks (ZIFs), metal oxalate coordination polymers, templated metal organic frameworks (MOFs) and solvent-free mineral separations.⁷ In accelerated aging reactions, only moisture and mild heating (all previous studies were conducted under room temperature or 45°C) were used to help the completion of solid-state reactions. With a high lattice energy resulting from interactions of trivalent bismuth cations and oxygen anions, bismuth oxide is a challenging feedstock for accelerated aging synthesis. However, at the same time, it is a good starting case for investigation, activation and separation of high-valent metal oxides/sulfides.

3.3 Experimental Section

Mechanochemical experiments: 1 gram of a solid reactant mixture in appropriate stoichiometric ratio was placed in a stainless steel grinding jar, along with 1 stainless steel ball of 10 mm diameter. The mixture was ground 90 min, in a Retsch MM200 mill at a frequency of 30 Hz. For LAG reactions, 250 μL ($\eta=0.25$ $\mu\text{L}/\text{mg}$) H_2O was added to the reaction mixture.⁸ For ILAG reactions, 50 mg salt was also added. The samples were washed with distilled water to remove the salt additive and dried in air.

Accelerated aging experiments: 0.5 g of a solid reactant mixture containing the starting materials in appropriate stoichiometric ratio was gently ground manually

with a mortar and pestle. The ground mixtures were then placed in an open vial and aged at 95 °C and 100% RH in a glass desiccator in which a constant humidity level was maintained by equilibrating the atmosphere with water. The desiccator was placed in a large volume incubator set at 95 °C. For large scale reactions, 10 g of a solid reactant mixture was ground and aged in large Petri dishes which enabled holding the reaction mixture in the form of a thin layer (usually not thicker than 3 mm).

Nanocluster synthesis: 1 g of bismuth disalicylate (**Bi-2**) was dissolved in 100 mL warm acetone (around 50 °C). The filtrate was slowly evaporated overnight to form crystals. The yield of crystallization is 71%. Dissolution of the **Bi-2** in other organic solvents such as DMF, 2-butanone and cyclohexanone gave clusters decorated with other solvent shells. The water-decorated cluster was formed by participation from acetone solution upon adding water (5 mL of water in 10 mL of the acetone solution).

Powder X-ray diffraction (PXRD): Room temperature PXRD patterns were collected in the 2θ range 3° to 40° on a Bruker D2 PHASER X-ray diffractometer using a CuK_α ($\lambda=1.54 \text{ \AA}$) source, equipped with a Linear detector LYNXEYE and a K_β filter. The X-ray tube was operating at the power setting of 30 kV and 10 mA. Data analysis was carried out using the Panalytical X'pert Highscore Plus program.

Infrared spectroscopy: Fourier transform infrared spectra were collected using a Perkin Elmer Fourier Transform Infrared Attenuated Total Reflectance spectrometer in the range 400 cm^{-1} to 4000 cm^{-1} .

Thermogravimetric analysis (TGA): TGA measurements were conducted on a TA Instruments Q500 Thermogravimetric System with a Pt pan under dynamic atmosphere of air with 40 ml/min balance flow and 60 ml/min purge flow. The upper temperature was around 600 °C depending on the sample, with a heating rate of 5 °C/min.

Solid-state NMR (C^{13}): Spectra were collected on a 400 MHz Varian VNMR equipped with a 4 mm CPMAS probe at a spin rate of 14 KHz. Cross-polarization (CP) spectra were collected with a contact time of 2 ms and recycle delay of 2 s while direct-polarization (DP) spectra were collected with a recycle delay of 10 s.

Dynamic light scattering (DLS): 0.2 mmol/L bismuth nanocluster solutions were made at room temperature by dissolving solid samples of the clusters decorated with different solvent molecules in their respective solvents. Measurements were performed on a Brookhaven Instruments Corporation system equipped with a BI-200SM goniometer, a BI-9000AT digital correlator and a Compass 315-150 CW laser light source from Coherent Inc. operating at 532 nm (150 mW).

Atomic force microscopy (AFM): Droplets of an aqueous suspension of bismuth nanoclusters decorated with water (Bi-NP-H₂O) were dried out on silica plates. Experiments performed with a MultiModeTM SPM connected to a NanoscopeTM IIIa controller, from the Digital Instruments Veeco Metrology Group.

Single Crystal Diffraction: The 2-butanone structure has been collected at 150 K on a Bruker diffractometer with an Incoatec Microsource at 100 K. The cyclohexanone material was collected on a Bruker Microstar diffractometer equipped with a rotating anode. Both structures have been collected using CuKalpha radiation.

3.4 Results and Discussions

Our initial efforts resulted in successful gram-scale synthesis of bismuth subsalicylate (**Bi-1**), bismuth disalicylate monohydrate (**Bi-2**) and bismuth trisalicylate (**Bi-3**) by modification of the reported ILAG method⁴, such as using large steel balls to increase the mechanical impact and extending the grinding time. After that, we focused on individual properties of these bulk products. Notably, we found that **Bi-2**, which is stable and insoluble in room temperature water, is completely hydrolyzed to **Bi-1** after 3 hours refluxing as slurry in boiling water. Conversely, when we milled a 1:1 stoichiometric solid mixture of **Bi-1** and salicylic acid (**H₂Sal**) with a catalytic amount of water for 90 min at room

temperature, **Bi-2** was readily obtained again. This synthetic cycle, we believe, is caused by a difference in solubility of salicylic acid in water at room temperature and at 100°C.⁹ Bulk material **Bi-3**, however, is very sensitive to moisture and is readily hydrolyzed to **Bi-2** and **H₂Sal** if left overnight in open air. (Figure 3.1)

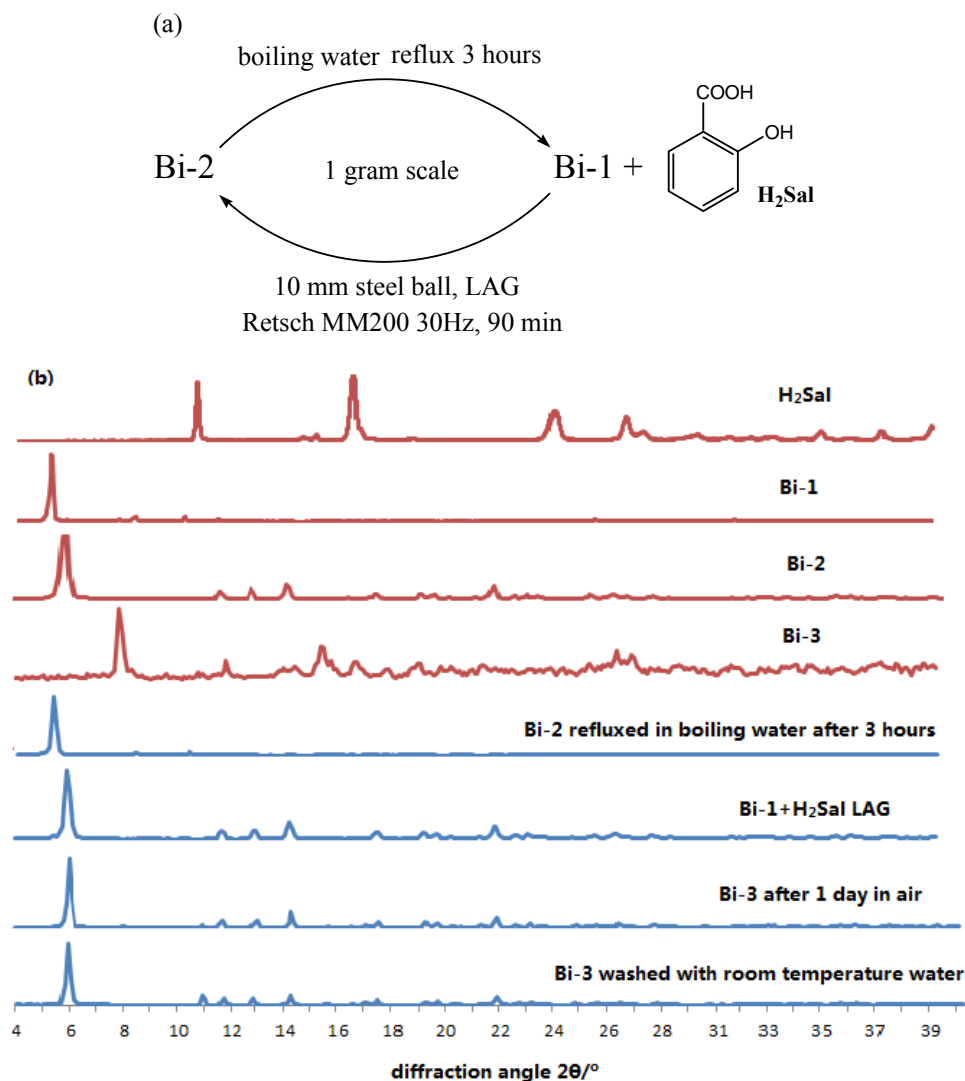


Figure 3.1. (a) The interconversion of **Bi-1** and **Bi-2**; (b) PXRD patterns for interconversion of **Bi-1**, **Bi-2** and **Bi-3**. From top to bottom: commercial **H₂Sal**; commercial **Bi-1**; synthesized **Bi-2** (washed by room temperature water and dried in the open air); synthesized **Bi-3** (kept in dry desiccator); **Bi-2** after reflux in boiling water for 3 hours; 1:1 mixture of **Bi-1** and **H₂Sal** after LAG with water ($\eta=0.25\mu\text{L}/\text{mg}$); **Bi-3** after 1 day in air; **Bi-3** washed with room temperature water.

Starting from a 1:4 solid mixture of bismuth oxide and salicylic acid expected to yield **Bi-2**, accelerated aging at 80°C and 100% RH proceeded very slowly. The inorganic salts typically used in mechanochemical ILAG synthesis⁴ do not provide a notable acceleration to the aging reactions. However, a slight increase in the temperature to 95°C results in complete and stoichiometric conversion to **Bi-2** in 3 days without adding any catalytic salts. The reaction towards **Bi-1** involves multiple steps. Starting from a 1:2 stoichiometric mixture of bismuth oxide and salicylic acid, the reaction initially follows the route of **Bi-2** synthesis, apparently consuming all salicylic acid and only part of bismuth oxide. The intermediate **Bi-2** then slowly reacts with remaining bismuth oxide and completely converts to **Bi-1** after 9 days (Figure 3.2). All aging reactions have been scaled up to 10 grams in large Petri dishes. Volume expansion is easily observed (Figure 3.2a), probably caused by the density difference between the initial mixture and the final product. Thin layer and large exposure area keep the rate of the large scale reaction similar to that of milligram scale reactions, indicating potential for larger (industrial) applications.

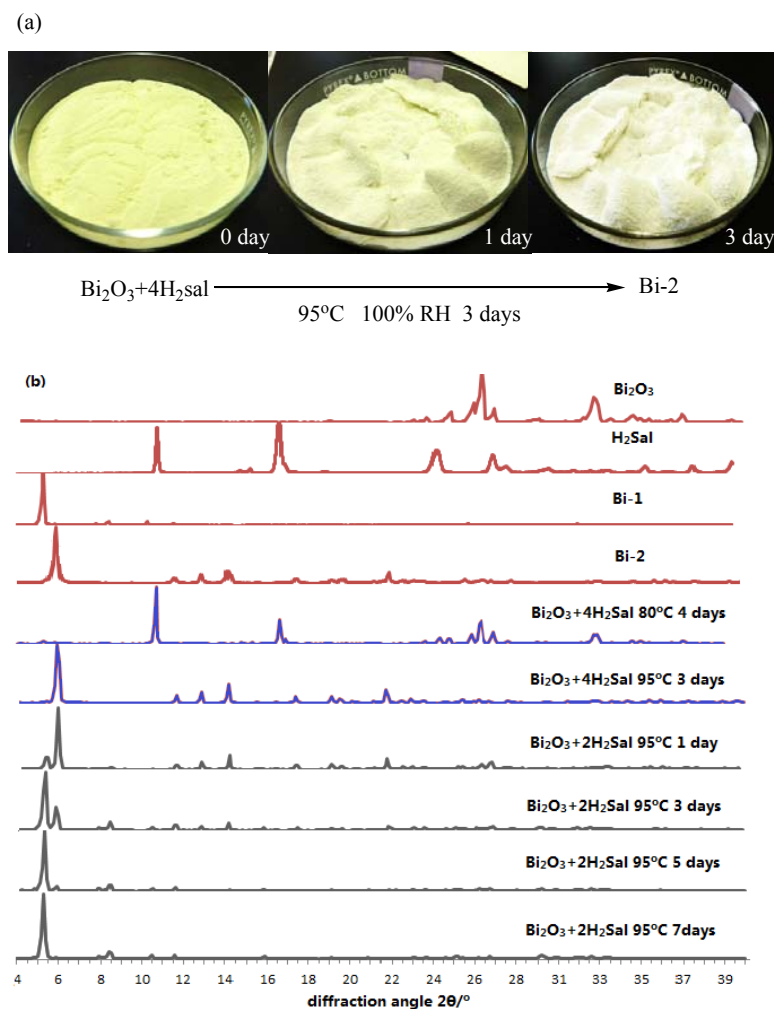


Figure 3.2. (a) Images of 10 gram scale accelerated aging reaction to form **Bi-2**; (b) PXRD patterns for accelerated aging reactions forming **Bi-2** and **Bi-1**. From top to bottom: bismuth oxide (Bi_2O_3); salicylic acid (H_2Sal); **Bi-1**; **Bi-2**; 1:4 mixture of Bi_2O_3 and H_2Sal after 4 days aging at 80°C 100% RH; 10 g scale 1:4 mixture of Bi_2O_3 and H_2Sal after 3 days aging at 95°C 100% RH; 1:2 mixture of Bi_2O_3 and H_2Sal after 1 day aging at 95°C 100% RH; 1:2 mixture of Bi_2O_3 and H_2Sal after 3 days aging at 95°C 100% RH; 1:2 mixture of Bi_2O_3 and H_2Sal after 5 days aging at 95°C 100% RH; 1:2 mixture of Bi_2O_3 and H_2Sal after 7 days aging at 95°C 100% RH;

The aging synthesis of **Bi-1** involves a 2:1 solid-state reaction of **Bi-2** and bismuth oxide, which are both stable and insoluble compounds at room temperature. In the

investigation of this intriguing solid-state reaction, the solid-state equilibrium-like behavior of **Bi-1** and **Bi-2** has been observed and systematically studied. (Figure 3.3) Under the same aging condition (95°C and 100% RH, reactions are too slow for monitoring at lower temperatures), reaction from both sides of the equilibrium achieves a similar solid-state composition after up to 11 days. Simple PXRD analysis using manually-made standard mixtures show that **Bi-1** content in final mixture lies between 10% and 20% by stoichiometric composition.

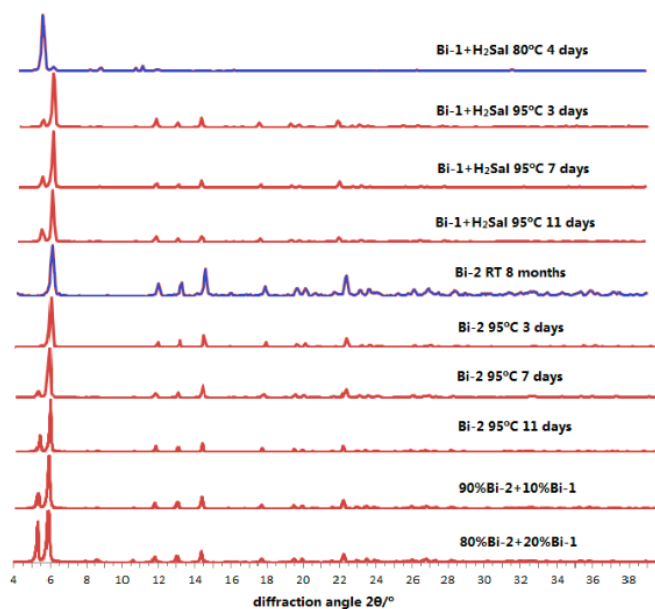
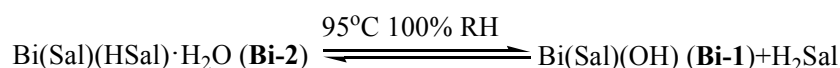


Figure 3.3. PXRD patterns for equilibrium study of **Bi-2** and **Bi-1+H₂Sal** at 95°C 100% RH aging condition. From top to bottom: 1:1 mixture of **Bi-1** and **H₂Sal** after 4 days aging at 80°C 100% RH (no reaction); 1:1 mixture of **Bi-1** and **H₂Sal** after 3 days aging at 95°C 100% RH; 1:1 mixture of **Bi-1** and **H₂Sal** after 7 days aging at 95°C 100% RH; 1:1 mixture of **Bi-1** and **H₂Sal** after 11 days aging at 95°C 100% RH; **Bi-2** after 8 months aging at room temperature 100%RH (no reaction); **Bi-2** after 3 days aging at 95°C 100%RH; **Bi-2** after 7 days aging at 95°C 100%RH; **Bi-2** after 11 days aging at 95°C 100%RH; 10% **Bi-1**+90% **Bi-2** manually mixture; 20% **Bi-1**+80% **Bi-2** manually mixture.

We believe that the observed equilibration behavior can be explained by the release of salicylic acid upon aging of **Bi-2** at 95°C and 100% RH. In the second step of **Bi-1** synthesis, the released salicylic acid subsequently reacts with remaining bismuth oxide which pushes the equilibrium towards the formation of **Bi-1**. As shown in Figure 3.4, four equivalents of **Bi-1** are produced within each cycle, while two equivalents of consumed **Bi-2** can be regenerated by the reaction of released salicylic acid with bismuth oxide. Finally, as shown by PXRD analysis, only **Bi-1** is left at the end of the reaction.

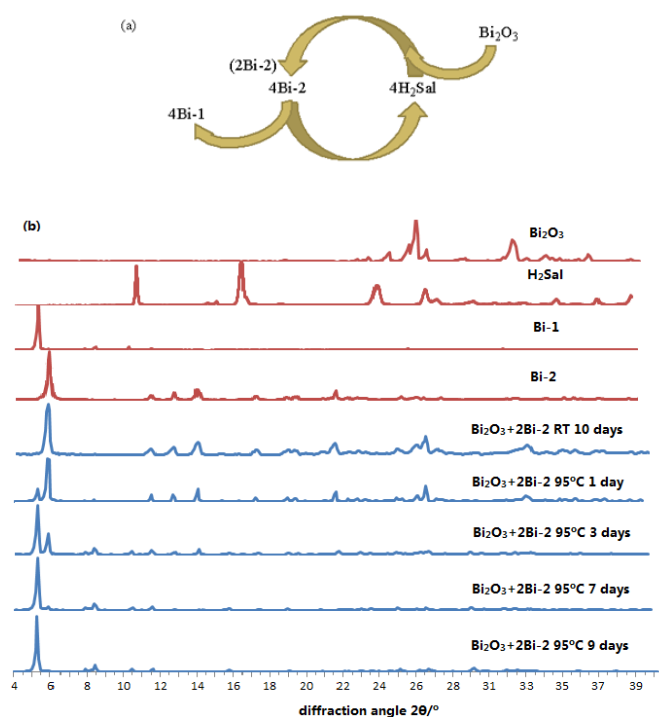


Figure 3.4. (a) Proposed mechanism of the **Bi-2** and Bi_2O_3 aging reactions; (b) PXRD patterns for **Bi-2** and Bi_2O_3 aging reactions, from top to bottom: bismuth oxide (Bi_2O_3); salicylic acid (H_2Sal); **Bi-1**; **Bi-2**; 2:1 stoichiometric mixture of **Bi-2** and Bi_2O_3 after 10 days aging at room temperature and 100% RH (no reaction); 2:1 mixture of **Bi-2** and Bi_2O_3 after 1 day aging at 95°C and 100% RH; 2:1 mixture of **Bi-2** and Bi_2O_3 after 3 days aging at 95°C and 100% RH; 2:1 mixture of **Bi-2** and Bi_2O_3 after 7 days aging at 95°C 100% RH; 2:1 mixture of **Bi-2** and Bi_2O_3 after 9 days aging at 95°C 100% RH.

The previous investigation of **Bi-2** revealed⁴ that upon recrystallization from acetone it readily forms nanosized clusters of bismuth oxide, decorated with salicylate ligands and acetone molecules with composition of $\text{Bi}_{38}\text{O}_{44}(\text{HSal})_{26}(\text{Me}_2\text{CO})_{16}(\text{H}_2\text{O})_2$,³ which led us to explore the ability to use **Bi-2** as a versatile precursor for a more general synthesis of such bismuth oxo-clusters (detailed procedure has been illustrated in Experimental Section). The first target in such a study was to establish the ability to scale-up the previously reported work.⁴ This led to a reliable recrystallization-based procedure which provided the acetone-decorated bismuth oxo-clusters in 71% isolated yield from 1 gram of **Bi-2** after overnight evaporation of 300 mL of an acetone solution. According to single crystal diffraction data, the resulting product crystals only contained the expected oxo-clusters based on the $\text{Bi}_{38}\text{O}_{44}(\text{HSal})_{26}$ core, decorated by acetone and water molecules. As the next step in our study, we explored recrystallization of **Bi-2** from other ketones, in expectation to obtain oxo-clusters based on the $\text{Bi}_{38}\text{O}_{44}(\text{HSal})_{26}$ core but decorated with a diversity of organic molecules. Indeed, recrystallization of **Bi-2** from 2-butanone and cyclohexanone gave well-developed crystals whose preliminary structural characterization revealed the expected 2-butanone- and cyclohexanone-decorated oxo-nanoclusters (Figure 3.5a). While the 2-butanone-decorated clusters adopted a crystal packing structure that was identical to that seen with acetone and DMF⁴, using cyclohexanone as the cluster decorating agent led to a change in space group and molecular packing. This observation indicates that changes in decorating molecule lead to different recognition properties of the decorated clusters. In addition to X-ray single crystal diffraction, the decorated clusters were also investigated in solution using dynamic light scattering (DLS), which indicated cluster sizes resembling those seen in the solid state (Figure 3.5b). The decoration of oxo-clusters with different solvent molecules in the solid state was also apparent from the comparison of their FTIR-ATR spectra (Figure 3.5c).

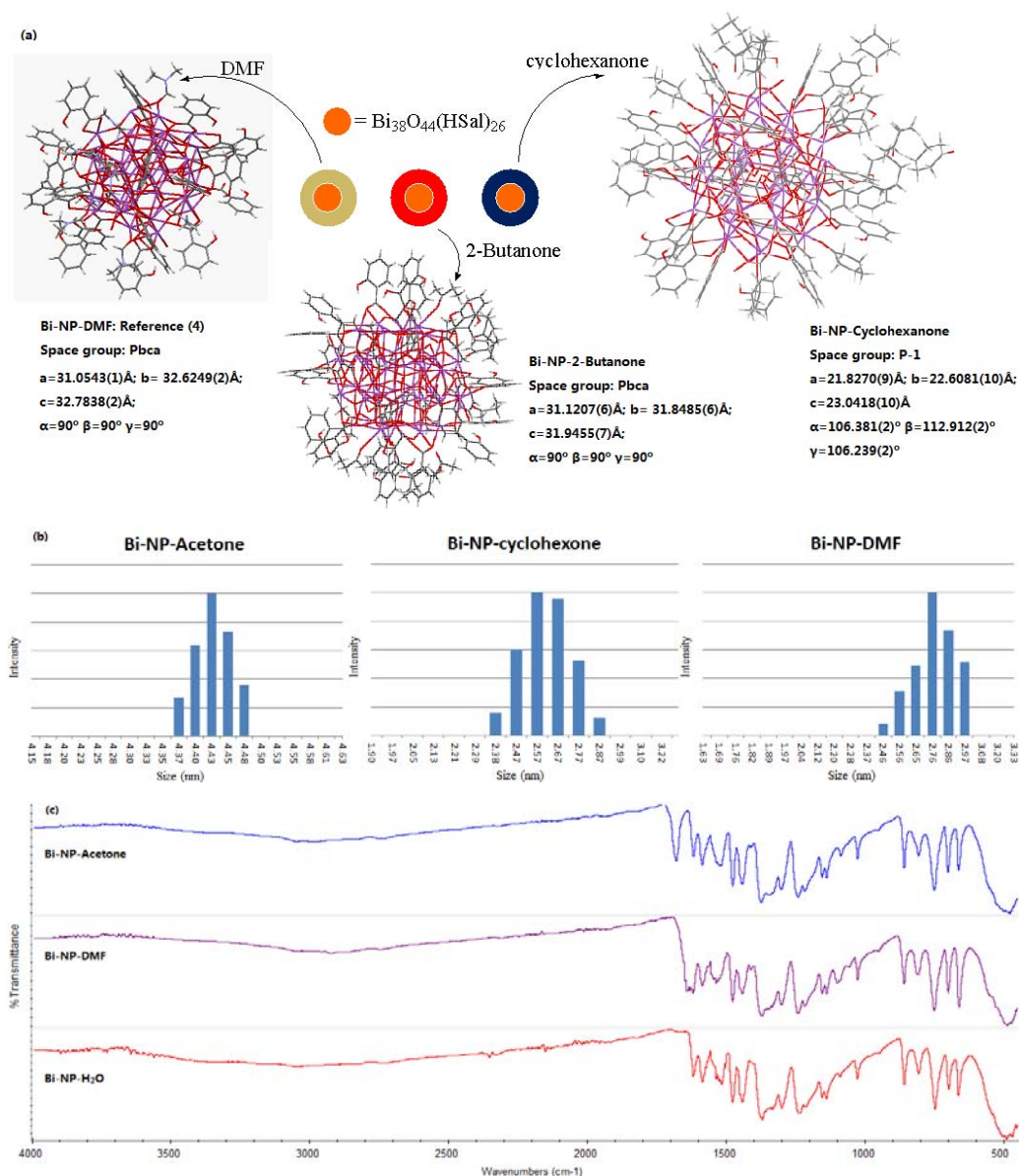


Figure 3.5. (a) A series single crystals of surface-decorated bismuth salicylate oxo-nanoclusters; (b) DLS measurements of the size of nanoclusters in their respective solvents of decoration; (c) FTIR-ATR spectra of different decorated nanoclusters. The characteristic absorption bands are located in the 1500-1700 cm⁻¹ region.

We have also explored the ability to decorate the oxo-nanoclusters with water molecules only, by precipitating the acetone solutions of **Bi-2** with water. This led to an insoluble white powder that could not be readily recrystallized.

Consequently, we addressed its structure through SSNMR (C^{13}) and TGA. The solid-state NMR spectrum in the 100 ppm - 180 ppm region was found to be identical to those of DMF- and acetone-decorated oxo-nanoclusters. Also, the results of TGA were consistent with the formula $Bi_{38}O_{44}(HSal)_{26}(H_2O)_5$. We believe that these clusters, decorated with water molecules only, might have considerable potential for the development of nanopharmaceuticals. We also used AFM to explore the aqueous suspensions of these water-decorated nanoclusters and found the formation of aggregates with nanoscale heights and diameters (Figure 3.6).

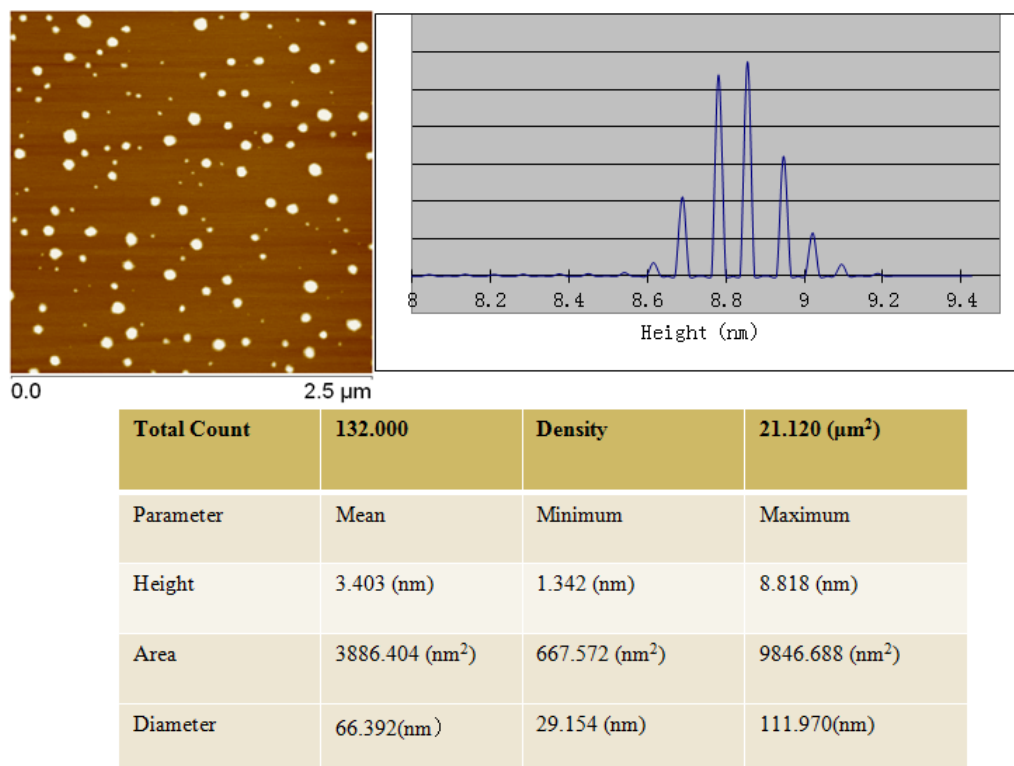


Figure 3.6. AFM image and analysis of aqueous suspension of proposed water-decorated bismuth salicylate oxo-nanoclusters.

3.5 Conclusions

We have demonstrated the interconversions of different bismuth salicylates and the versatile role of bismuth disalicylate in the synthesis of bismuth subsalicylate

and decorated bismuth oxo-nanoclusters. Conditions and mechanisms of accelerated aging reactions towards bismuth subsalicylate and bismuth disalicylate have been discussed in detail. In the future are planned further investigations of supramolecular assembly of bismuth salicylic oxo-nanoclusters and their potential pharmaceutical applications.

Reference

- (1) G. G. Briand and N. Burford, *Chem. Rev.*, **1999**, *99*, 2601.
- (2) J. H. Thurston, E. M. Marlier and K. H. Whitmire, *Chem. Commun.*, **2002**, 2834.
- (3) P. C. Andrews, G. B. Deacon, C. M. Forsyth, P. C. Junk, I. Kumar and M. Maguire, *Angew. Chem. Int. Ed.* **2006**, *45*, 5638.
- (4) V. André, A. Hardeman, I. Halasz, R. S. Stein, G. J. Jackson, D. G. Reid, M. J. Duer, C. Curfs, M. T. Duarte and T. Frišćić, *Angew. Chem. Int. Ed.* **2011**, *50*, 7858.
- (5) T. Frišćić, D. G. Reid, I. Halasz, R. S. Stein, R. E. Dinnebier, M. J. Duer, *Angew. Chem. Int. Ed.* **2010**, *49*, 712.
- (6) G. Berti, M. D'Acunto and F. De Marco, *Advances in X-ray Analysis.* **2002**, *45*, 60.
- (7) (a) M. J. Cliffe, C. Mottillo, R. S. Stein, D-K. Bučar and T. Frišćić, *Chem. Sci.* **2012**, *3*, 2495; (b) C. Mottillo, Y. Lu, M-H. Pham, M. J. Cliffe, T-O. Do and T. Frišćić, *Green Chem.*, **2013**, *15*, 2121; (c) F. Qi, R. S. Stein and T. Frišćić, *Green Chem.*, **2013**, DOI: 10.1039/C3GC41370E.
- (8) T. Frišćić, S. L. Childs, S. A. A. Rizvi and W. Jones, *CrystEngComm.*, **2009**, *11*, 418.
- (9) A. Shalmashi and A. Eliassi, *J. Chem. Eng. Data*, **2008**, *53*, 199.

Chapter 4. Conclusions, Contributions to Original Knowledge and Ideas for Future Work

This thesis introduced mechanochemical milling and accelerated aging, two remarkable solvent-free, low-energy synthetic approaches for MOMs synthesis and mineral processing. The accelerated aging method has been focused on and a comprehensive biography of this newborn method has been illustrated, including the inspiration from geological biomineralization, its relationship and comparison with mechanochemical milling, its standard and alternative reaction conditions, its kinetics and thermodynamics, its applications for different MOMs synthesis (coordinated polymers, MOFs, metallodrugs) and its metallurgical use for non-ferrous mineral separations.

Contributions to original knowledge include:

1. The first systematic study of the synthesis of MOFs and coordination polymers directly from metal oxides by accelerated aging technique.
2. Cheap and inert mineral feedstocks (metal oxides and sulfides) across periodic table have been successfully activated and stoichiometrically converted to MOMs with controlled topology (coordinated polymers, MOFs, metallodrugs) by accelerated aging for the first time.
3. It was proven that ammonium oxalates have templating effect on solid-state synthetic pathways, such as accelerated aging.
4. It was systematically studied how accelerated aging is influenced by different environmental factors, including temperature, humidity, particle size and defects (the last two are modified by pre-milling).
5. Kinetics and thermodynamics of accelerated aging reactions have been studied case by case, including polymorphic transformations of manganese oxalate dihydrate, solid state equilibrium of bismuth disalicylate and

bismuth subsalicylate, and the mechanism of bismuth subsalicylate accelerated aging synthesis.

6. For most of the chosen compounds, up to 10 gram scale accelerated aging reactions have been successfully conducted. Thin layer and large exposure area keep the rate of the large scale reaction similar to that of milligram scale reactions, indicating potential for industrial applications.
7. Based on kinetics of accelerated aging, a new solid-state separation method has been developed for industrial mineral processing. A provisional patent (US 61/826,172) has been obtained, aiming to lower the cost, risks and pollution of current metallurgical techniques.
8. ILAG syntheses of bismuth salicylates have been scaled up to 1 gram.
9. Transformations between different bismuth salicylates have been reported for the first time. Bismuth disalicylate has been proved to be a highly versatile precursor for the synthesis of bismuth subsalicylate and bismuth oxo-nanoclusters
10. A series of decorated bismuth oxo-nanoclusters have been synthesized and structurally determined. Some of them, especially the water-decorated bismuth oxo-nanocluster have great potential for the application of nano-pharmaceuticals.

At this point, it is not possible to clearly evaluate the cost of scaling up demonstrated transformations to the industrial level. However, as a part of future development, we are currently looking for industrial partners that would support scaling up of these processes to a pilot plant level, which could open a door to cleaner mining processing. In order to extend the applications of accelerated aging, more types of minerals such as carbonates, phosphates and high-valent metal oxides/sulfides need to be explored for activation and used as feedstocks in the future. More complicated and useful MOFs can be targeted and synthesized from inexpensive minerals in order to lower the cost and pollution associated with their production and makes them more readily available for potential application. Organic and biochemical reactions can be

investigated in the solid state under accelerated aging conditions, especially those conducted in water. Gas compositions of accelerated aging can also be changed: pure nitrogen for air-sensitive reactions, pure oxygen for redox reactions, or even pure hydrogen, *e.g.* for making hydrogen storage materials directly from hydrogen gas. Microscopic and synchrotron studies of accelerated aging reactions are necessary to understand the underlying mechanisms and self-assembly. Systematic studies of the relationships of pre-milling time, particle size and reaction rates are important for building the fundamentals of the solid-state mineral separation. In the field of bismuth chemistry, decorated bismuth oxo-nanoclusters can be used as building blocks for supramolecular chemistry. More modifications on the surface of such nanoclusters, for example, the attachment of hydrophilic or charged groups, may improve the water solubility of these bismuth salicylate oxo-nanoclusters and extend their applications towards the fields of materials and pharmaceutical science.